SIMULATION OF A MAXIMUM POWER POINT TRACKING SYSTEM FOR IMPROVED PERFORMANCE OF PHOTOVOLTAIC SYSTEMS

VINCENT NDEGWA LENGOIBONI

MASTER OF SCIENCE

(Mechatronic Engineering)

JOMO KENYATTA UNIVERSITY OF AGRICULTURE AND TECHNOLOGY

2015

Simulation of a maximum power point tracking system for improved performance of photovoltaic systems

Vincent Ndegwa Lengoiboni

A thesis submitted in partial fulfillment of the requirement for the award of the degree of Master of Science in Mechatronic Engineering in the Jomo Kenyatta University of Agriculture and Technology

2015

DECLARATION

This thesis is my original work and has not been presented for a degree in any other University.

Sign..... Date.....

Vincent N. Lengoiboni

This thesis has been submitted for examination with our approval as the University Supervisors:

Sign..... Date.....

Prof. George N. Nyakoe

JKUAT, Kenya

Sign..... Date.....

Dr. James N. Keraita

DeKUT, Kenya

DEDICATION

I dedicate this work to Lisa, the joy of my life.

ACKNOWLEDGEMENTS

I would like to acknowledge my supervisors, Prof. George N. Nyakoe and Dr. James N. Keraita for their invaluable guidance and advice throughout my studies.

I would like to thank Dedan Kimathi University of Technology for granting me the scholarship that enabled me to undertake my studies and hence achieve one of my personal goals. My heartfelt appreciation goes to my course mates, Sultan Hamid, Khamis Karama, Nicholas Mhusa, James Wamai and Ambrose Mungai for their encouragement, positive criticism and good co-existence especially during my course work.

I express my sincere thanks to all members of staff and all postgraduate students in Mechanical and Mechatronic Engineering departments of Jomo Kenyatta University of Agriculture and Technology for their input to my work during postgraduate seminars through their comments and suggestions.

Finally, I express my appreciation to my father, Mr. Gabriel Lengoiboni, mother, Prof. Eunice Kairu, sibling, Dr. Timothy Lengoiboni and lovely fiancee, Winfred Nyawira for their prayers, encouragement, guidance, love and unwavering belief in me, which kept me going.

TABLE OF CONTENTS

LIST OF TABLES

LIST OF FIGURES

LIST OF APPENDICES

LIST OF ABBREVIATIONS

AC	Alternating Current
DC	Direct Current
FF	Fill Factor
FL	Fuzzy Logic
FLC	Fuzzy Logic Controller
GP	Global Peak
GMPP	Global Maximum Power Point
InCond	Incremental Conductance
MPP	Maximum Power Point
MPPT	Maximum Power Point Tracking
NN	Neural Network
OC	Open Circuit
P-I	Power-Current
P&O	Perturb and Observe
PV	Photovoltaic
P-V	Power-Voltage
SC	Short Circuit
V-I	Voltage-Current

NOMENCLATURE

$\boldsymbol{A}$	Diode Ideality Factor
$\boldsymbol{C}$	Capacitance $[F]$
$\boldsymbol{D}$	Diode
$\boldsymbol{E_{g0}}$	Band Gap Energy for Silicon $[eV]$
$\boldsymbol{G}$	Incident Irradiance on Surface $[Wm^{-2}]$
$\boldsymbol{G_n}$	Nominal Irradiance $[1000Wm^{-2}]$
$\boldsymbol{\Delta G}$	Change in Irradiance $[Wm^{-2}]$
$\boldsymbol{I}$	Solar Cell Output Current $[A]$
$\boldsymbol{I_D}$	Diode Current $[A]$
$\boldsymbol{I_L}$	Light Generated Current/ Photo-generated Current $[A]$
$\boldsymbol{I_{MPP}}$	Current at MPP $[A]$
$\boldsymbol{I_0}$	Dark Saturation Current/ Diode Saturation Current $[A]$
$\boldsymbol{I_{rs}}$	Reverse Saturation Current $[A]$
$\boldsymbol{I_{R_{SH}}}$	Shunt Resistance Current $[A]$
$\boldsymbol{I_{SC}}$	Short Circuit Current $[A]$
$\boldsymbol{I_{scn}}$	Short Circuit Current at STC $[A]$
$\boldsymbol{K_i}$	Temperature Coefficient of Short Circuit Current
$\boldsymbol{K_v}$	Temperature Coefficient of Open Circuit Voltage
$\boldsymbol{L}$	Inductance $[H]$
$\boldsymbol{P}$	Solar Cell Output Power $[W]$
$\boldsymbol{q}$	Charge of an Electron $[C]$
$\boldsymbol{R}$	Resistance $[\Omega]$
$\boldsymbol{R_S}$	Series Resistance of Solar Cell $[\Omega]$
$\boldsymbol{R_{SH}}$	Shunt Resistance of Solar Cell $[\Omega]$
$\boldsymbol{S}$	Electronic Switch
$\boldsymbol{T}$	Absolute Temperature/ Actual temperature $[^\circ K]$
$\boldsymbol{\Delta T}$	Change in Temperature $[^\circ K]$
$\boldsymbol{T_n}$	Nominal/ Reference Temperature $[25^\circ C]$
$\boldsymbol{V}$	Solar Cell Output Voltage $[V]$
$\boldsymbol{V_{MPP}}$	Voltage at MPP $[V]$
$\boldsymbol{V_{OC}}$	Open Circuit Voltage $[V]$
$\boldsymbol{V_{OC}^{STC}}$	Open Circuit Voltage at Standard Temperature and Conditions $[V]$
$\boldsymbol{V_t}$	Junction Thermal Voltage $[V]$

$\boldsymbol{\alpha_v}$	Coefficient of Proportionality for Fractional Open Circuit Voltage
$\boldsymbol{\alpha_i}$	Coefficient of Proportionality for Fractional Short Circuit Current
$\boldsymbol{k}$	Boltzman Constant

ABSTRACT

In line with global trends, Kenya is increasingly turning to renewable sources of energy, namely Hydro, Solar, Wind and Geothermal to boost its capacity feed to the national grid. As such, Photovoltaic (PV) power generation has a key role to play. Compared to other renewablel sources of power (like wind and geothermal), PV power has the advantage of being installed in places that would otherwise have no other use such as roof tops. However, due to the equipment required, it still remains expensive to small scale dosmetic users. To counter this, delibarate efforts are being made to make them more competitive by increasing their efficiency. The major cause of energy losses in PV arrays has been recognized to occur when the PV arrays are operating at non-uniform conditions such as in a case where part of the modules are under shade while the rest are receiving the nominal solar radiation. Under partial shading conditions PV characteristics get more complex with multiple peaks. Because of multiple Maximum Power Points (MPPs), a considerable amount of available electrical energy may be lost when the module is operating at a local Maximum Power Point (MPP) with low power instead of the global MPP. Hence, it is necessary to understand the occurence of multiple MPPs under partial shading in order to extract maximum power.

This thesis explores the effect of partial shading on the power-voltage (P-V), power-current (P-I) and current-voltage (I-V) characteristic curves through models of the PV array created in MATLAB/SIMULINK software. It also sought to determine the effectiveness of employing a conventional MPP technique, namely the Perturb and Observe (P&O) in tracking the MPP in the prescence of multiple peaks and compared results with that of a proposed two-tier maximum power point tracking technique. This technique aims to locate the global MPP on the P-I curve of the interconnected PV arrays by bypassing any local maximum that may trap the conventional MPPT schemes. The technique is split into two parts with the first stage being used to find a point that bypasses any local maximum and moves the operating point of the PV arrays near the global MPP. The second stage then finds the global MPP and sets the operating point of the PV arrays at this maximum. The system consists of two series PV array, A DC-DC converter, a load and the proposed technique. Operation of the model employing the proposed MPPT technique was verified by measurements of electrical characteristics of a PV array under partial shading.

Simulation results show the existence of only one peak on the P-V and P-I characteristic curves and one step on the I-V characteristic curve under uniform insolation. However,

under partial shading, there exists multiple peaks on the P-V and P-I characteristic curves and multiple steps in the I-V characteristic curve with power peaks being displaced from each other by a multiple of 8% of open circuit voltage. Simulation results also show that in the prescence of multiple peaks, the Perturb and Observe (P&O) can unexpectedly track the global peak, be trapped at a local peak for some time but continue to track the global peak or totally be unable to track the global peak. The results also showed that compared to the conventional P&O algorithm, the proposed MPPT algorithm provides improved performance in tracking the global MPP in the prescence of multiple peaks.

Experimental results of model validation show that the model of the PV module used was reliable and accurate. Experimental implementation of the proposed MPPT algorithm indicates that a significant amount of additional energy (an increase of about 130% of additional PV power) can be extracted from a PV module under partial shading when using the proposed technique as compared to when the P&O algorithm is used. This results in improved effciency in the operation of the PV system, which is expected to increase cost savings in the long term.

The results of this work can be applied to improve the operation of a partially shaded PV system by improving the maximum power point tracking of partially shaded PV arrays, resulting in the increase of power harvested from the PV system which is expected to increase cost savings in the long haul. Thus contributing to making PV-power generation a viable alternative to hydro-power generation.

1. CHAPTER ONE INTRODUCTION

1.1 Background

The annual world demand for Photovoltaic (PV) energy is growing and had reached 1727 MW in 2005 [1]. To meet meet future energy demands efficiently, energy security and reliability must be improved. One way of achieving this is by aggresively investigating alternative energy sources. An effective energy solution would be to utilize renewable energy sources. Of the many available renewable sources of energy, solar energy is a promising option because apart from being a green source, it is also extensively available [2]. Compared to other conventional sources of power (like hydro), PV power has the advantage of being installed in places that would otherwise have no other use such as roof tops or being used to produce electricity in remote locations where there is no electricity network. In the long term, PV power generation can also be an economically viable source of power [3].

To expand their usage as a preffered source of power generation, deliberate efforts are being made to make them more competitive. One way of achieving this is by reducing the cost of power generated by PV solar systems by increasing their efficiency [2].

The efficiency of a PV system (which varies between 8.8% and 28.8% for the different types of solar cells [4]) is affected mainly by three factors: The PV panel [5], the inverter [6] and the maximum power point tracking (MPPT) algorithm [7] - this is the process of locating the unique operating point on a PV module or array, where maximum power is obtained. Improving the efficiency of the PV panel and the inverter is not easy as it depends on the technology available. It may require better components, which can drastically increase the cost of the installation. Instead, improving the maximum power point tracking (MPPT) algorithm by modifying the already existing algorithms is easier and less expensive. This would lead to an immediate increase in PV power generation and consequently an increase in its efficiency.

Solar cell characteristics are nonlinear and vary with irradiation and temperature. In general, there is a unique point on the Voltage-Current (V-I), Power-Current (P-I) and

Power-Voltage (P-V) curves known as Maximum Power Point (MPP), at which the entire PV system operates with maximum efficiency and produces its maximum output power. The location of the MPP may not be known, but can be determined, either through calculation or by search algorithms. Therefore, Maximum Power Point Tracking (MPPT) techniques are needed to maintain the PV array operating point at its maximum power point (MPP) [8]. Furthermore, the daily solar irradiation constantly varies during the day and as such, the MPP changes continuously. To harness maximum energy from the PV system, the PV array operating point must be kept at its maximum power point continously by use of maximum power point tracking algorithms [8, 9].

There exist many methods for determining the MPP that have been developed. These techniques differ in aspects such as required sensors, complexity, range of effectiveness, convergence speed, popularity, among others. A partial review of the different MPPT algorithms can be found in Esram and Chapman [10].

1.2 Problem Statement

The cost of conventional energy in Kenya has gone up in the recent past and other non-conventional means of power generation, like solar, can be promising alternatives. Through parallel and series combination of PV cells electrical power can be generated depending on the prevailing atmospheric conditions. [11]. A growing trend towards installation of solar cells is rooftop PV installations. This increases the occurrence of partial array shading. In urban environments, shading of PV arrays originating from chimneys, roof vents, power poles, trees, neighbouring buildings, and other obstructions is often unavoidable.

The quantity of power supply from photovoltaic arrays is sensitive to the shading effects of single or multiple modules. In particular, the P-V and P-I curves present multiple maxima under partial shading conditions and as such, most MPPT algorithms cannot determine the global maximum or global point (GP) or global maximum power point (GMPP) [12]. This means that the energy yield of a partly shaded photovoltaic system is much lower than that which can be achieved from the nominal solar irradiance. Therefore there is a need to optimise PV system power generation by either selecting the right type or modifying the maximum power point tracking system in combination with a DC to DC converter.

1.3 Objectives

The main objective of this study was to investigate the effect of partial shading on a PV system and to develop an MPPT algorithm for a PV system to enable tracking of the MPP under partial shading conditions. To achieve this objective, the following specific objectives wereto be achieved:

1. Modelling a PV array and using it to investigate the behaviour of the MPP under both uniform insolation and partial shading conditions.
2. Development of an algorithm to track the MPP under partially shaded conditions.
3. Simulation of the response of the developed algorithm in tracking the MPP.
4. Experimental validation of the proposed algorithm in tracking the MPP under partial shading conditions.

1.4 Justification

Many techniques for determining the MPP of photovoltaic cells have been developed and implemented, thus improving the quality of output power of the PV arrays and expanding their use as an alternative source of power. The Perturb and Observe MPPT algorithm which has been in use for a long time, has limitations (such as the tendancy to track the local peak as opposed to global peak under partial shading conditions) that need to be overcome for these expanding applications of PV power. There is a need to study the response of this algorithm when the PV array is under partial shading to ensure maximum power delivery from the PV system. A study of the MPPT algorithm under partial shading will add knowledge which is useful in implementing the technique in future.

1.5 Outline of the Thesis

This thesis contains 5 chapters: Chapter 1 gives an introduction of the subject of this research work. An overview of PV power generation, maximum power point tracking techniques, definition of partial shading, governing mathematical equations used in

modelling and literrature review are discussed in Chapter 2. Relevant mathematical equations of DC-DC converters necessary in design of a PV system and the methodology that was applied to achieve the objectives of this work is covered in Chapter 3, while Chapter 4 deals with the results and their interpretations and discussions. Chapter 5 carries the conclusions and recommendations for future work.

2. CHAPTER TWO
LITERATURE REVIEW

As explained in Chapter 1, the quality of PV power is sensistive to shading effects on single or multiple modules resulting in the occurence of multiple maxima on P-V, P-I curves. The resultant effect is that most MPPT algorithms are unable to track the global peak, leading to a much reduced energy yield than can be achieved. This chapter looks at the concept behind PV power generation, introduces key terminology and unique points of interest in characteristic curves of PV modules and looks in detail into the mathematical equations employed in modelling a PV array. Maximum power point tracking algorithms employed in tracking the maximum power point are also detailed. The concept of partial shading is explained and recent advances in the field of maximum power point tracking of PV modules under both uniform insolation and partial shading is captured.

2.1 Types of Solar Cells

According to Lynn [13], silicon is almost the only material used for manufacturing solar cells. Although other materials and techniques have been developed, silicon is used in more than the 80 percent of the production. The abundance of Silicon (in the form of silicon dioxide) being one of the contributing factors to its wide usage. Monocrystalline and polycrystalline silicon solar cells are the two major types of silicon solar cells. The author cites a third type, amorphous silicon, but the efficiency is less than the previous two so it is less used.

2.1.1 Monocrystalline Silicon

Monocrystalline silicon solar cells are the most efficient ones. They are made of single crystals obtained from pure molten silicon. These single crystals are highly ordered thus have uniform and predictable properties. However the manufacturing process occurs at high temperatures, which is expensive [13].

2.1.2 Polycrystalline Silicon

These cells are also made from single crystals obtained from pure molten silicon. However, the crystal structure is random because as the silicon cools, it crystallizes simultaneously in many different points producing an irregular structure. These structures are not as ideal as in the monocrystalline cells so the efficiency is lower. However the manufacturing process is less expensive, so the lower efficiency is compensated in some way [13].

2.1.3 Amorphous or Thin-film Silicon

Amorphous silicon is the non-crystalline form of the silicon and it can be deposited as thin-films onto different substrates. The deposition can be made at low temperatures. The manufacturing process is simpler, easier and cheaper than in the crystalline cells. The weak point of these cells is their lower efficiency. However, the performance under weaker or diffuse irradiation, such as that in cloudy days, can be higher than in crystalline cells. Amorphous silicon is also a better light absorber than crystalline silicon [13].

Over recent years, one more type of silicon has been developed known as microcrystalline silicon [13]. It can also be deposited as thin-films onto different substrates, minimizing the quantities of crystalline silicon needed and improving the efficiency of amorphous silicon. However, the light absorption of microcrystalline silicon compared to amorphous silicon is poor. This type of silicon is not yet a commercial technology and more research and development is needed.

2.2 Operating Principle of a Solar Cell

Solar cells are the basic components of photovoltaic panels. Most are made from silicon even though other materials are also used.

A solar cell is basically a p-n junction which is made from two different layers of silicon doped with a small quantity of impurity atoms. The n-layer contains atoms with one more valence electron (donors) while the p-layer contains atoms with one less valence electron (acceptors). When the two layers are joined together, the free electrons of the

n-layer are diffused in the p-side near the interface leaving behind an area positively charged by the donors. Similarly, the free holes in the p-layer are diffused in the n-side, leaving behind a region negatively charged by the acceptors. This creates an electrical field between the two sides that is a potential barrier to further flow. This electric field pulls the electrons and holes in opposite directions so the current can flow in one way only. Electrons move from the p-side to the n-side and the holes in the opposite direction. An illustration of the p-n junction under the effect of the mentioned electric field is shown in Figure 2.1.

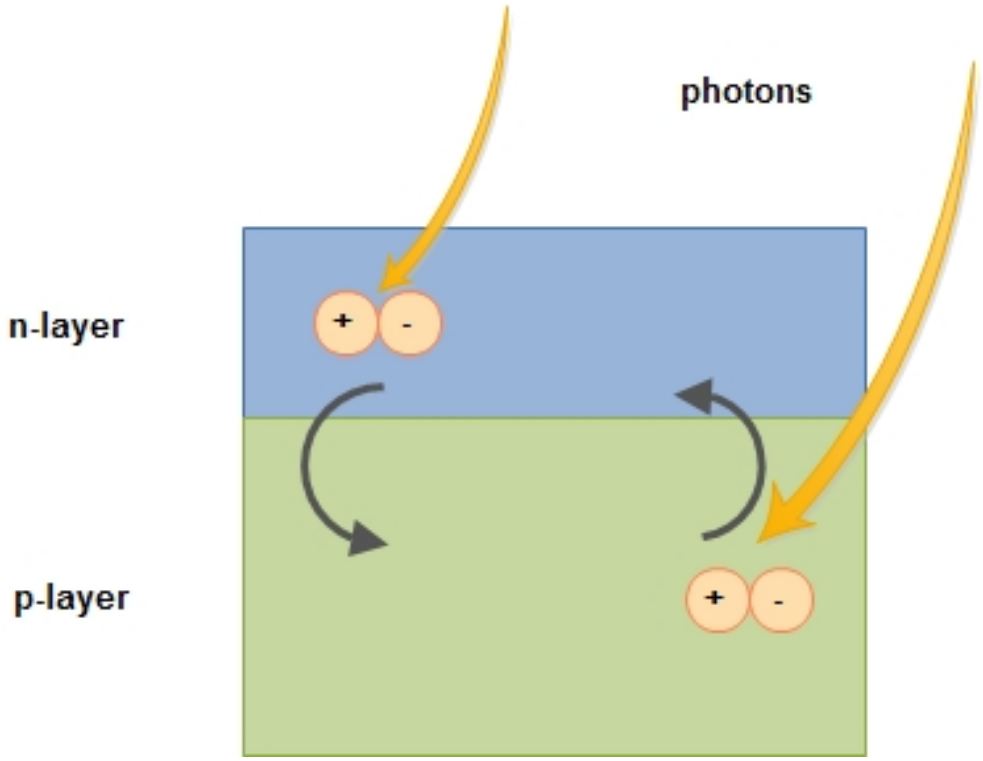

Figure 2.1: The solar cell P-N junction

Metallic contacts are added at both sides to collect the electrons and holes so the current can flow. In the case of the n-layer, which is facing the solar irradiance, the contacts consist of several metallic strips (called fingers) so as to allow the light to pass to the solar cell.

When photons of the solar radiation shine on the cell, some of the photons are reflected from the top surface of the cell and metal fingers. Those that are not reflected penetrate in the substrate. Those with less energy, pass through the cell without causing any

effect while those with energy level above the band gap of the silicon create an electron-hole pair. These pairs are generated at both sides of the p-n junction. The electric field sweeps these pairs away in opposite directions (electrons towards the n-side, holes towards the p-side) generating a current in the cell, which is collected by the metal contacts at both sides. This is the light-generated current (photo-generated current or simply photo current) which depends directly on the irradiation. The higher it is, the more photons with enough energy to create more electron-hole pairs and consequently more current is generated by the solar cell.

2.3 Electrical Model of a Solar Cell

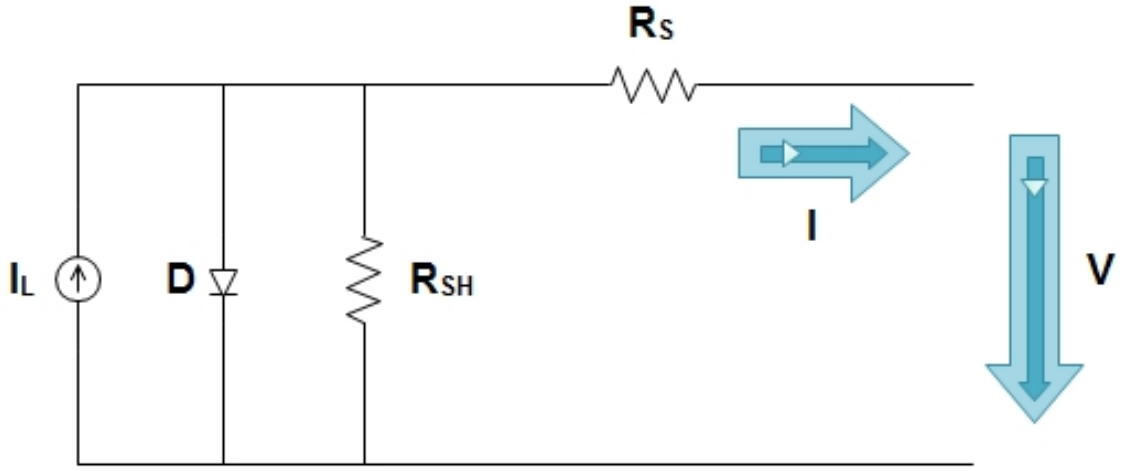

Figure 2.2: Electrical Model of a solar cell

The solar cell can be represented by the electrical model shown in Figure 2.2 [15]. Its current-voltage characteristic is expressed by the following equation.

$$I = I_L - I_0 \left(e^{\frac{q(V - IR_S)}{AkT}} - 1 \right) - \frac{V - IR_S}{R_{SH}} \tag{2.1}$$

Where

I is the solar cell output current,
V is the solar cell output voltage,
I_0 is the dark saturation current,

I_L is the light generated current,
q is the charge of an electron,
A is the diode quality(ideality) factor,
k is the Boltzman constant,
T is the absolute temperature,
R_S is the series resistance of the solar cell,
R_{SH} is the shunt resistance of the solar cell.

The origin of this equation emanates by applying Kirchoff's current law on the common node of the current source, diode and resistances, to attain the PV output current as:

$$I = I_L - I_D - I_{R_{SH}} \tag{2.2}$$

where

I is the PV Output Current,
I_L is the Photoelectric Current (generated under a given insolation),
I_D is the Diode Current,
$I_{R_{SH}}$ is the Shunt Resistance Current.

2.3.1 Photoelectric Current

The photoelectric current I_L is affected by solar irradiance and temperature and is calculated thus [16].

$$I_L = \left(\frac{G}{G_n}(I_{scn} + K_i(T - T_n))\right) \tag{2.3}$$

where

G is the Incident Irradiance on the Surface,
G_n is the Nominal Irradiance at $1000W/m^2$,
I_{scn} is the Short Circuit Current at STC (obtained from data sheet),
K_i is the Temperature Coefficient of Short Circuit Current (obtained from data sheet),

T is the Actual Temperature,
T_n is the Nominal/Reference Temperature at 25 C.

The term $(T - T_n)$ is described as the deviation of the operating temperature from the reference temperature [15].

2.3.2 Diode Current

The current through the diode is described by the Schockley Equation [17]:

$$I_D = I_0 \left(exp \left[\frac{V + R_s I}{V_t A} \right] - 1 \right) \tag{2.4}$$

where

I_0 is the Diode Saturation Current,
V_t is the Junction Thermal Voltage,
V is the PV Output Voltage,
R_s is the Series Resistance,
A is the Diode Ideality Factor.

It was noted that the value of the diode ideality factor (A), lies between 1 and 2, for monocrystalline silicon modules [18]. According to Said et. al., the diode ideality factor is also dependent on the PV Technology and is represented in the Table 2.1 [19].

The diode saturation current I_0, is dependent on temperature and can be represented by [15].

$$I_0 = I_{rs} \left(\frac{T}{T_n} \right)^3 exp \left[\frac{qE_{g0}}{Ak} \left(\frac{1}{T_n} - \frac{1}{T} \right) \right] \tag{2.5}$$

where

I_{rs} is the Reverse Saturation Current,
q is the Charge of an Electron,
E_{g0} is the Band Gap Energy for Silicon,

Table 2.1: Dependence of Diode Ideality Factor on PV Technology

Technology	**A**
Si-mono	1.2
Si-poly	1.3
A-Si:H	1.8
A-Si:H tandem	3.3
A-Si:H triple	5
CdTe	1.5
CIS	1.5
AsGa	1.3

k is the Boltzman Constant.

The value of the band gap energy of silicon semiconductors, E_{g0}, is between 1.1 and 1.2 eV [15].

The reverse saturation current I_{rs}, can be calculated for a certain temperature by [19].

$$I_{rs} = \frac{I_{scn}}{exp\left(\frac{qV_{oc}}{kAT}\right) - 1} \tag{2.6}$$

where

V_{oc} is the Open Circuit Voltage.

The terms representing the Junction Thermal Voltage, V_t are:

$$V_t = \frac{kT}{q} \tag{2.7}$$

Equation (2.6) can then be re-written as;

$$I_{rs} = \frac{I_{scn}}{exp\left(\frac{V_{oc}}{AV_t}\right) - 1} \tag{2.8}$$

Substituting Equation (2.8) into Equation (2.5), the diode saturation current I_0 can be written as;

$$I_0 = \frac{I_{scn} + K_i(T - T_n)}{exp\left[\frac{V_{oc}+K_v(T-T_n)}{AV_t}\right] - 1} \tag{2.9}$$

where

K_v is the Temperature Coefficient of Open Circuit Voltage determined from the PV datasheet.

2.3.3 Shunt Resistance Current

The current through the shunt resistance is given by [19];

$$I_{R_{SH}} = \frac{V + IR_S}{R_{SH}} \tag{2.10}$$

R_S is the resistance offered by the contacts and the bulk semiconductor material of the solar cell. The origin of the shunt resistance R_{SH} is related to the non-ideal nature of the pn junction and the presence of impurities near the edges of the cell that provide a short-circuit path around the junction [13]. In an ideal case R_S would be zero and R_{SH} infinite. Sometimes, to simplify the model, the effect of the shunt resistance may be ignored [20]. When R_{SH} is considered infinite, the last term in Equation (2.1) is neglected.

2.3.4 PV Output Current

Substituting Equations (2.3), (2.4) and (2.10) into Equation (2.2), then PV output current, I, can be written by:

$$I = I_L - I_0\left(exp\left[\frac{V + R_S I}{V_t A}\right] - 1\right) - \frac{V + R_S I}{R_{SH}} \tag{2.11}$$

A PV module is composed of many solar cells, which are connected in series and parallel

so that the output current and voltage of the PV module are high enough to meet the requirements of the grid or equipment. Taking into account this point and the simplification mentioned in section 2.3.3 about the shunt resistance current, the output current-voltage characteristic of a PV panel can be expressed by Equation (2.12).

$$I = n_P I_L - n_P I_0 \left(e^{\frac{q(V - IR_s)}{AkTn_S}} - 1 \right) \tag{2.12}$$

Where n_P and n_S are the number of solar cells in parallel and series respectively [13].

2.4 Open Circuit Voltage, Short Circuit Current and Maximum Power Point

Two important points of the current-voltage characteristic must be pointed out. The open circuit voltage V_{OC} and the short circuit current I_{SC}. At both points, the power generated is zero. V_{OC} can be approximated from Equation (2.1) when the output current of the cell is zero and is represented in Equation (2.3) assuming an ideal cell with R_{SH} neglected. The short circuit current I_{SC} is the current at short circuit and is approximately equal to the light generated current I_L.

$$V_{OC} = \frac{AkT}{q} ln \left(\frac{I_L}{I_0} + 1 \right) \tag{2.13}$$

The maximum power is generated by the solar cell at a point of the current-voltage characteristic where the product VI is maximum. This point is known as the MPP and is unique, as can be seen from Figure 2.3.

The values of open circuit voltage, short circuit current and maximum power point are not constant and vary depending on prevailing conditions of irradiation and temperature.

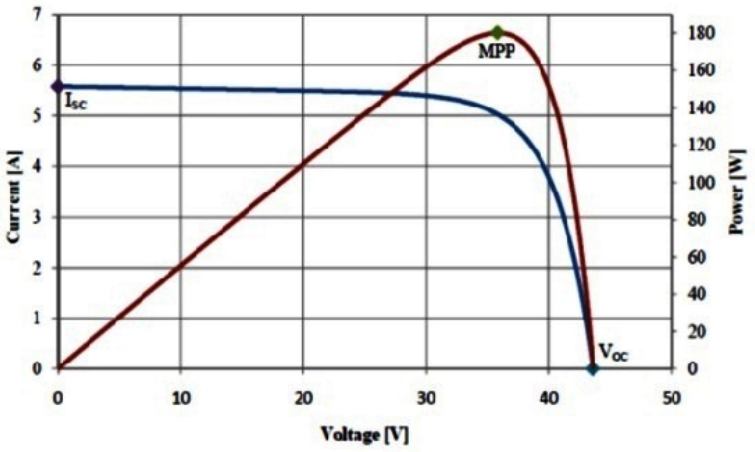

Figure 2.3: Important points in the characteristic curves of a solar panel [21]

2.5 Temperature and Irradiance Effects

Two important factors that have to be taken into account in PV energy generation are the irradiation and the temperature [22]. They strongly affect the characteristics of solar modules. As a result, the MPP varies during the day and that is the main reason why the MPP must constantly be tracked to ensure that the maximum available power is obtained from the panel.

The effect of the irradiance on the V-I and P-V characteristics is depicted in Figure 2.4. The photo-generated current is directly proportional to the irradiance level, so an increment in the irradiation leads to a higher photo-generated current. The short circuit current is directly proportional to the photo-generated current therefore it is directly proportional to the irradiance. When the operating point is not the short circuit, in which no power is generated, the photo-generated current is also the main factor in the PV current, as is expressed by equations (2.1) and (2.2). For this reason, the voltage-current characteristic varies with the irradiation.

From Figure 2.4, it can be seen that the change in current (from 0.4 A to 1 A) is much more than the change in voltage (from 0.9 V to 1 V). In practice, the voltage dependency on the irradiation is often neglected [23]. As the effect on both the current and voltage is positive (both increase) when the irradiation rises, the effect on the power is also positive (the more irradiation, the more power is generated).

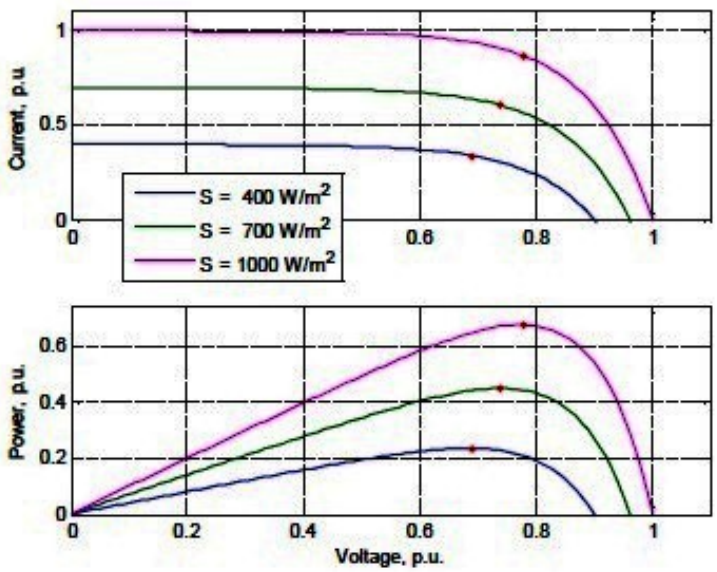

Figure 2.4: V-I and V-P curves at constant temperature (25C) and three different insolation values [23].

On the other hand, temperature mostly affects the voltage. The open circuit voltage is linearly dependent on the temperature, as shown in the following equation:

$$V_{oc} = V_{oc}^{STC} + \frac{K_v}{100}(T - 273.15) \tag{2.14}$$

where

V_{oc} is the Open Circuit Voltage,
V_{oc}^{STC} is the Open Circuit Voltage at Standard Temperature and Conditions,
K_v is the Temprature Co-efficient of Open Circuit Voltage.

According to Equation (2.15), the effect of the temperature on V_{OC} is negative, because K_V is negative, i.e. when the temperature rises, the voltage decreases. There is a very slight increase in current due to temperature rise which does not compensate the decrease in the voltage caused by the given temperature rise. That is why the power also decreases. As the effect of the temperature on the current is really small, it is usually neglected [23]. Figure 2.5 shows how the voltage-current and the voltage-power characteristics change with temperature.

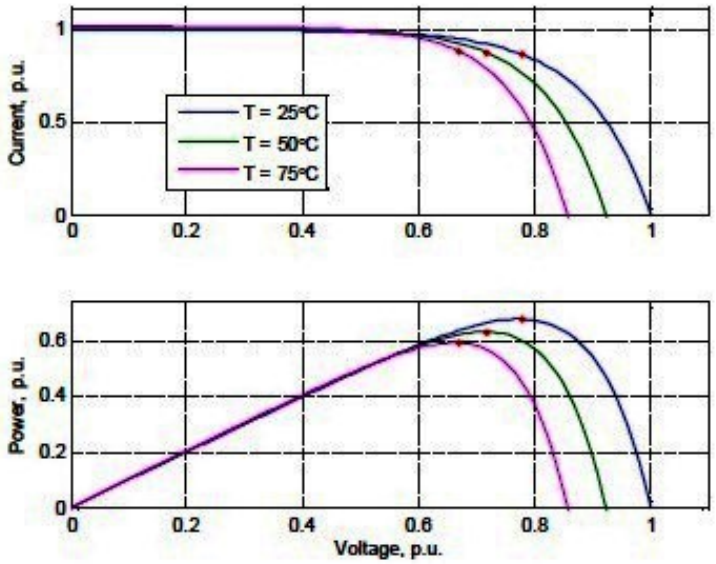

Figure 2.5: V-I and P-V curves at constant irradiation (1 kW/m2) and three different temperatures [23].

The temperature and the irradiation depend on the atmospheric conditions, which are not constant during the year and not even during a single day they can vary rapidly due to fast changing conditions such as clouds. This causes the MPP to move constantly, depending on the irradiation and temperature conditions. If the operating point is not close to the MPP, considerable power losses occur. Hence it is essential to track the MPP in any conditions to ensure that the maximum available power is obtained from the PV panel.

2.6 Grid Photovoltaic Configuration

PV modules generate DC current and voltage. However, to feed the electricity to the grid, AC current and voltage are needed. Inverters are the equipment used to convert DC to AC. Just like choppers, they can be used to keep the operating point of the PV array at the MPP.

There are different inverter configurations depending on how the PV modules are connected to the inverter [13, 24]. These configurations have their merits and demerits and the choice of which to use is mainly based on the environmental conditions and financial constraints.

2.6.1 Central Inverter

In this configuration, branches consisting of series connected PV panels are connected in parallel to obtain the desired output power. The resulting PV array is connected to a single inverter, as is shown in Figure 2.6. In this configuration all branches operate at the same voltage, which may not be the MPP voltage for all of them [13].

If the branches are receiving different irradiations (due to partial shading or other problems), the true MPP is difficult to find and consequently there are power losses.

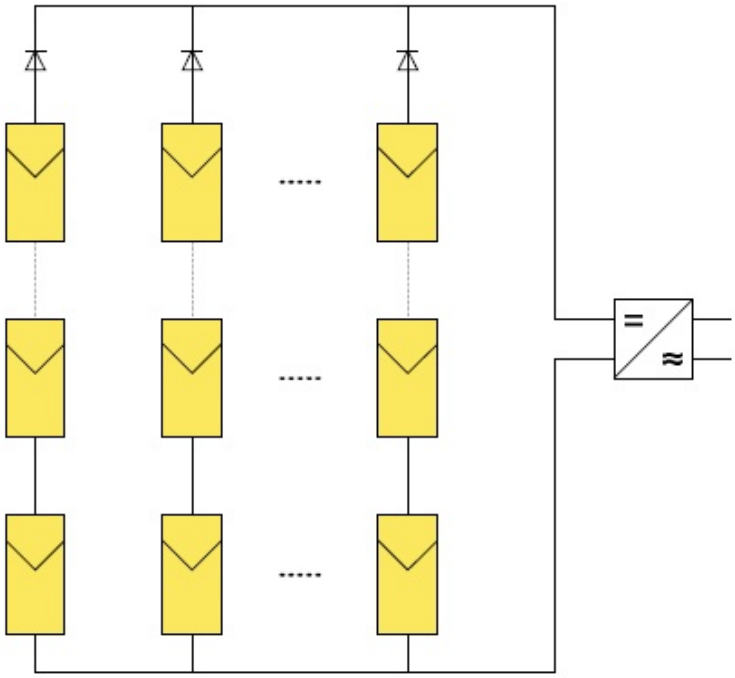

Figure 2.6: Central inverter configuration.

2.6.2 String Inverter

In this configuration, every branch of PV panels connected in series is connected to a different inverter, as can be seen in Figure 2.7. This can improve the MPP tracking because each branch can operate at a different MPP if necessary, whereas in the central inverter there is only one operating point which may not be the MPP for each branch, thus leading to power losses. On the other hand, the number of components of the system increases as well as the installation cost, as an inverter is used for each branch. [13]

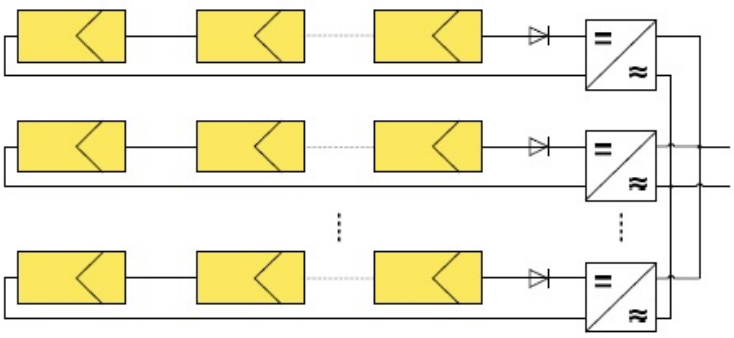

Figure 2.7: String inverter configuration.

2.6.3 Multi-string Inverter

In this configuration, each branch is connected to a different DC to DC converter which is in charge of the MPP tracking of the branch and the converters are connected to a single inverter, as depicted in Figure 2.8. The advantages related to MPP tracking are the same as in the string configuration, as each branch can have a different MPP. [13]

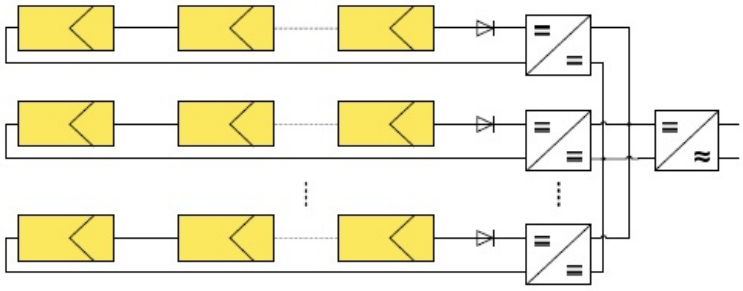

Figure 2.8: Multi-string inverter configuration.

2.6.4 Module Integrated Inverter

In this configuration,as shown in Figure 2.9, each PV module in a branch is connected to a different inverter and consequently the maximum power is obtained from each panel as the individual MPP is tracked by each inverter. This configuration can be used when the differences in the operating point of the different modules are large. However, it is more expensive because each panel has its own inverter. [13]

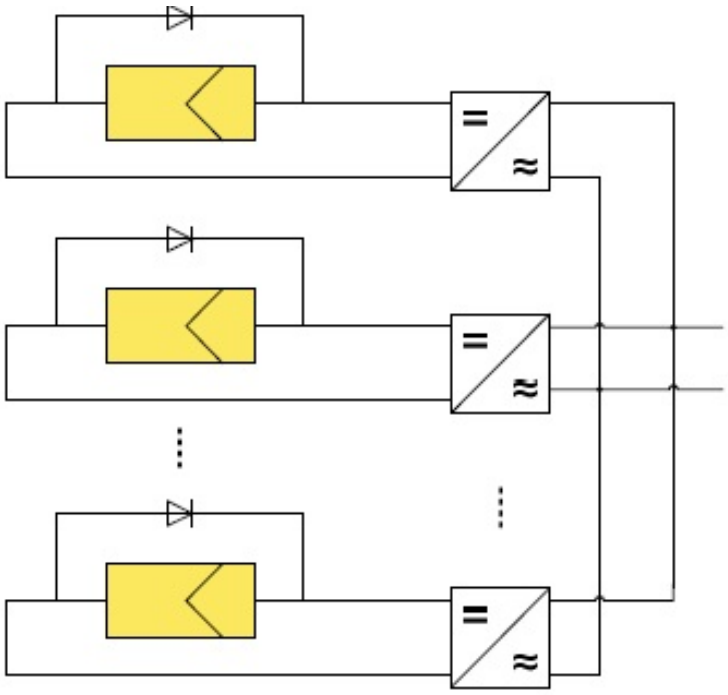

Figure 2.9: Module integrated inverter configuration.

2.7 Maximum Power Point Tracking Algorithms

2.7.1 Perturb and Observe

This technique involves varying the duty cycle of the power converter and thus varying the opertaing voltage in the link between the PV array and the power converter [10]. The sign of the last change and the sign of last increment in the power are then used to decide what the next variation of duty cycle should be.

In Figure 2.10, on the left of the MPP, incrementing the voltage increases the power whereas on the right, incrementing the voltage decreases the power. If there is an increment in the power, the perturbation should be kept in the same direction and if the power decreases, then the next perturbation should be in the opposite direction. The process is repeated until the MPP is reached. A flowchart of this method is shown in Figure 2.11.

This technique has two drawbacks. Firstly, when the changes in the voltage and current

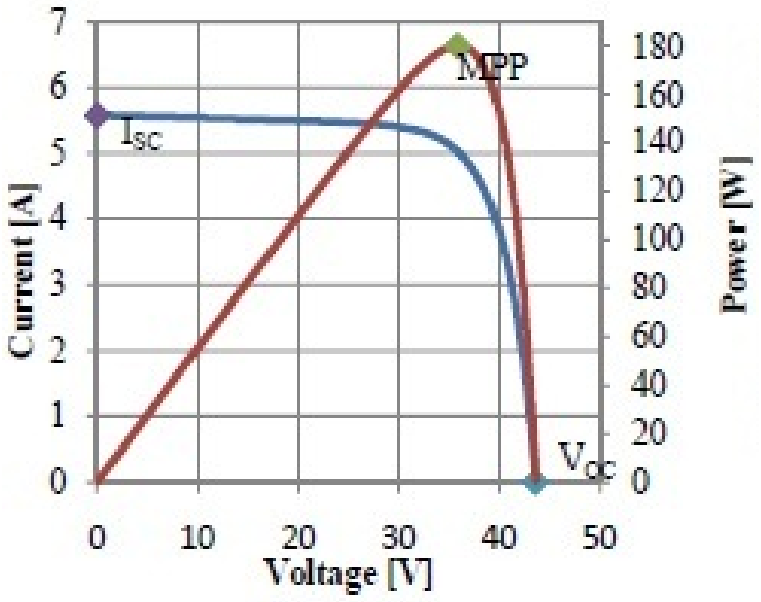

Figure 2.10: PV panel characteristic curves [21].

are not only due to the intentional variation of the voltage (like voltage change caused by change in irradiation) it is not possible for the algorithm to determine whether the change in the power is due to its own voltage increment or due to the change in the irradiation. Secondly, it experiences oscillations of voltage and current around the MPP due to the fact that the voltage and current are not constantly at the MPP but oscillating around it [25].

2.7.2 Incremental Conductance

The incremental conductance algorithm is based on the fact that the slope of the P-V (P-I) curve of the PV module is zero at the MPP, positive (negative) on the left of it and negative (positive) on the right, as can be seen in Figure 2.10. By comparing the increment in the power with the increment in the voltage (current) between two consecutives samples, the change in the MPP voltage can be determined. A flowchart of the algorithm is shown in Figure 2.12.

Like in the previous technique, this method has the drawback of experiencing oscillations of voltage and current around the MPP due to the fact that the voltage and current are not constantly at the MPP but oscillating around it.

2.7.3 Fractional Open Circuit Voltage

This method relies on the approximating a constant between voltage at the MPP and open circuit voltage as given in the following equation [26].

$$V_{MPP} \simeq \alpha_v \times V_{OC} \tag{2.15}$$

where

α_v is the Coefficient of Proportionality for Open Circuit Voltage.

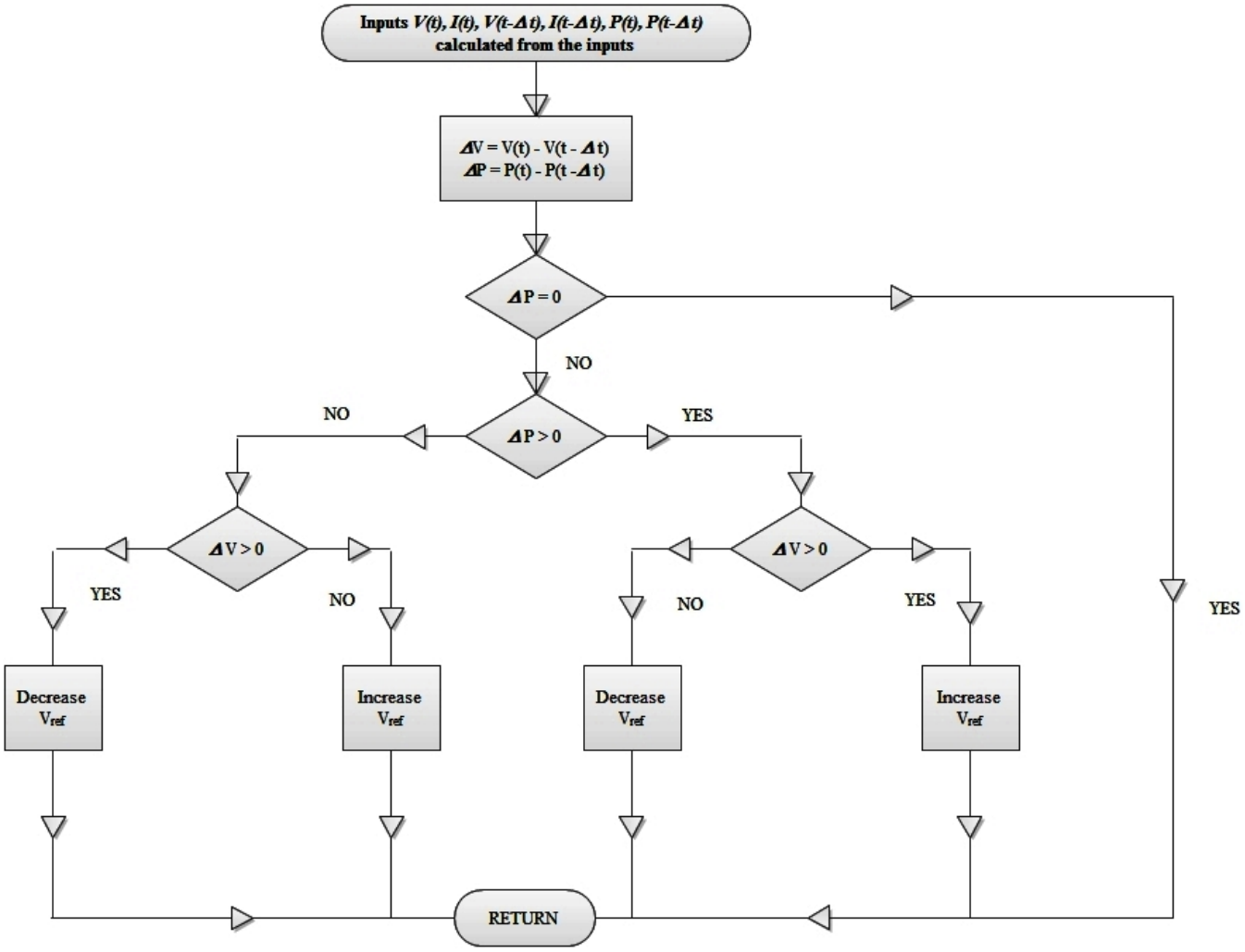

Figure 2.11: Flowchart of the P&O algorithm [10].

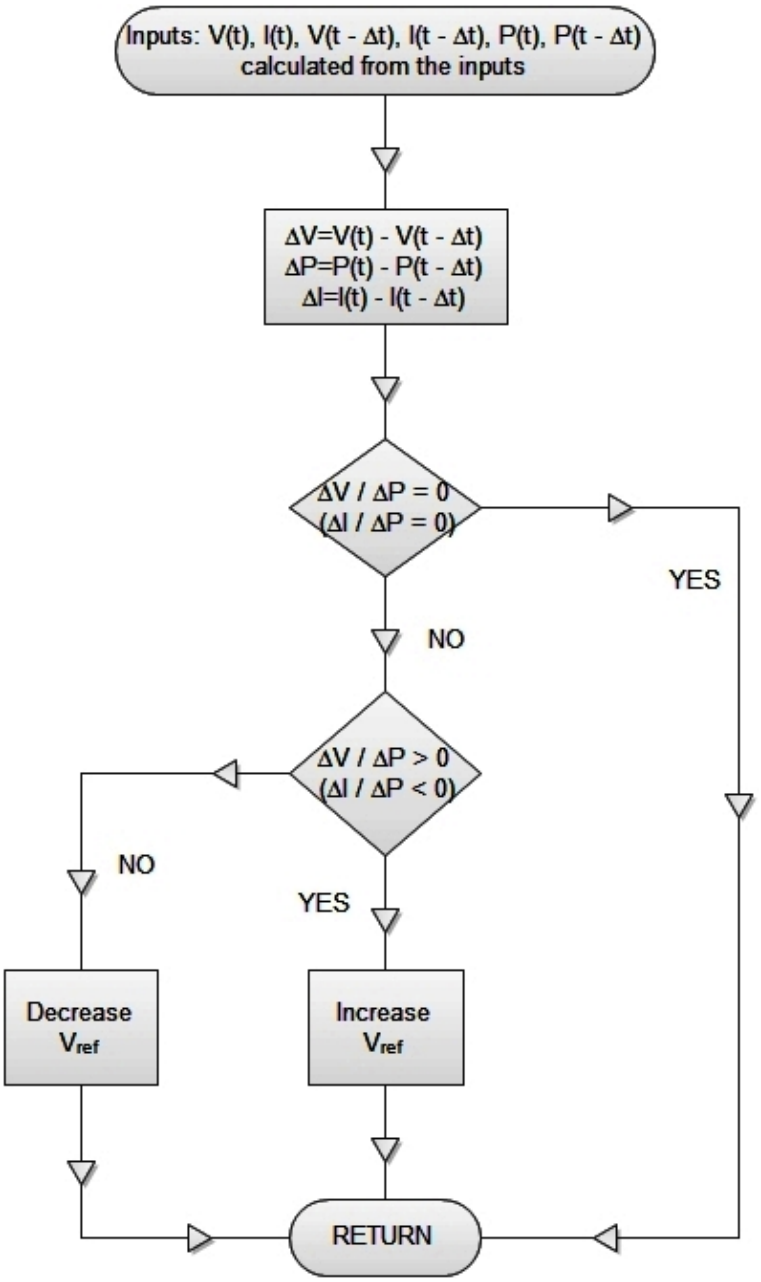

Figure 2.12: Flowchart of the Incremental Conductance algorithm [10].

The solar panel is temporarily separated from the converter and the open circuit voltage measured. The voltage at the MPP is then calculated using the above equation. α_v is a constant that depends on the characteristics of the PV array and it has to be determined beforehand by determining the voltage at MPP and voltage at open circuit for different levels of irradiation and different temperatures. According to Onat [26] the constant α_v is usually from 0.73 to 0.80.

The drawback of this technique is that to measure open circuit voltage, the power converter has to be shut down momentarily causing a loss of power in each measurement. The other drawback is that the MPP reached is not the real one because the relationship between voltage at the MPP and open circuit voltage is approximate.

2.7.4 Fractional Short Circuit Current

This method relies on approximating a constant between short circuit current and current at the MPP as given in the following equation [26].

$$I_{MPP} \simeq \alpha_i \times I_{SC} \tag{2.16}$$

where

α_i is the Coefficient of Proportionality for Short Circuit Current.

α_i has to be determined according to each PV array as in the previous method. To measure the short circuit current while the system is operating, an additional switch is added to the power converter to periodically short the PV array and measure the short circuit current. The current at the MPP is then determined using the above equation. According to Onat [26] the constant α_i is usually from 0.78 to 0.92.

As in the fractional open circuit voltage method, power from the converter has to be temporarily cut off to measure the short circuit current causing a loss of power during each measurement. The system also does not reach the real MPP because the relationship between current at the MPP and short circuit current is approximate.

2.7.5 Fuzzy Logic Control

The fuzzy logic control consists of three stages. Fuzzification, inference system and defuzzification. Fuzzification comprises the process of transforming numerical crisp inputs into linguistic variables based on the degree of membership to certain sets. Membership functions, like the ones in Figure 2.13, are used to associate a grade to each linguistic term. To improve the accuracy of the controller, the number of membership functions are

normaly varied and in some cases the membership functions are chosen less symmetric or even optimized for the application [10].

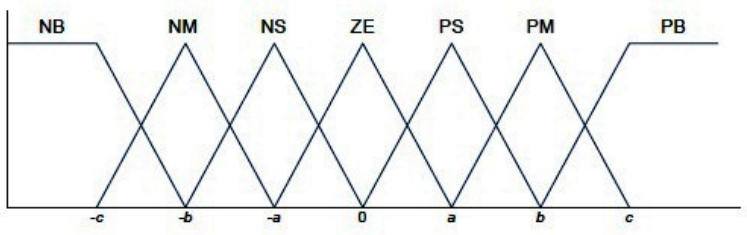

Figure 2.13: Membership functions

The inputs of the fuzzy controller are usually an error, E, and the change in the error,ΔE. The error can be chosen by the designer, but usually it is chosen as $\Delta P/\Delta V$ because it is zero at the MPP. Then E and ΔE are defined as follows:

$$E = \frac{P(k) - P(k-1)}{V(k) - V(k-1)} \tag{2.17}$$

$$\Delta E = E(k) - E(k-1) \tag{2.18}$$

The output of the fuzzy logic controller is usually a change in the duty ratio of the power converter, ΔD, or a change in the reference voltage, ΔV. The rule base, also known as rule base lookup table or fuzzy rule algorithm, associates the fuzzy output to the fuzzy inputs based on the power converter used and on the knowledge of the user. The rule base contains the fuzzy logic rules, which may be defined as the collection of conditional statements in the form: IF x is A THEN y is B. Fuzzy rules are therefore in the form of if-then rules and make us of Fuzzy descriptors (A and B in our case). In the last stage of the fuzzy logic control, defuzzification, the output is converted from a linguistic variable to a numerical crisp variable again using membership functions as those in Figure 2.13 usualy using the center of gravity method [27].

The disadvantage of the fuzzy logic control method is that the effectiveness of the controller depends a lot on the skills of the designer in not only on choosing the right error computation, but also in coming up with an appropriate rule base.

2.7.6 Neural Networks

The simplest example of a Neural Network (NN) has three layers called the input layer, hidden layer and output layer, as shown in Figure 2.14. More complicated NNs are built by adding more hidden layers. The number of layers and the number of nodes in each layer as well as the function used in each layer vary depending on the user knowledge. The input variables usually are parameters of the PV array such as V_{OC} and I_{SC}, atmospheric data as irradiation and temperature or a combination of these. The output is usually the duty cycle or the reference voltage.

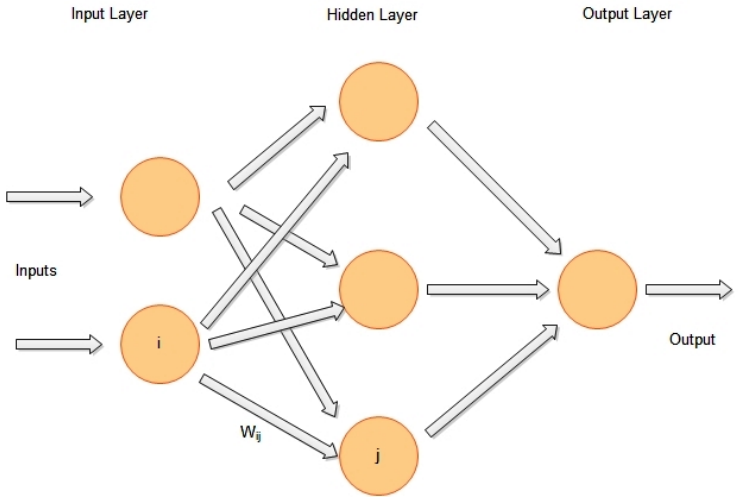

Figure 2.14: Structure of a neural network

The performance of the NN depends on the functions used by the hidden layer and how well the neural network has been trained. The links between the nodes are usually weighted. In Figure 2.14 the weight between the nodes i and j is labelled as W_{ij}. To train the NN, data of the patterns between inputs and outputs of the neural network are recorded over a period of time and used to adjust the weights [27].

The main disadvantage of this MPPT technique is that the data needed for the training process has to be specifically acquired for every PV array and location, as the characteristics of the PV array vary depending on the model and the atmospheric conditions vary depending on the location. Also, the neural network has to be periodically trained as these characteristics change with time [27].

2.8 Recent Work on MPPT Under Uniform Insolation

A research by Panda et al. [28] considered the maximum power point tracking of a PV module using a fuzzy logic controller under varying atmospheric conditions of irradiation and temperature. They analysed the performance by simulating the PV module along with the MPPT controller in MATLAB/Simulink software. They tracked the voltage, current and power at maximum power point first at varying irradiation and constant temperature of 25 degrees centigrade then at varying temperature and constant irradiation of 1000W/m^2. The simulation results demonstrated the peak power tracking capability of the proposed fuzzy logic scheme. It was also demonstrated that the fuzzy logic controller method improves the tracking performance as compared to the perturb and observe method. It was also determined that the fuzzy based MPPT controller reduced the maximum power tracking time by 88.18%.

A study by Elgharbi et al. [29] investigated the possibility of applying artificial neural networks (ANN) to extract the maximum power point of a photovoltaic generator feeding a motor-pump through a PWM inverter. The output of the ANN was set to be the optimal voltage which was compared to the PV generator voltage and then passed through an integrator to ascertain the stator frequency which is given to the PWM control of the inverter. Training of the ANN was accomplished by an algorithm developed by the authors and the whole training technique was simulated and studied using MATLAB software. Simulation studies were then carried out to verify the proposed artificial neural network method. The obtained results showed that the proposed approach could furnish a new interesting point of view in tracking the maximum power point of PV systems.

A study by Salhi and El-Bachtiri [30] investigated the use of a new maximum power point tracking system for photovoltaic applications by considering a photovoltaic panel system supplying a resistance load. For using the PV at optimal operating point, they used a DC/DC boost converter. This converter was controlled by a PI regulator. Synthesis of this regulator was achieved by using the Bode method. For the transfer function of the system, they used a small signal method for the step by step modelling. This enabled the global model to give off a system transfer function, with which they synthesized a suitable PI regulator for controlling the boost converter in order to get the system operating at the PV maximum power. A simulation study was made to illustrate the response of

the system to rapid temperature and solar irradiance changes. For this purpose, the irradiance and the temperature, which are initially 1000 W/square meter and 320.18 K, are switched at 0.3s and 0.7s, to 100 W/square meter and 260.18 K respectively and vice versa.

A research by Azab [31] proposed the use of a new maximum power point tracking algorithm for photovoltaic arrays. The major difference between the proposed algorithm and other techniques is that the proposed algorithm was used to control directly the power drawn from the PV. This was done by computing the maximum power and then directly controlling an ON/OFF power controller. The controller in turn controlled the operation of a buck chopper ensuring that the power drawn from the PV was set to the computed value. Previous methods attempted to reach the maximum point by the knowledge of the voltage or the current corresponding to that optimum point. The algorithm was then tested under various operating conditions and the obtained results have proved that the MPP could be tracked even under sudden changes in the level of irradiation.

2.9 Operation of PV Modules under Partial Shading

Due to low voltage and power ratings, PV cells are normally connected in series to form PV modules, which are the basic building blocks of a power generator. PV modules are further connected in series and/or parallel to increase the voltage and power levels of the whole PV power generator forming a PV array [14].

Partial shading refers to the instance when the operating conditions of the PV cells are not identical, such as when certain PV cells in a module receive lower than the nominal irradiation or when PV modules in a PV array receive lower than the nominal irradiation. [32]. Series connection of PV cells are prone to mismatch losses when they are not operating under uniform conditions due to partial shading [33]. In particular, the shaded cells produce lower current than the non shaded cells. If the current of the PV power generator is higher than the current of the shaded cell, the cell will be reverse biased due to other cells in the series connection. The shaded cell will then act as a load in the series connection dissipating part of the power generated by the other cells leading to power losses. These losses can lead to "hot-spot" heating in the shaded cell which can irreversibly damage the cell [34].

Under partial shading conditions, the PV characteristics become more complex with development of multiple peaks on the P-V curve. This makes MPP tracking more complicated because of the existence of local and global peaks [35]. The conventional MPPT algorithms described in Section 2.7 work well in detecting the MPP of a PV array when it is uniformly shaded. However under partial shading, they may converge to a local MPP of the array rather than the global one resulting in under-utilization of the PV array [12].

2.10 Recent Work on MPPT Under Partial Shading Conditions

Noguchi et. al. [36] proposed a new MPP tracking algorithm to track the MPP under partial shading conditions. The technique involved using an additional circuit to scan P-V curve, then inducing a "short current pulse" to determine the optimum operating current where the maximum output power was obtained by taking a product of the "short current pulse" and a parameter "r" since the optimum operating current was exactly proportional to the "short current pulse" under various conditions of irradiation and temperature.

Ahmed and Miyatake [37] proposed an improved Fibonacci search algorithm to realize a simple control system to track the real maximum power point even under non-uniform insolation conditions. The variable x was set as the voltage (current) of the PV array and the function f(x) was set as the output power. An initialization function was then introduced for initializing the search condition (when sudden or partial change in insolation is detected) and doing a wide search which led to the real maximum power.

Nguyen and Low [38] proposed a new MPPT algorithm to track the global peak of a partially shaded module by directly searching for the global peak on the P-V curve using a two mode dividing rectangles method. Once the direct search tracks the global peak, the method activates the P&O method to maintain the operating point at this global peak.

Mishima and Ohnishi [39] proposed a system that can control the output power of the array on a PV string basis, which contributes to a more efficient and simpler implemen-

tation of the PV power compensation system than that by individual controls of PV modules. The basic idea was to feed the bias voltage into the shaded PV string so that it generates the maximum power at the same operation voltage as the other blocks. A single partially shaded PV string was chosen by a selector and fed a bias voltage. If there occured partial shadings in more than one PV string, the bias voltage was controlled separately due to the fact that the shading level or pattern was not the same in all strings. This necessitated a different biasing voltage for each shading string. For this reason, if a complicated partial shading occurs, this method can-not be used.

Miyatake et. al. [40] proposed a line search algorithm in conjunction with a Fibonacci sequence to find the global MPP when the PV array is partially shaded. However, this approach did not guarantee global point tracking under all conditions. As an improvement to this, Kobayashi et. al. [41] proposed a two stage MPPT control process. The first stage used the concept of equivalent resistance being proportional to the ratio of open circuit voltage to short circuit current. The values of open circuit voltage and short circuit current were measured online and the system moved to a point referred to as the load line, calculated by this measured values. The second stage was then used to search for the global MPP. However, in this method, it was observed that if the global point lies on the left side of the load line, the operating point was shifted to 90% of open circuit voltage, hence missing the global peak.

Swathy and Archana [42] proposed a modified InCond algorithm to track the global peak. This involved using a controller that combines incremental conductance algorithm with the particle swarm optimization (PSO) technique. The PSO was initialized by defining the particle position as the duty cycle of the boost converter. The values of voltage and current were measured directly and the power calculated. Using this value of power, values known as Pbest and Gbest were updated by comparing the new power against the previous power. Then using these values, the duty cycle was updated. When the maximum number of iterations was met, the algorithm stopped and the Gbest solution was output.

The random numbers in the conventional PSO algorithm reduce the searching efficiency significantly. For example, during the search process, if a low valued random number is multiplied with the present information of control variable (voltage, current or duty cycle), only a small change in the velocity term of the PSO equation is obtained. This small perturbation may be insufficient to bring the operating point to near the desired

value. Consequently, further iterations need to be carried out and there is no guarantee that the random number in the subsequent iteration will track GP. To solve this, Ishaque and Salam [44] proposed a deterministic particle swarm optimization teachnique (DPSO) to improve the maximum power point (MPP) tracking capability for PV systems under partial shading conditions. The main idea was to remove the random number in the accelerations factor of the conventional PSO velocity equation. Additionally, the maximum change in velocity was restricted to a particular value obtained from the PV characteristics during partial shading.

Shankar and Mukherjee [12] proposed a hybrid PSO algorithm (HPSO) consisting of continous genetic algorithm (CGA) and particle swarm optimization (PSO) techniques to track the global peak of a partially shaded PV array.

Karatepe et. al. [43] proposed a power compensation strategy to overcome the problem of partial shading and obtain power more efficiently. This system was realized by using a chopper for each string as opposed to the PV module. The shaded modules are de-activated by forward biasing a corresponding bypass diode according to the shading level of the PV module. The bias voltage to be applied to each shaded PV module was set by ascertaining how many modules will be deactivated for each string. Particularly, the number of de-activated shaded modules was determined by monitoring and comparing the operating voltages of each PV module.

2.11 Summary of Review

From researches carried out, it can be seen that considerable effort has been put into tracking the maximum power point of photovoltaic modules under both uniform and partial shading conditions. However, this research has not been conclusively exhausted as there is still lacking MPPT techniques that are able to directly predict the occourence of the global peak of a partially shaded PV module under all conditions as most techniques have to make do with the disadvantage of having to scan the P-V curve. Further, the random numbers in the conventional PSO algorithm significantly reduce the efficiency thus further research is required to reduce the number of iterations and guarantee tracking of the global peak. As such, there is still work to be done to develop an optimal method. This research aims at using a modified P&O algorithm that combines a search algorithm with conventional P&O algorithm to track the global peak.

3. CHAPTER THREE METHODOLOGY

In this chapter, the Matlab/Simulink models employed in modelling the PV module and PV array are presented. The proposed two-tier technique for tracking the MPP under partial shading is presented in detail and the experimental process employed in validating the operation of the PV module is discussed together with the procedure used in experimentally evaluating the performance of the proposed technique under partial shading.

3.1 Modelling the PV Module Under Uniform and Partial Shading Conditions

To model the PV module, the current - voltage equation derived in Chapter 2 is employed. To generate the P-V, P-I and I-V charecteristic curves under uniform insolation, the voltage is varied from zero to open circuit voltage and corresponding values of current and power are obtained. For this purpose, the model of Figure 3.1 was developed. Some of the values of constants used in modelling were obtained from the PV modue datasheet. A complete documentation of the values of constants used in modelling are given in the Table 3.1. The PV module sub-block was modelled as shown in Figure 3.2.

To generate the P-V, P-I and I-V characteristic curves of a PV array under partial shading conditions, three PV modules were connected in series with the modules receiving different levels of irradiation (250, 500 and 100 W/m^2). The current through the three modules was then varied from zero to short circuit and values of voltage and power of the PV array obtained. The simulink model is as shown in Figure 3.3.

Table 3.1: Constants Used in Modelling the PV Module

Label	Description	Value
V_{PV}	Array Voltage	(V)
I_{PV}	Array Current	0→ 3.28 (A)
G	Solar Irradiance	W/m^2
T	Cell Temperature	$°K$
T_r	Reference Temperature	301.15 $°K$
A	Diode Ideality Factor	1.6 [18]
K	Boltzman Constant	1.3805e-23
q	Electron Charge	1.6e-16
R_S	Series Resistance of Cell	0
R_{SH}	Shunt Resistance of Cell	∞
I_{SCR}	PV Cell Short Circuit Current	3.28 (A) [45]
K_i	Short Circuit Temperature Co-efficient	0.060 (%/K) [45]
K_v	Open Circuit Temperature Co-efficient	-0.36 (%/K) [45]
I_{0r}	Saturation Current at T_r	2.0793e-6 (A) [45]
E_{g0}	Band Gap For Silicon	1.1 eV
N_S	No. of series cells in the array	36 [45]
N_P	No. of parallel cells in the array	1 [45]

3.2 Proposed Two-tier Algorithm and Simulation of the PV System

3.2.1 The Two-tier Algorithm

To solve the problem of tracking the local peak as opposed to the global peak, when presented with multiple peaks as is the case during partial shading, an algorithm that uses a two tier technique was proposed. The technique can be divided into two stages. The first stage, monitors the irradiance (G) and temperature (T) of the two PV arrays and plots the resultant P-I curves. It then approximates the GP using the variables of power and current. The second stage then locates the actual MPP of the characteristic curve, starting from the estimated point of the first stage.

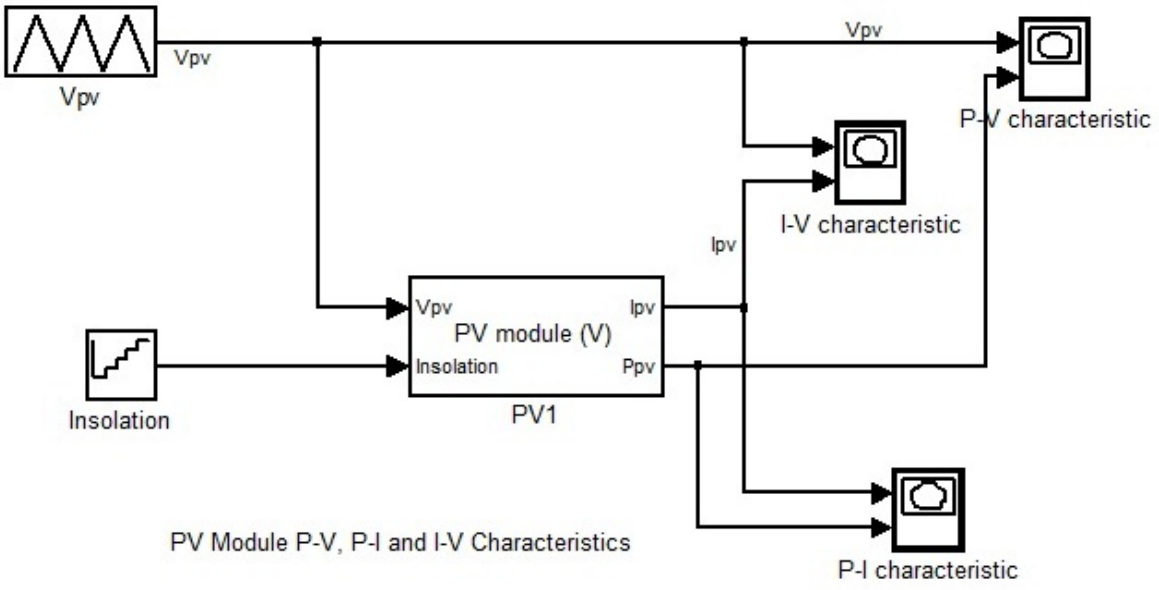

Figure 3.1: Model for simulating P-V, P-I and I-V characteristics under uniform insolation

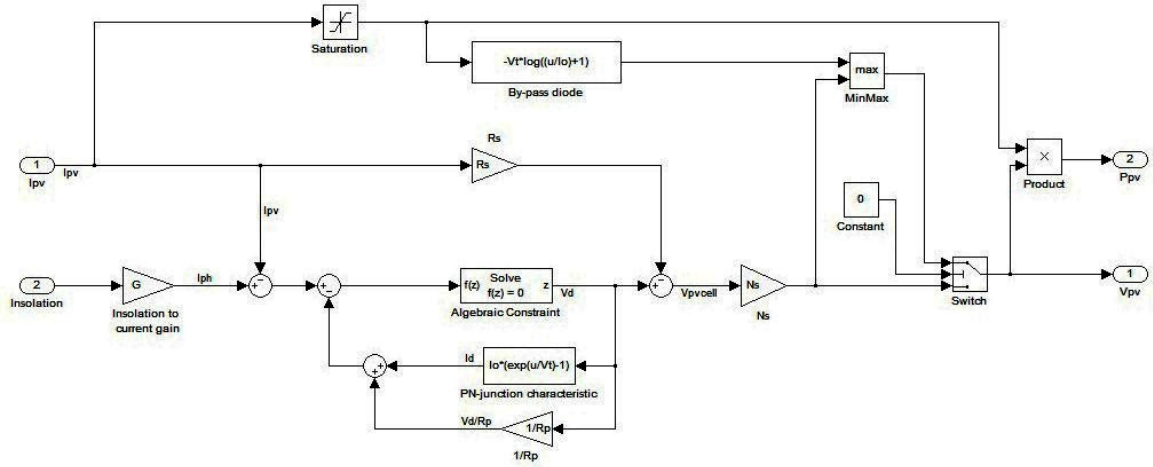

Figure 3.2: Sub model of the PV module block

In the first stage, a change in irradiance (ΔG) or temperature (ΔT) on the PV module automatically generates the P-I curve of the array and all the maxima are located. The approximate location of the global maximum is then determined so as to guide the controller in the general region of the GMPP. As would be expected, (ΔG) and (ΔT) are not constant and keep on varying. Thus, prior to running this stage, a change detection mechanism to determine if the change in irradiance or temperature was significant enough

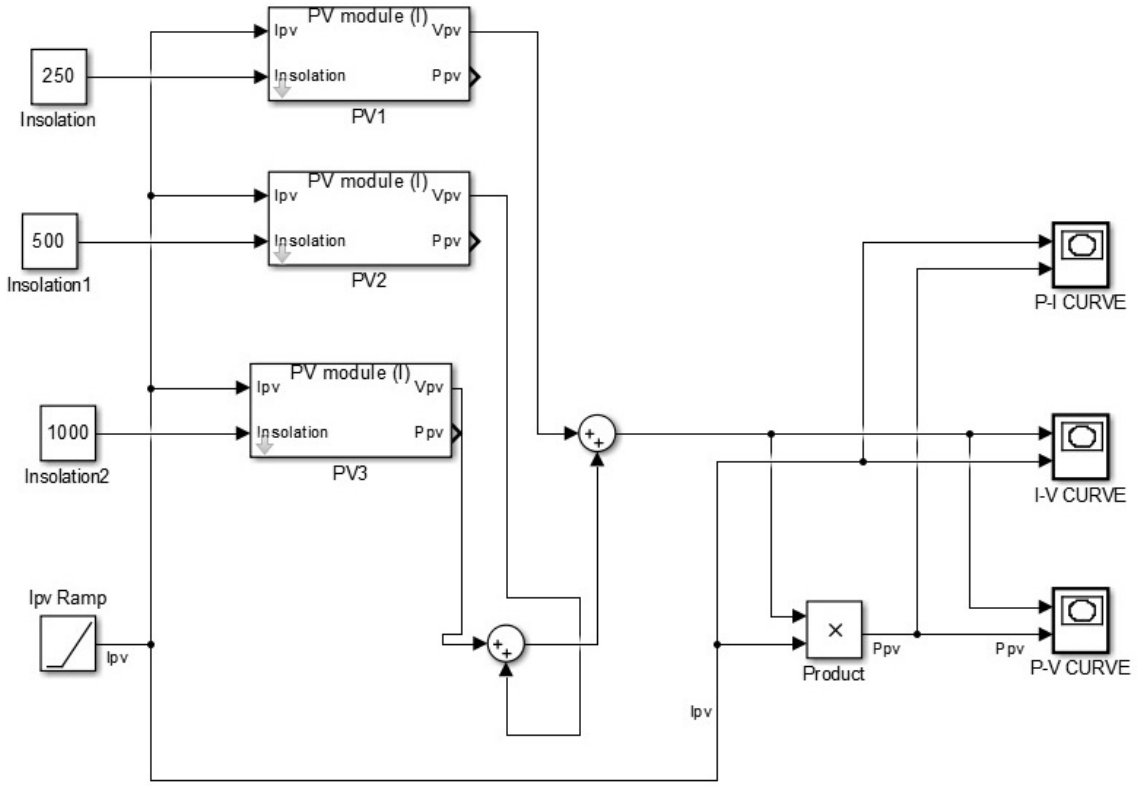

Figure 3.3: Model for simulating P-V, P-I and I-V characteristics under partial shading conditions

to cause a change in the GP was necessary. Change in these conditions above the set threshold would trigger generation of the P-I curve for the PV array and determination of the approximate GMPP (basically, the first stage to be executed). If the change is not significant, then the system would continue to execute the second stage without running the first stage since the assumption is that the change in these conditions is not significant to affect the arrangement of peaks on the P-I curve. Thus, the overall objective of the first stage is to determine the approximate location of the GP which serves as the starting point of the second stage. This serves to guide the escond stage as to which point to start tracking to GMPP and enables the controller to bypass any local maxima that would cause it to be trapped at the local peak, thus increasing the chances of tracking the global peak.

In the second stage, the estimated MPP from the first stage serves as the starting point for the second stage in tracking the global maximum. This starting point helps the controller bypass any local maxima that may cause the P&O algorithm to get stuck. Control is then passed to the conventional P&O algorithm that tracks the global maximum. A

flowchart of the proposed two-tier algorithm to solve the partial shading problem is shown in Figure 3.4 while the flowchart of the first tier of the algorithm is shown in Figure 3.5.

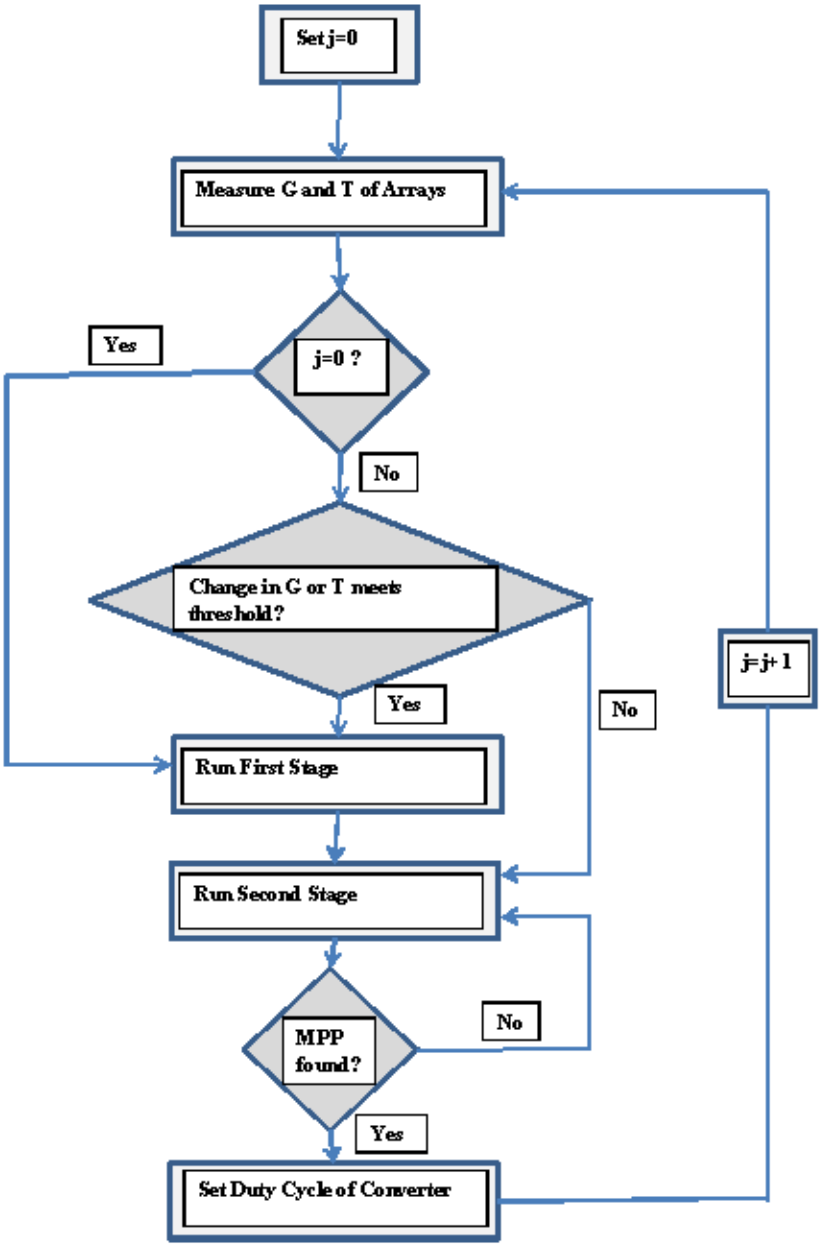

Figure 3.4: Flowchart of the proposed two-tier algorithm

To evaluate the simulated response of the proposed two-tier algorithm, the PV system comprising the PV array, First stage model, Second stage model and boost converter

are modelled in Matlab/Simulink. The output of the boost converter was connected to a battery, and as such, it was maintained at a certain, pre-determined DC level. The parameters of temperature and irradiance were varied to obtain the performance of the proposed technique and documented in Chapter 4 on a case by case basis.

The battery was modeled as a constant source of voltage in order to reduce the effects of its dynamics on the system. The boost converter was also modeled by its exact circuit, to negate the effect of its ripple current and voltage. It was also noted that the switching time of the converter did affect the simulation time of the whole process.

3.2.2 Modelling the PV Array

For this research, the central inverter grid photovoltaic configuration was employed due to its ease of implementation and its reduced cost of actual implementation. The model of the PV module takes the temperature (T), irradiance (G) and PV array current (I_{PV}) as inputs and gives the PV array voltage (V_{PV}) as output. The simulink model of the PV Array with two series connected modules is as shown in Figure 3.6.

In the above model, the inputs to each of the PV modules is the temperature and irradiance (G1, T1, G2 and T2). The voltage output of each of the module is then added together to generate the PV array voltage. This PV array voltage is multiplied by the PV array current to obtain the PV array power. The PV module is modelled as an embedded matlab function that has input variables of current, irradiance and temperature. The current is varied from 0 to 3.28 (short circuit current) for a given level of irradiance and temperature and the function gives an output of PV module voltage.h

3.2.3 Modelling the Boost Converter

The boost converter boosts up a dc voltage and is common in MPPT applications where the maximum voltage that the PV module is capable of producing is less than the required DC voltage. In the particular application applying to this thesis, the maximum voltage that the PV module is capable of producing is 40V while the required voltage is 48V thus necessitating the use of boost converter as opposed to the Buck or Buck-Boost converters. The circuit of the boost converter is shown in Figure 3.7.

It is desirable that the conversion in the converter be made with low losses. Therefore, the transistor is operated as a switch using a control signal delivered to the switch, which is held high for a time t_{on} and low for a time t_{off}; with the sum total of the time $t_{on}+t_{off}$ being equal to the switching period T_s of the transistor, which is held constant.

The duty cycle, D, is a real value in the interval 0 to 1 and it is equal to the ratio of the width of a pulse to the switching period. That is, $D = \frac{t_{on}}{t_{on}+t_{off}} = \frac{t_{on}}{T_s}$.

From Figure 3.7, when the switch S is on, the inductor current builds up and energy is stored in the inductor since D is off. When the switch is turned off, the inductor (now acting as a source) and the input voltage source both feed the load through the diode and charge the capacitor.

For this study, the boost converter was modelled in its exact circuit as opposed to modelling it as an ideal converter. To achieve this, the design equations of the boost converter given below [46] were used to select the values of the capcitor and inductor required.

$$I_{LB} = \frac{V_0}{2Lf} D\,(1-D) \tag{3.1}$$

$$\Delta V_0 = \frac{V_0 D T_S}{RC} \tag{3.2}$$

The main input-output equation assuming a lossless converter, is shown in Equation (3.3)

$$\frac{I_0}{I_{in}} = \frac{V_{in}}{V_0} = \frac{1}{1-D} \tag{3.3}$$

From the KL050 data sheet [45], the input voltage range (V_{in}) is between 5V and 40V; while the maximum value of PV array current is (I_L) =3.28A. The value of the desired voltage ripple (ΔV_0) is below 2V.

Re-arranging Equation (3.3), the value of the duty cycle, D, can be calculated for the various values of V_{in} , given that in this case, the value of V_0 is constant.

$$D = 1 - \frac{V_0}{V_{in}} \tag{3.4}$$

For V_0 =48V, then, for V_{in} =5V, D=0.896; and forV_{in} =40V, D=0.16667

Equation (3.1) can be re-arranged as follows.

$$L = \frac{V_0}{2fI_{LB}} D\,(1 - D) \tag{3.5}$$

For f=10KHz and I_{LB} =3.28A, then L=68.183 μH.

Equation (3.2) can be re-arranged as follows.

$$C = \frac{V_0 D T_S}{R \Delta V_0} = \frac{I_0 D T_S}{\Delta V_0} \tag{3.6}$$

because $V_0/R = I_0 S$, and $T_S/R = 1/f_S$, then C=15.23 μF

Thus, for operating in the continuous conduction mode, a vaule of L >68.183μH was needed, since this is the boundary between continuous and discontinuous conduction modes. The value of L=22 mH was used in simulation because it was readily available. To achieve a maximum output ripple of 2V, a value of C>15.23μF was needed. A value of C=220 μF was chosen for the same reasons. Using these values of inductance and capacitance, the boost converter was modelled as shown in Figure 3.8.

3.2.4 Modelling the First Stage of Proposed MPPT System

The first stage of the proposed two-tier technique can be modeled as three main parts, referred to as blocks in this thesis. The first block detects the percentage change of irradiance and temperature of the two PV modules (i.e. the four values of G1, T1, G2, and T2) and generates the P-I curve of the PV array, the second block contains the search algorithm and the third block generates the duty cycle.

The percentage change detection and P-I curve generation block detects changes in the values of G1, T1, G2 and T2. The detections are then connected to an OR gate so that if any of the values changes by a certain percentage, then a pulse is generated. Once the pulse is received, the counter counts from 0 to 328, which is then divided by 100 to get 3.28 (as will be shown in the counter sub-block). This value of 3.28 represents

the maximum current that can be drawn from the PV modules, thus the output of the counter is the PV array current varying from 0 to 3.28A. The voltage of the two modules are calculated within this range and then added to determine the PV array voltage.

The simulink model of the percentage change detection and P-I curve generation block is as shown in the Figure 3.9 while Figures 3.10 and 3.11 show the model of the counter sub-block and change detection sub-block respectively.

In the global peak search algorithm block, the P-I curve can have only two peaks since the model contains only two PV arrays. One of these will be the local maximum while the other will be the global maximum. Each peak has the associated value of power and current, that is to say, each peak will have an MPP and using the same analogy, one peak will be the local MPP while the other will be the global MPP. The algorithm searches for the first peak and stores the associated value of current and power. It also searches for the second peak and similarly stores its associated value of current and power. The value of the power at the global maximum is found using the max function. This value of power is compared to the value of power stored for the second peak. If they are equal, then the second peak is the global MPP otherwise the first peak is the global MPP. The simulink model of this block is as shown in Figure 3.12. Figures 3.13 and 3.14 show the simulink models of the first peak detection and second peak detection sub-blocks.

In the duty cycle implemntation block, Equation (3.3) is used to determine the value of the duty cycle with V_0 as the voltage that should be fed to the battery (48V in our case) and V_{in} as the voltage from the PV array (obtained by adding up the voltages of each of the PV modules).

The simulink model of this block is as shown in Figure 3.15.

3.2.5 Modelling the Second Stage of Proposed MPPT System

The duty cycle from the first stage is fed to the converter. This necessitates a delay before the second stage is run to give the system time to settle. The second stage searches for the real MPP commencing with the region generated by the first stage. The simulink model of the second stage is as shown in Figure 3.16.

As mentioned, a delay in running the second stage is necessary. The delay chosen before running the model is 5ms. The input variables needed for the second stage is the duty cycle set from the first stage so as to decide on whether to increment or decrement the duty cycle based on the current duty cycle. The values of the current and previous values of power and voltage are needed as well.

3.3 Experimental Validation of the MPPT System

For data collection, The Sunshine Solar AP-PM-20 solar panel was used. The module has a maximum power output of 20 W and a 20.5 V open-cuircuit voltage at an irradiation of 1000 W/m^2 at 25 °C.

The configuration of the experimental set-up adopted and pictorial configuration of the experimental set-up are shown in Figure 3.17 and Figure 3.18, respectively. Data collection using the above set-up was done on a clear sunny day. A clear sunny day was chosen to ensure a constant solar irradiation was available since the cuircuit does not include ways of measuring the solar irradiation level.

The complete set-up used in data collection consists of the PV module, the DC-DC converter, the microcontroller, the laptop computer and a user defined software for data collection. This set-up was achieved by connecting the input side of the DC-DC converter to the PV array and the output side to the load. The microcontroller was then connected to the set-up through the voltage and current sensing circuitry. This circuitry enabled the collection of values of voltage and current at certain time intervals as programmed in the microcontroller. These values of voltage and current were then sent to the laptop computer connected to the set-up via a USB data cable and logged into a software created by the author for purposes of this experiment. The purpose of the software was primarily to log the data values of voltage and current collected by the microcontroller. From these values, the value of power was calculated in an excel sheet and the variation of power for a certain period of time (the main output of the experimental process) was then plotted.

The switch used for the DC-DC converter was tested separately to ensure it's switching period worked effectively to turn on and off for the converter to function optimumly. The circuit used to test the switch is shown in Figure 3.19.

The sensing cuircuitry (used to sense the voltage and current) and interface of the user defined software are shown in Figure 3.20 and Figure 3.21, respectively.

To validate the accuracy of the PV model, experimental measurements of electrical characteristics of the PV module were carried out and compared with the simulated characterstics of the PV module.To achieve this, the system load was varied from short circuit to open circuit while values of current and voltage were being taken. Values of PV array power were then generated from these values of current and voltage obtained. The values obtained were then used to generate the P-V, P-I and I-V experimental characteristic curves, which were then compared to those attained through simulation. In the experimental implementation of the proposed two-tier algorithm, the measurement procedure may be considered as two main parts. Firstly, the values of voltage and current were monitored and then the variation of power with time plotted when the P&O algorithm was primarily used to track the MPP of the partially shaded PV array. Secondly, The proposed algorithm was then implemented in the microcontroller and again the values of voltage and current monitored with the output being the variation of array power for a certain time interval. The variation of power for the two instances was then compared to determine the effectiveness of the proposed algorithm to experimentally track the GMPP under partial shading conditions.

3.4 Summary

In this chapter the modified P&O algorithm offered as a solution to mitigate the effect of partial shading on PV arrays has been presented in detail. It involves a two-tier technique in which these stages have been discussed. The system models employed to achieve modelling of the PV module, PV array, the boost converter and both stages of the proposed MPPT algorithm in Matlab/Simulink have also been presented in detail. The experimental set-up required to validate the accuracy of the models and evaluate the effectiveness of the proposed MPPT algorithm in tracking the MPP under partial shading has also been presented, including the ciruitry used to test the working of the switch used in the DC-DC converter.

An important note is that, to investigate the effect of partial shading in tracking the maximum power point with the Perturb and Observe and the proposed maximum power point tracking algorithm, simulations were performed under time-variant conditions. The respective models were simulated in order to determine a data set consisting of the expected global maximum power and the achieved/tracked maximum power under different values of solar irradiation. The global maximum power during the simulation at each run was recorded for comparison with the achieved/tracked global maximum power.

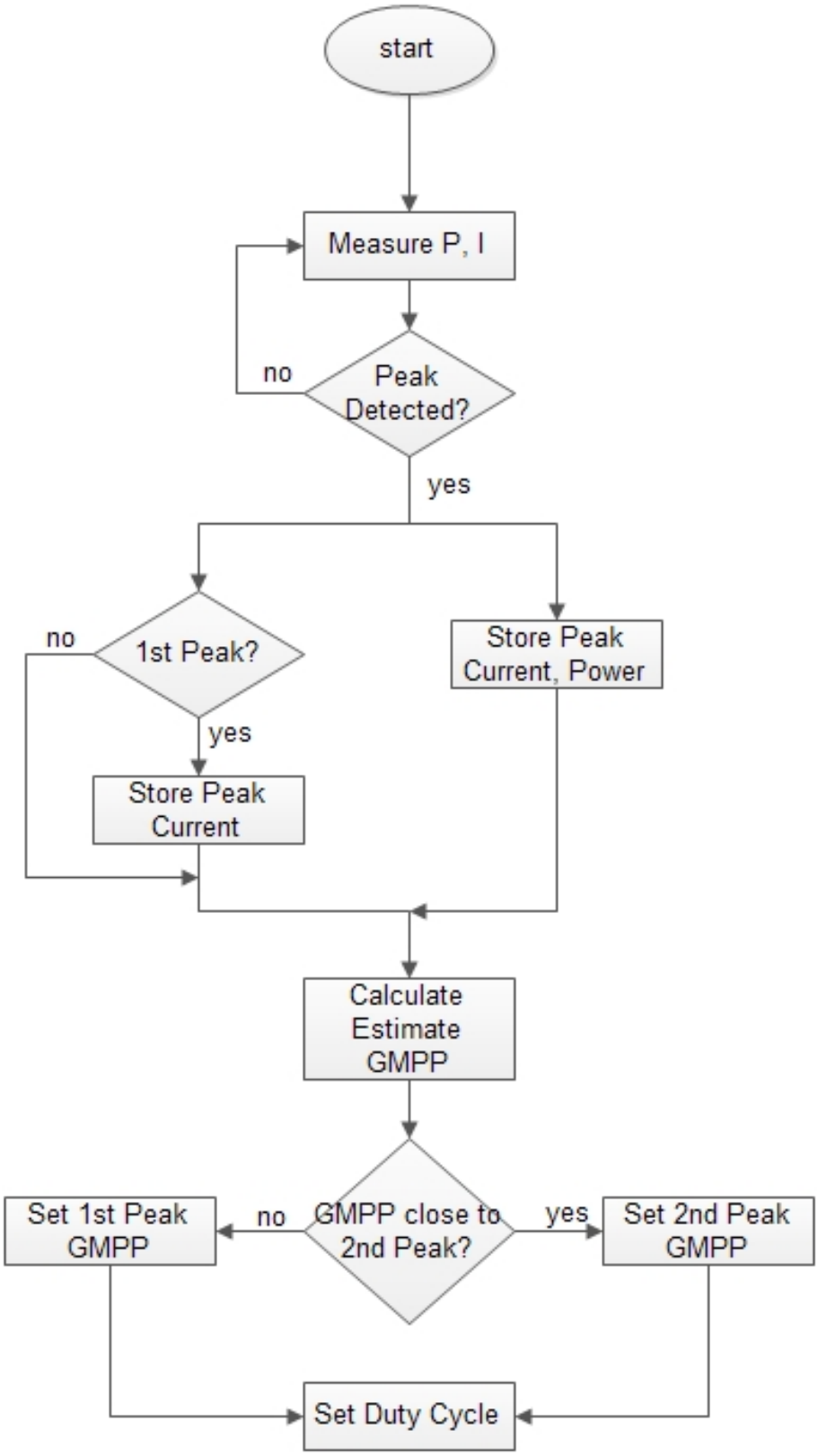

Figure 3.5: Flowchart of the 1st stage

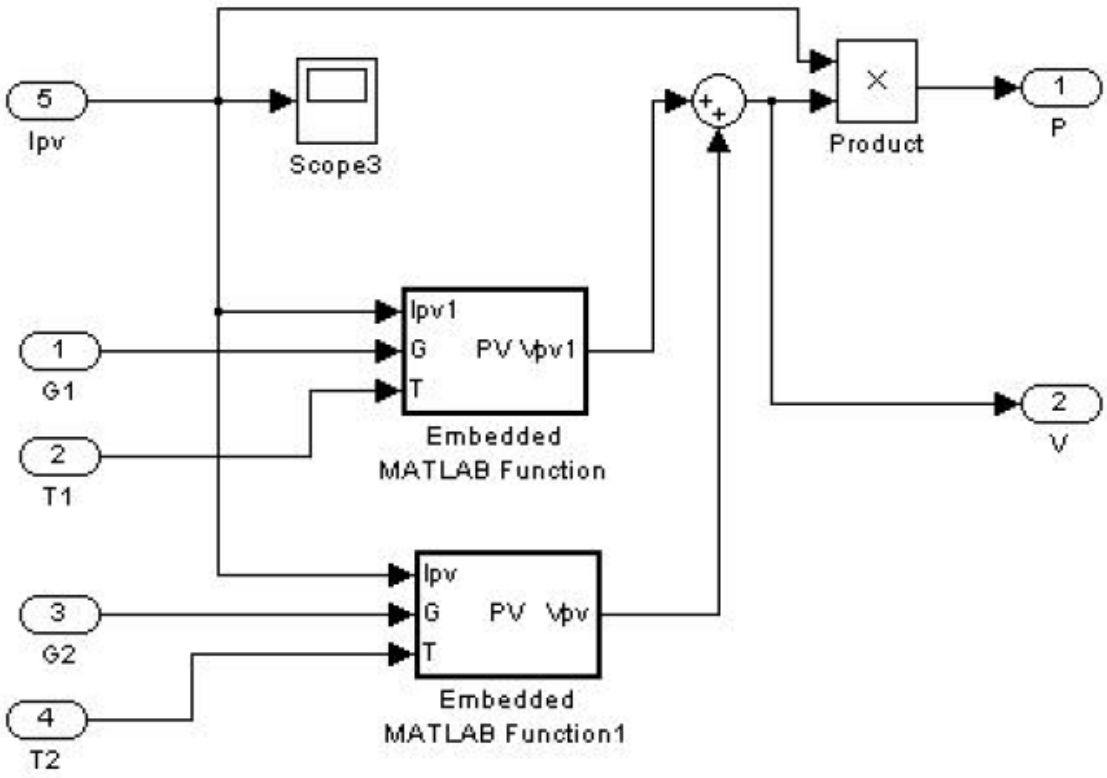

Figure 3.6: Model of the PV array

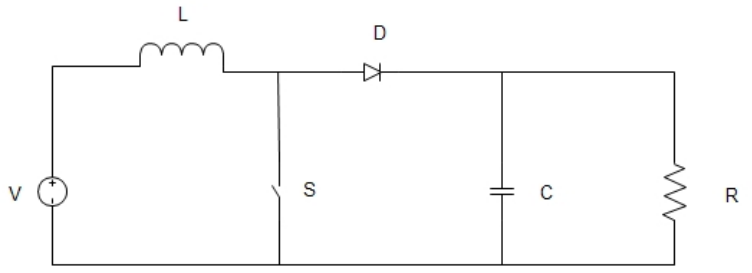

Figure 3.7: Schematic of boost converter

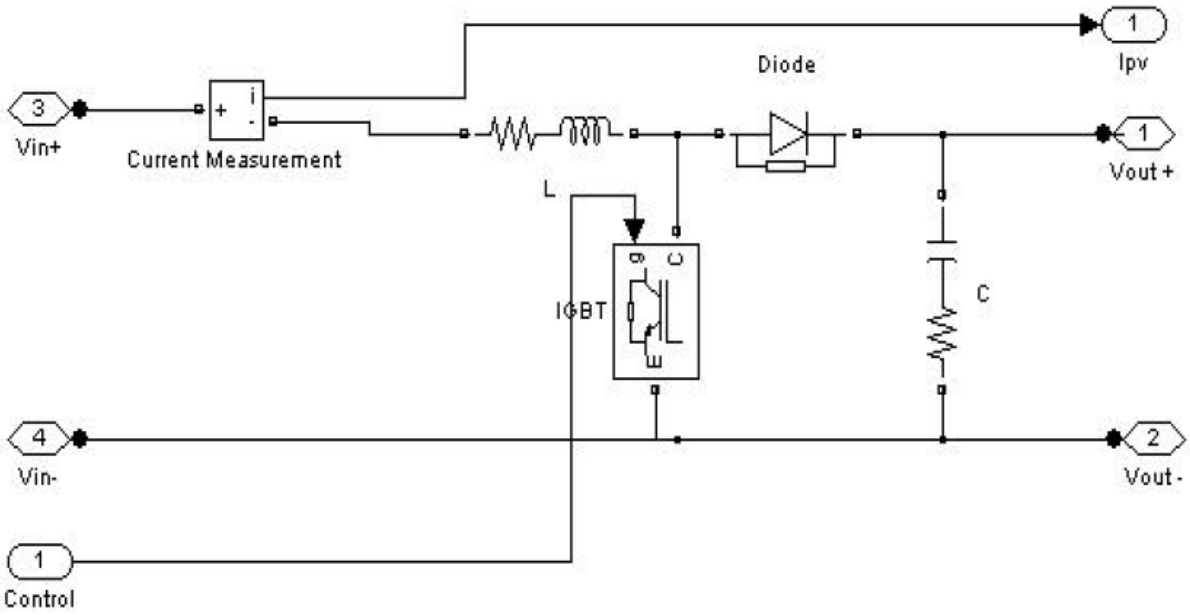

Figure 3.8: Model of the boost converter

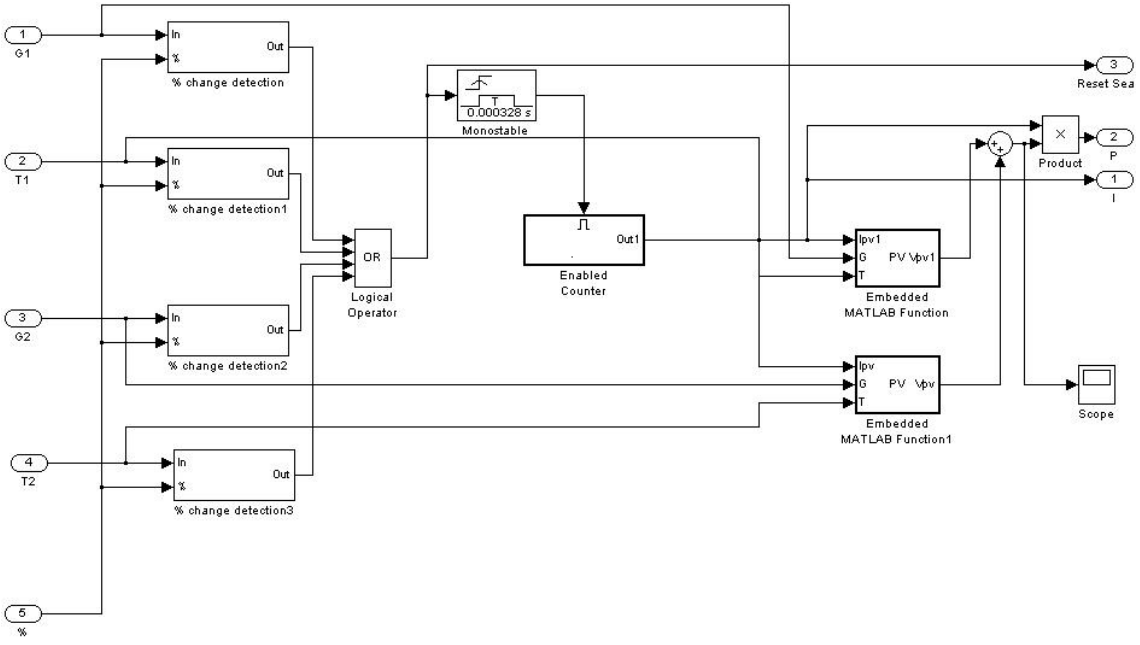

Figure 3.9: Model of percentage change detection and P-I curve generation block

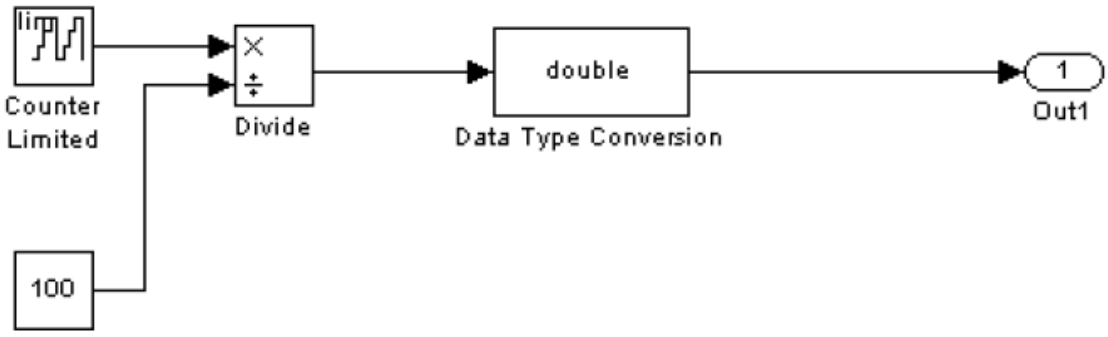

Figure 3.10: Model of counter sub-block

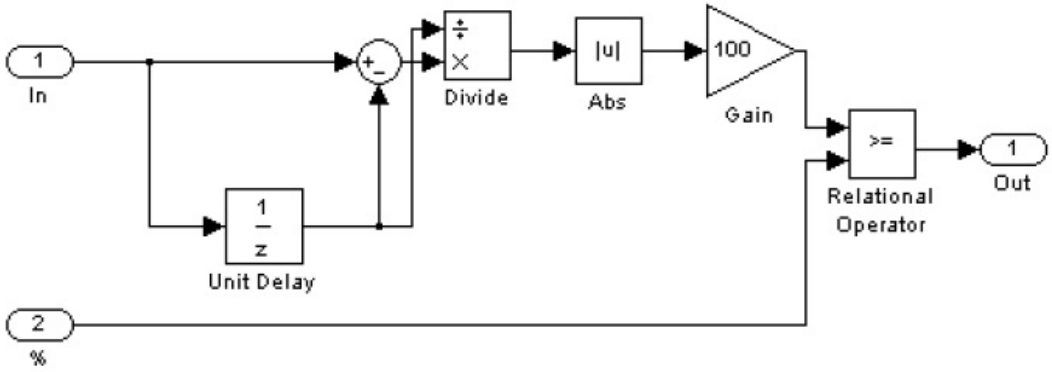

Figure 3.11: Model of change detection sub-block

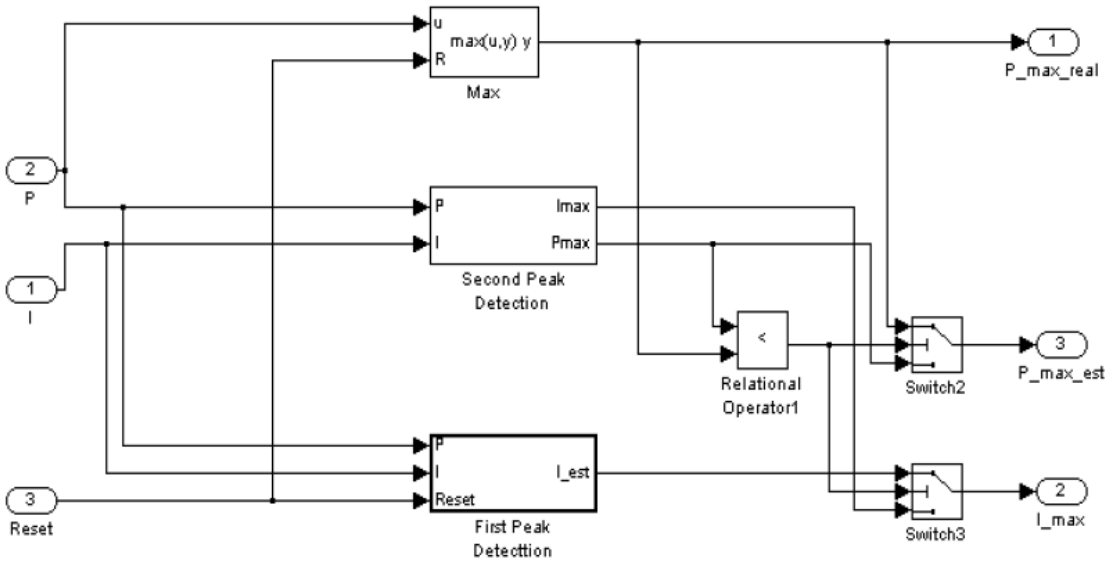

Figure 3.12: Model of the global peak search algorithm block

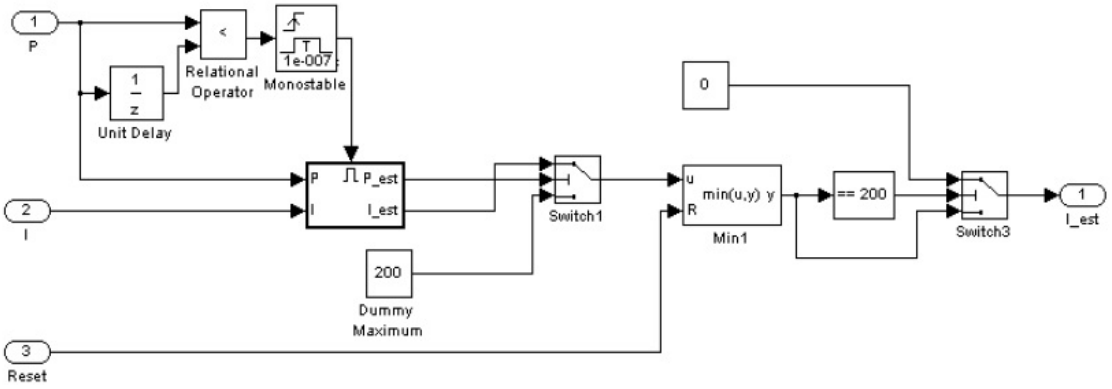

Figure 3.13: Model of the first peak detection sub-block

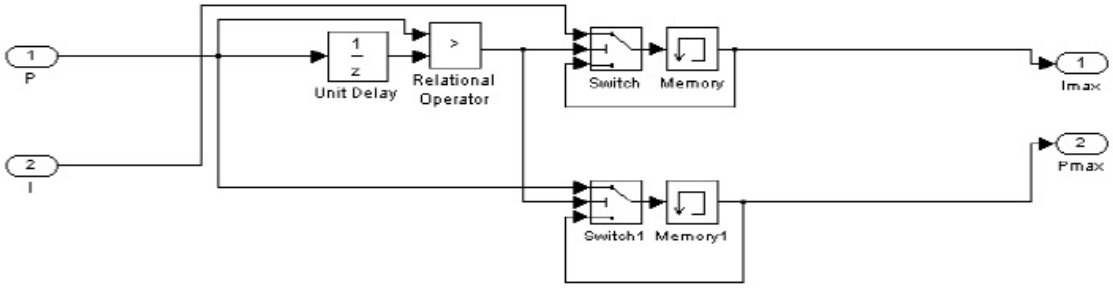

Figure 3.14: Model of the second peak detection sub-block

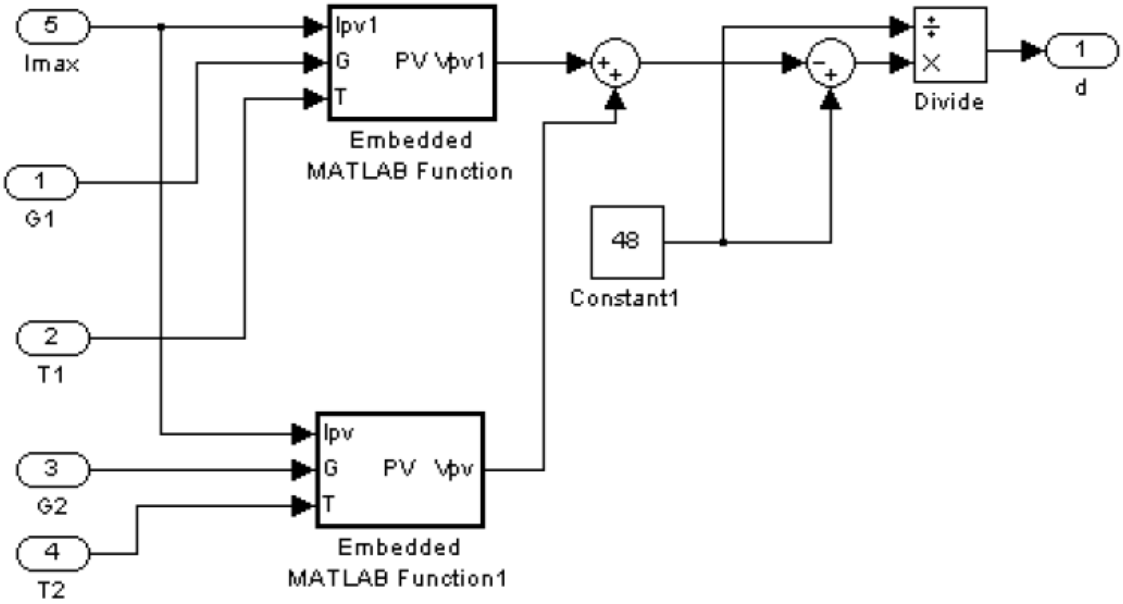

Figure 3.15: Model of the duty cycle implementation block

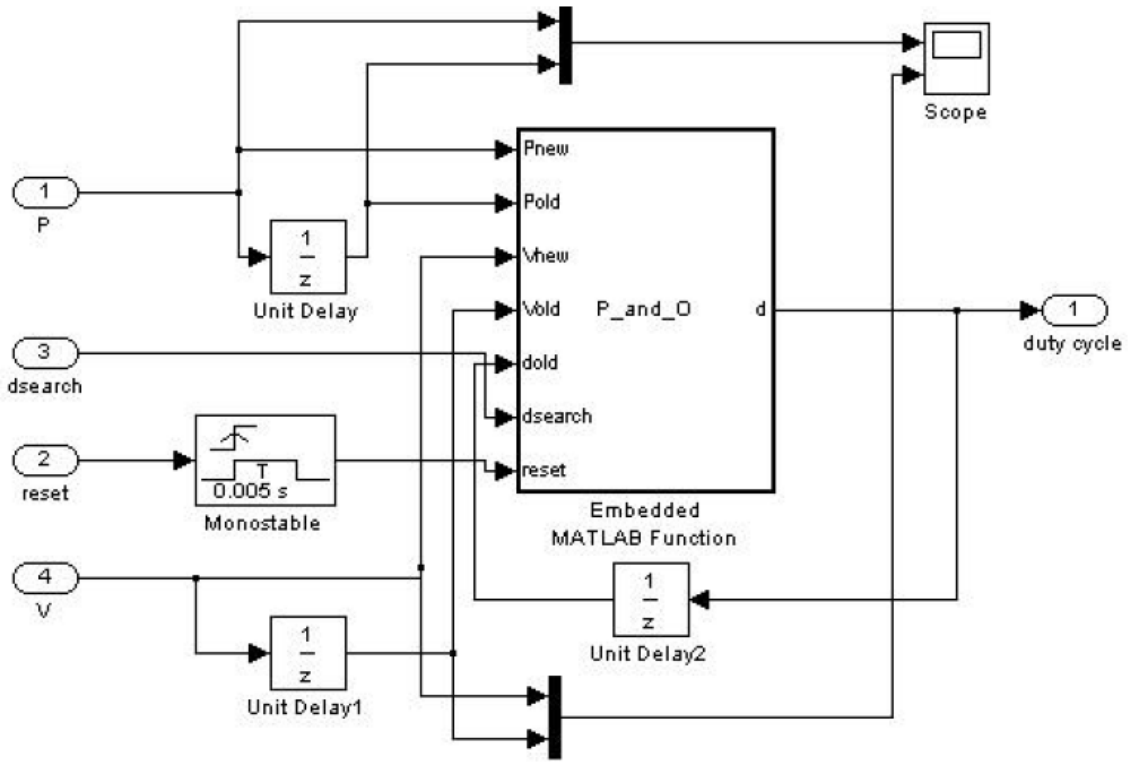

Figure 3.16: Model of the second stage of the MPPT system

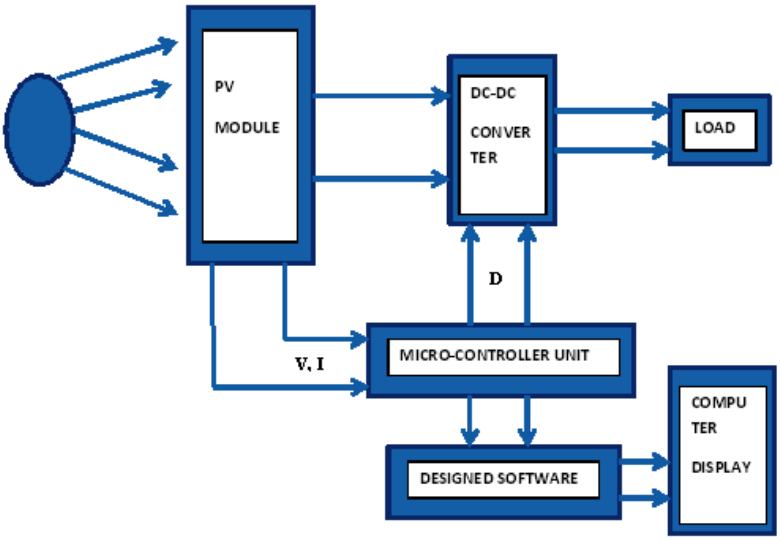

Figure 3.17: Configuration of experimental set-up

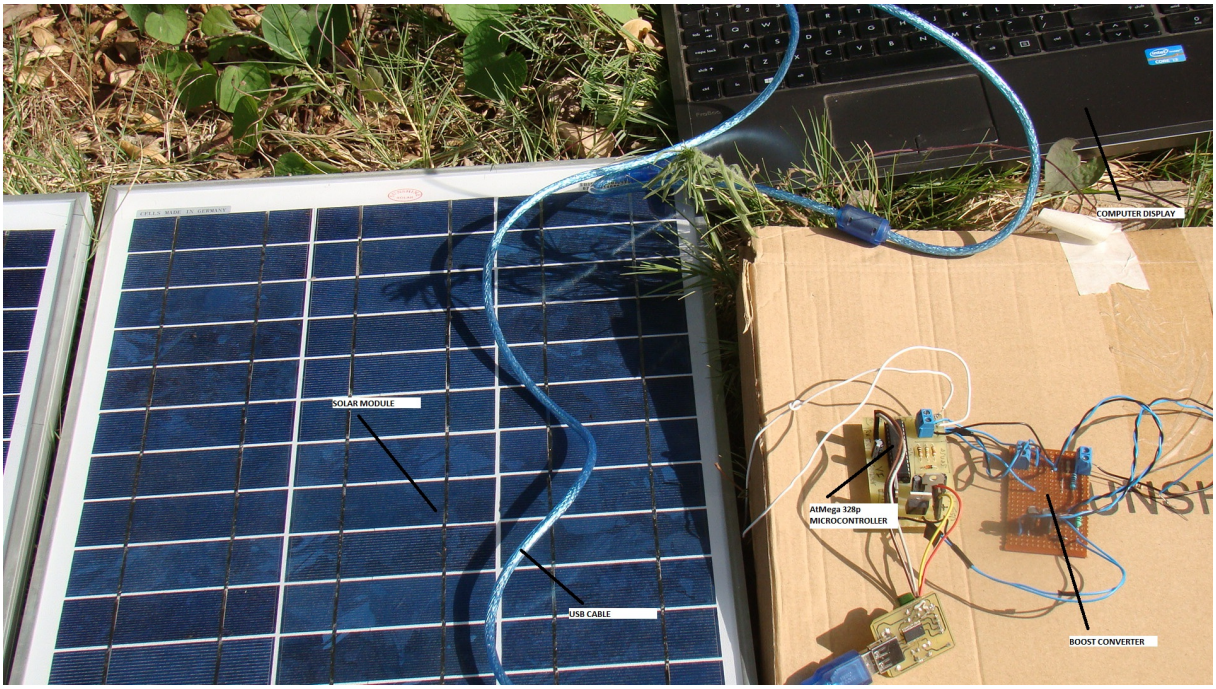

Figure 3.18: Pictorial configuration of experimental set-up

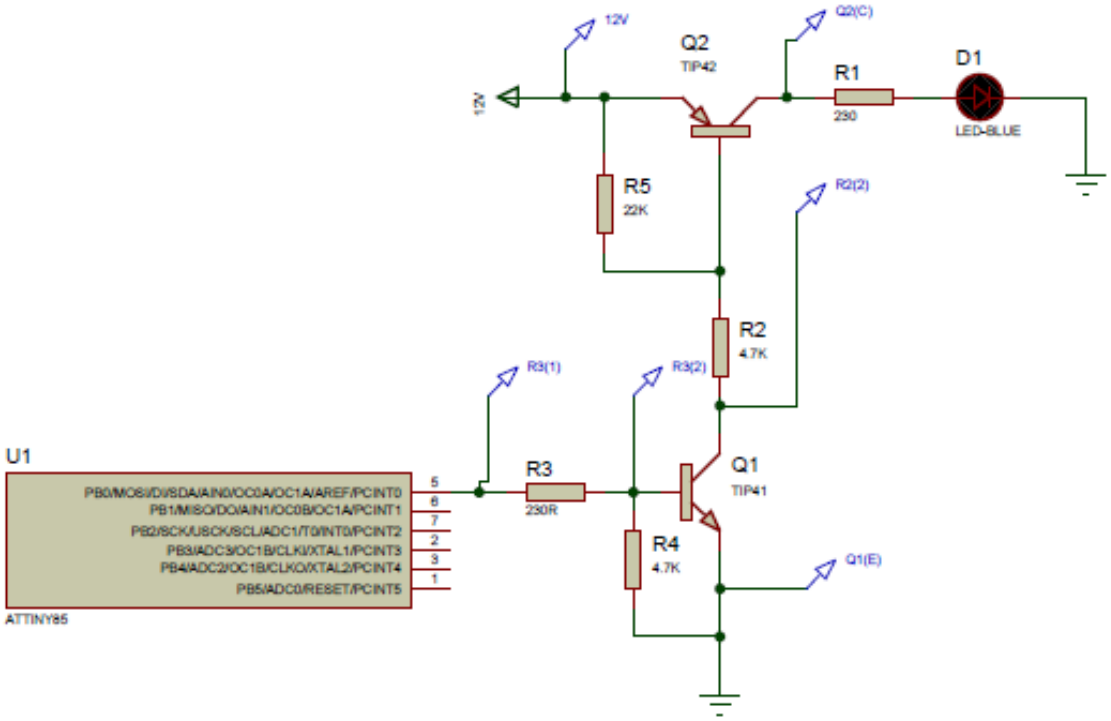

Figure 3.19: Switch test circuit

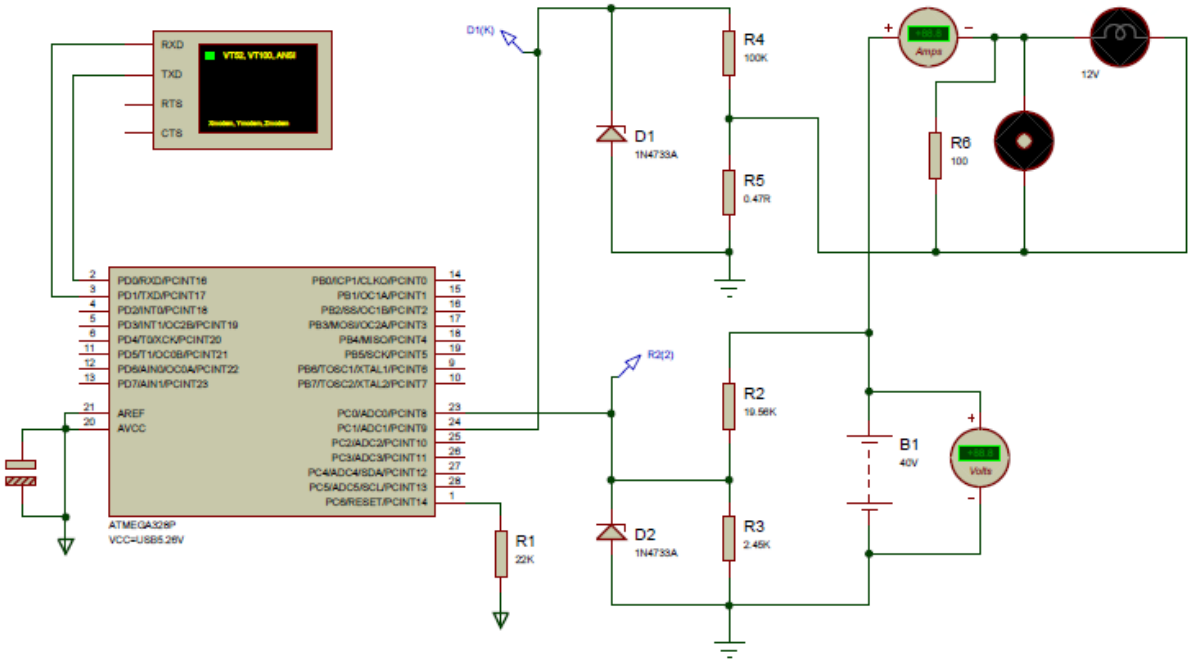

Figure 3.20: Voltage-current sensing circuit

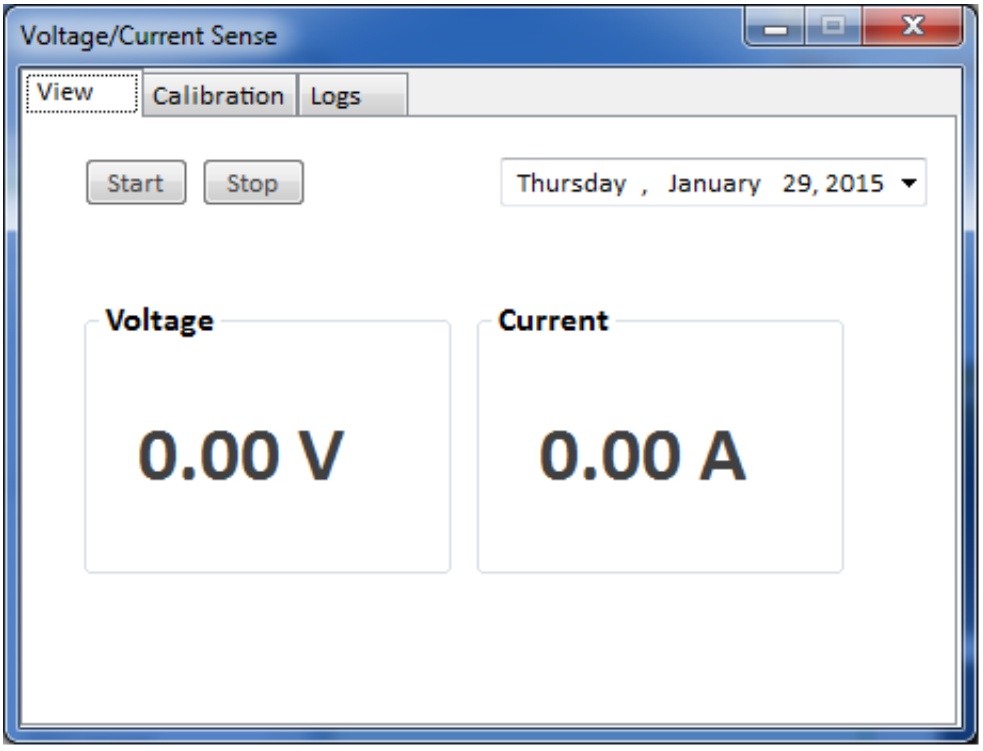

Figure 3.21: GUI interface of the user defined software

4. CHAPTER FOUR
RESULTS AND DISCUSSIONS

4.1 Overview

This chapter presents results of the running the PV module model to generate simulated electrical characteristics under uniform insolation, the PV array model to generate simulated electrical characteristics under partial shading, the MPPT system model incoporating the conventional P&O algorithm to generate the simulated electrical characteristic of PV array power and finally the MPPT system model incoporating the proposed solution to partial shading to genrate the simulated electrical characteristic of PV array power. Experimental results to validate the accuracy of the model and evaluate the effectiveness of the proposed solution in tracking the MPP under partial shading are also presented. In particular, a computer was used for data acquisition and storage, as well as display and analysis of the results obtained.

4.2 P-V, P-I and I-V Curves

To investigate the effect of partial shading on PV array charactersistics, the simulations in the following section were carried out on the PV module model under uniform insolation and the PV array model under varying insolation. The conditions under which the simulations were carried out are also presented.

4.2.1 P-V, P-I and I-V Curves Under Uniform Insolation

This section presents the standard P-V, I-V and P-I curves of a PV module under uniform insolation. On a clear sunny day, this insolation is at 1000 W/m^2. Thus, the insolation used in the simulation was set at this value. The P-V, I-V and P-I curves under uniform insolation for a PV module are shown in Figures 4.1, 4.2 and 4.3 respectively.

From Figure 4.1, it can be observed that the curve has two important points being displayed. These are, the maximum power point (MPP) where maximum power is generated

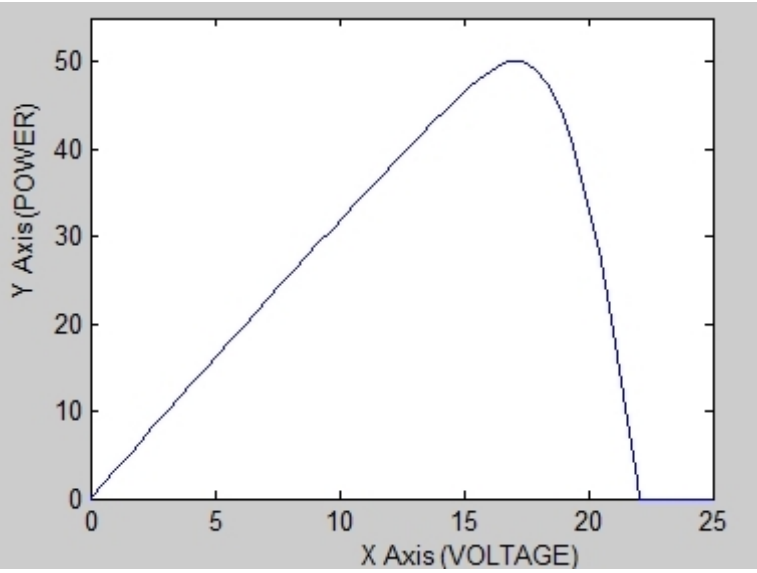

Figure 4.1: P-V graph of a module under uniform insolation

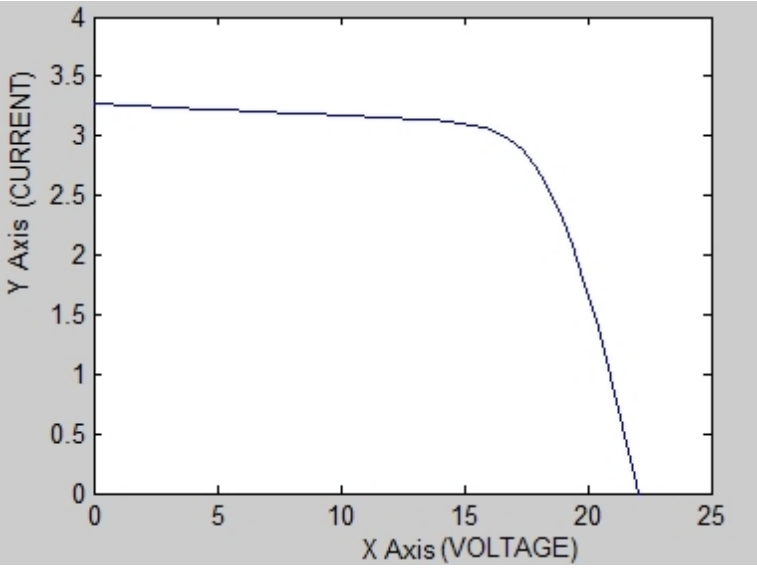

Figure 4.2: I-V graph of a module under uniform insolation

from the PV module and open circuit voltage (OCV), at which point, no power will be generated by the PV module. Similarly, from Figure 4.2, it can be observed that the curve has three important points being displayed. These are, the maximum power point (MPP) where maximum power is generated from the PV module, short circuit current (SCC) and open circuit voltage (OCV), at which point, no power will be generated by the PV module. From Figure 4.3, it can be observed that the curve has two important points being displayed. These are, the maximum power point (MPP) where maximum

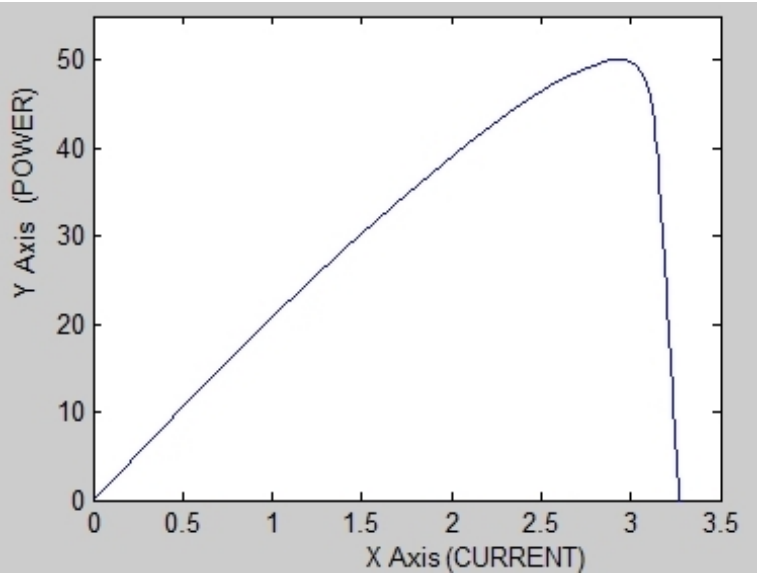

Figure 4.3: P-I graph of a module under uniform insolation

power is generated from the PV module and short circuit current (SCC), at which point, no power will be generated by the PV module.

It was also noted that though the P-V and P-I curves are different, they have a similar trend, where power gradually increases from zero to a certain point when it starts to decrease to a value of zero. A fundamental difference between the two curves is that the power decreases more gradually in the P-V curve as compared to the rapid decrease in power on the P-I curve. This can be explained by the fact that even though a given change in insolation causes an increase in the values of voltage and current, there is a much greater increase in current as compared to the voltage.

4.2.2 P-V, I-V Curves Under Partial Shading Conditions

Under partial shading conditions, the PV array does not receive uniform insolation, with the PV modules receiving different insolation due to the shading. Thus for this simulation, the three PV modules constituting the PV array were set to receive different insolation levels of 1000 W/m^2, 500 W/m^2 and 250 W/m^2. The P-V, I-V and P-I curves under partial shading conditions for the PV array are as shown in Figures 4.4, Figure 4.5 and Figure 4.6 repsectively.

From Figures 4.4, 4.5 and 4.6, it was noted that the P-V, I-V and P-I characterstic curves

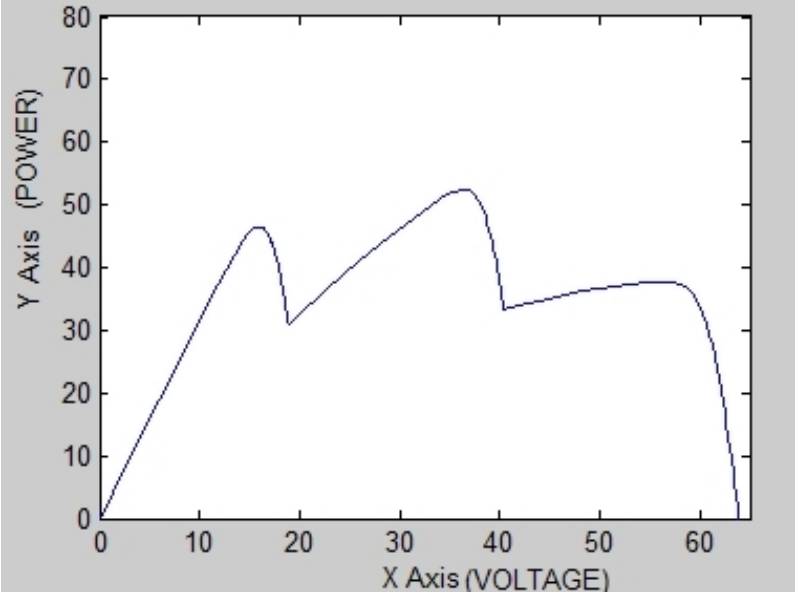

Figure 4.4: P-V graph of a array under partial shading

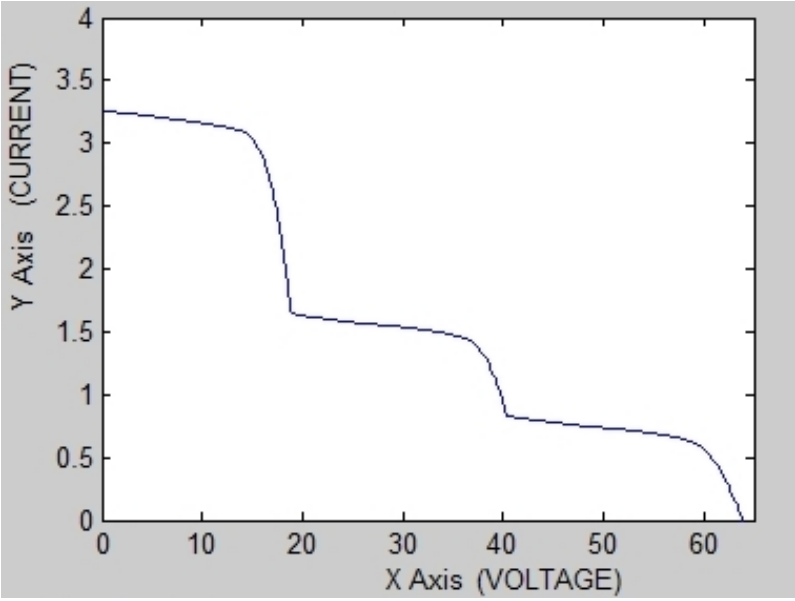

Figure 4.5: I-V graph of a array under partial shading

under partial shading conditions differ from those obtained under uniform insolation. In particular, the P-V and P-I curves develop multiple peaks with one peak being the global maximum and the other peaks being the local maxima. It can also be noted that each of these peaks has a maximum power point (MPP). In this thesis, that of the global maximum will be reffered to as global MPP or GMPP or global peak, while that of the local maxima will be reffered to as local MPP or local peak. The I-V curve as well

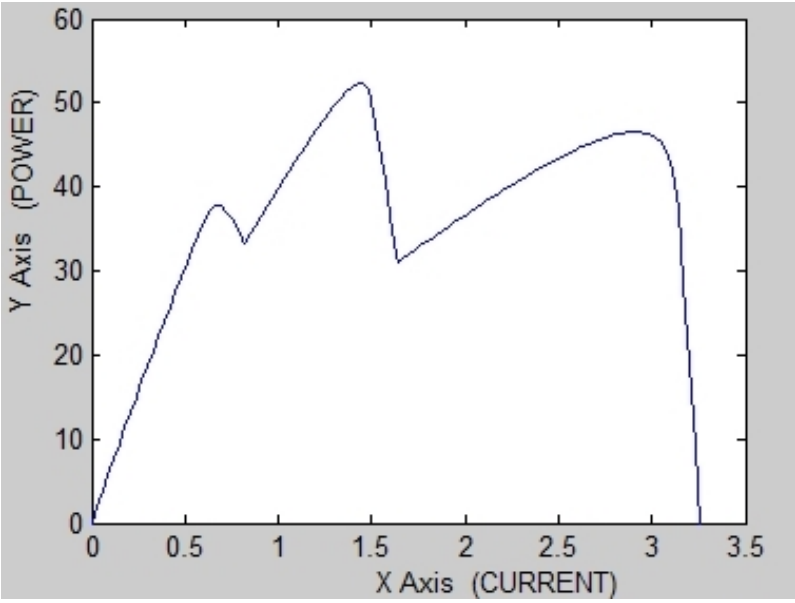

Figure 4.6: P-I graph of array under partial shading

develops multiple steps as compared to that obtained during uniform insolation. This can be explained by the fact that the different levels of irradiation incident on the PV array cause a comensurate level of peaks to develop on the characteristic curves. As such, three different levels of irradiation on the PV modules in the array would cause the formation of three peaks on the characteristic curves.

Also from Figures 4.4 and 4.5, it can be noted that the first peak occours at 14 V, the second peak (which happens to be the global peak) occurs at 35 V and the third peak occours at 58 V. The first peak occours at voltage $V_1 = 9 \times 1.72V = 15.48V$, where 1.72 is 8% of the open circuit voltage $V_{OC} = 21.5V$, of the module. A similar analogy can be applied to the other two peaks, which occour at $V_2 = 20 \times 1.72V = 34.5V$ and $V_3 = 34 \times 1.72V = 58.48V$, respectively. A significant outcome of this observation is that power peaks are displaced from each other by a multiple of 8% of V_{OC} of the PV module. That is; $(n \times 0.08 \times V_{OC})$

From the results, it was observed that the magnitude of the global peak and the voltage at which it occours is not only dependent on insolation at that particular instance but also on the shading pattern across the solar cells. Thus, the value at which the global peak accours varies and is not constant. It was also noted that the number of peaks that are observed in the P-V, P-I and I-V curves under partial shading conditions are directly related to the different levels of irradiation incident on the PV array. This is to

imply that if two values of irradiation are incident on the PV array, then only two peaks develop while if three values of irradiation are incident on the PV array, then only three peaks develop as in the simulations above.

4.3 MPP Tracking of the PV System With Pertub and Observe Algorithm

The simulations in the following section were carried out on the modelled PV system under both uniform insolation and partial shading conditions, with the P&O algorithm being primarily used to track the MPP of the system. The solver used is "ode23s stiff/-Mod. Rosenbrock, which is used with the power systems toolbox. Different scenarios were considered as presented below.

4.3.1 Temporary Trapping at a Local Peak

The irradiance and temperature changes for this run are shown in Figure 4.7 while the P-I curves of the PV arrays for every 0.02s are shown in Figure 4.8.

As can be seen in Figure 4.8, there are five curves (A, B, C, D and E), with each curve generated after 20ms such that curve A is generated within the first 20ms of simulation, curve B is generated in the subsequent 20ms of simulation and so on till curve E is generated. Curves A and E having multiple peaks as a result of the solar module is experiencing partial shading during the period of generation of these curves, while curves B, C and D having just one peak as a result of the solar module is experiencing uniform insolation during the period of generation of these curves. This could be explained by the fact that from Figure 4.19 in curves A and E, the iradiation incident on the array during this period of simulation causes the two modules to receive different levels of irradiation. While in curves B, C and D, the irradiation incident on the modules in the array is equal.

Table 4.1 shows the theoretical values of the power, voltage and current at MPP and the actual value of the MPP tracked by the P&O while the waveform of the PV array power against time are shown in Figure 4.9.

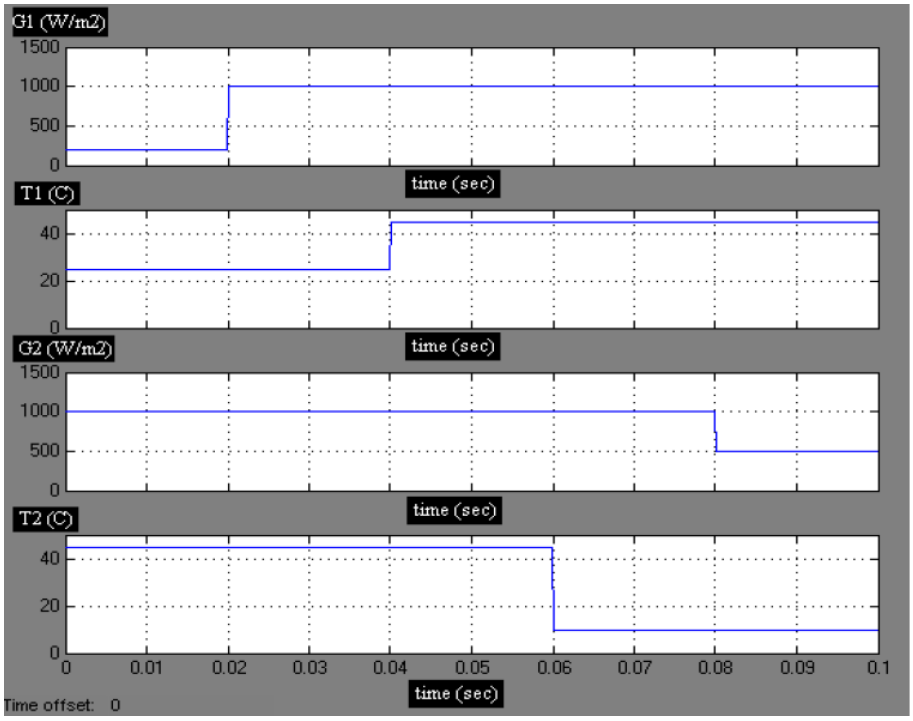

Figure 4.7: Graphical display of irradiance and temperature changes for temporary trapping at a local peak

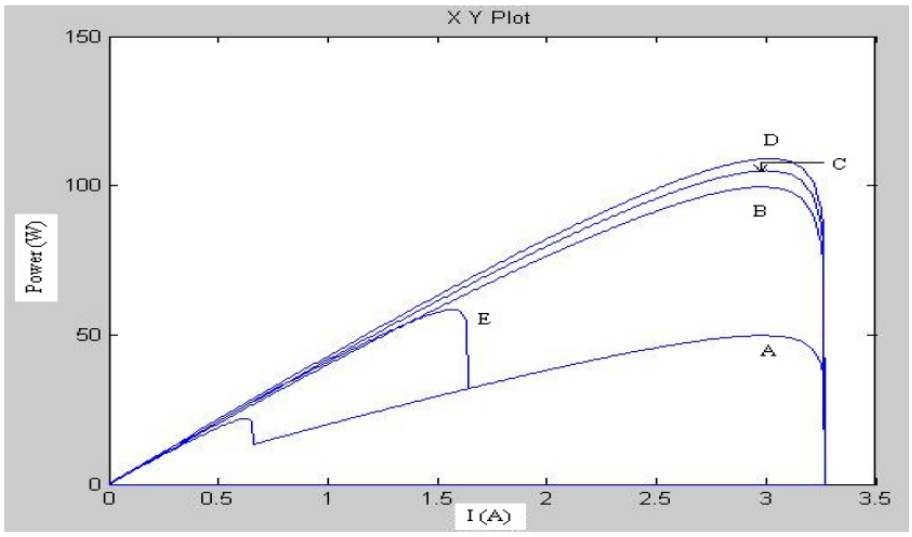

Figure 4.8: P-I curves when temporary trapping at a local peak occours

In curve A (Figure 4.8), the P&O was trapped at the first peak because it climbs the P-I curve as long as the power is increasing, so when it reaches the first peak, it cannot go beyond it since the power starts actually decreasing. The theoretical value of the power at the global peak is 49.78W shown as a dotted line in Figure 4.9 which is different from

Table 4.1: MPP Data for Temporary Trapping at a Local Peak

Time	**Curve**	$P_{MPP}(W)$	$I_{MPP}(A)$	$V_{MPP}(V)$	**Tracked Power (W)**
$t < 0.02$	A	49.78	2.98	16.7	18
$0.02 < t < 0.04$	B	105	3	34.99	105
$0.04 < t < 0.06$	C	99.55	2.98	33.41	100
$0.06 < t < 0.08$	D	109	3.01	36.22	109
$0.08 < t < 1$	E	58.5	1.58	37.03	58

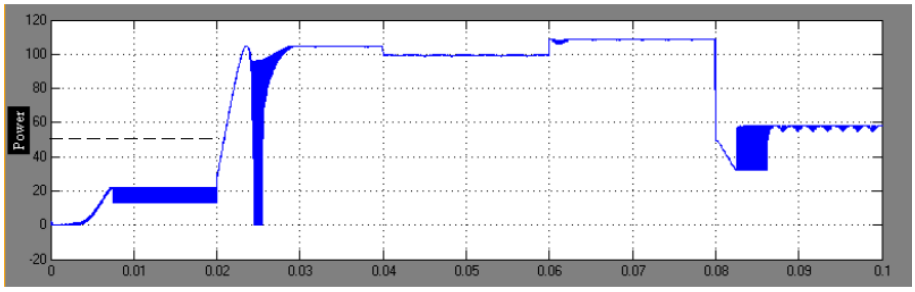

Figure 4.9: Graph of PV array power against time for temporary trapping at a local peak

the tracked power at $t < 0.02$seconds. For the reason mentioned above, the P&O fails in tracking the global MPP of curve A. This outcome is expected since the curve has two peaks, the local one and the global one; and in this case, the P&O tracks the local peak.

The P&O continued to find the actual global MPP for curves B, C, and D. This outcome is expected since these curves have only one peak. However, when the curve changed from D to E, which also has multiple peaks, it was expected that the P&O would not track the global MPP as happened in curve A. However, it can be seen from Figure 4.9 that the P&O was able to track the value of the power at the global peak, 58 W by coincidence. This may be explained by the fact that as the curve changed from D to E, the array current was approximately 3 A. Due to the high inductance value in the boost converter, instantaneouse change in current was not possible, forcing the operation of the PV system to shift from the P-I curve to the P-V curve. The array voltage was very close to the voltage at the GMPP and hence, the system was able to track the GMPP by sheer coincidence.

It can be considered that the P&O was trapped at the local peak for a short while when tracking the MPP of a P-I curve with multiple peaks and then reached the global MPP of

the P-I curve by sheer coincidence when tracking the MPP of curve E. The result of this run goes to show that the P&O can be trapped at a local peak. It can be considered that when temporary trapping at a local peak occours, output power from the PV system is lower than the actual maximum power at the GMPP for the short duration when the PV system is operating at the local peak.

4.3.2 Prolonged Trapping at a Local Peak

The irradiance and temperature changes for this run are shown in Figure 4.10 while the P-I curves of the PV arrays for every 0.02s are shown in Figure 4.11.

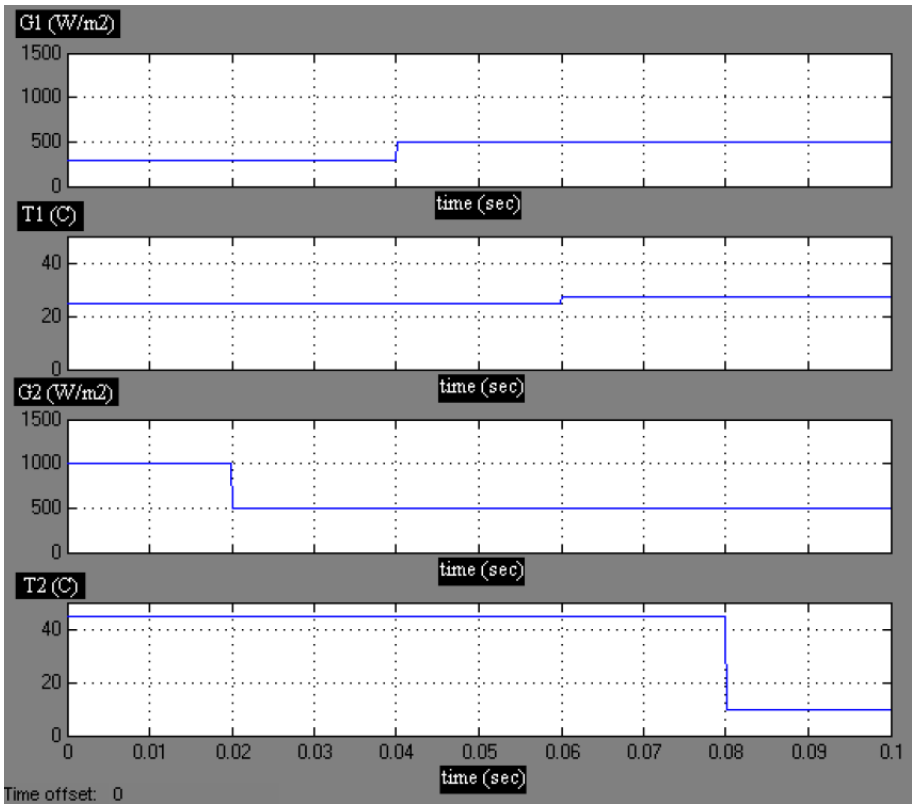

Figure 4.10: Graphical display of irradiance and temperature changes for prolonged trapping at a local peak

As can be seen in Figure 4.11, there are five curves (A, B, C, D and E), with each curve generated after 20ms such that curve A is generated within the first 20ms of simulation, curve B is generated in the preceding 20ms of simulation and so on till curve E is generated. Curves A and B have multiple peaks (meaning the solar module

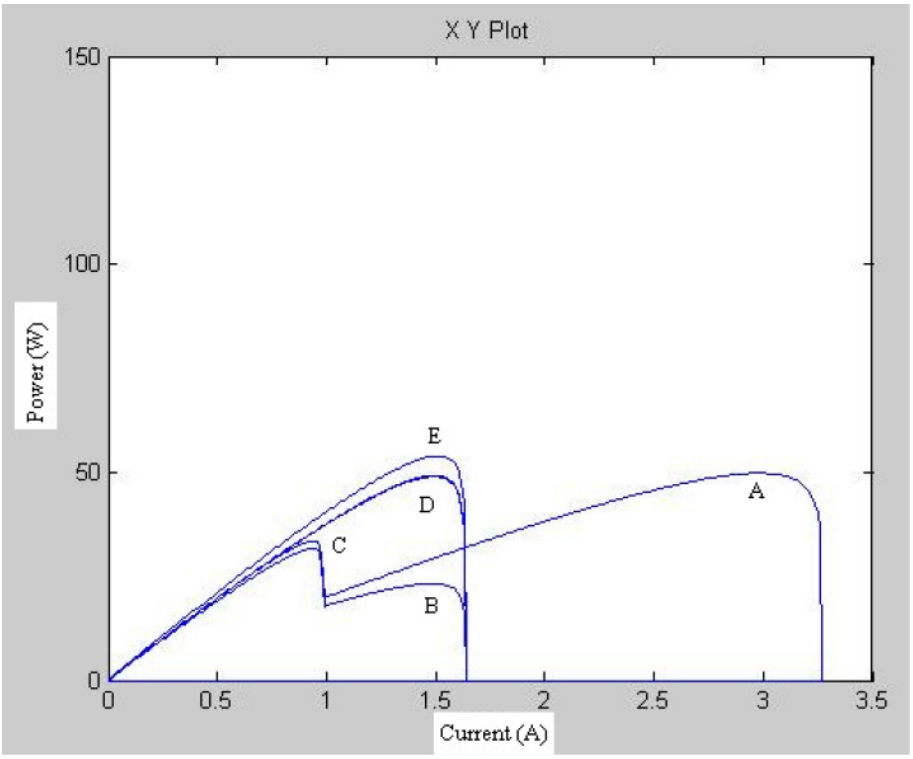

Figure 4.11: P-I curves for prolonged trapping at a local peak

is experiencing partial shading during the period of generation of these curves) while curves C, D and E have just one peak (meaning the solar module is experiencing uniform insolation during the period of generation of these curves). This could be explained by the fact that from Figure 4.10 in curves A and B, the iradiation incident on the array during this period of simulation causes the two modules to receive different levels of irradiation. While in curves C, D and E, the irradiation incident on the modules in the array is equal.

Table 4.2 shows the theoretical values of the power, voltage and current at MPP and the actual value of the MPP tracked by the P&O while the waveform of the PV array power against time are shown in Figure 4.12.

From Table 4.2, it is seen that during curve A and B, the tracked power was different from the theoretical value of the P_{MPP}. The theoretical value of the P_{MPP} for curve A (49.78W) and curve B (31.63W) are shown as dotted lines in Figure 4.12, where these are different from the tracked power for $t <$ 0.02seconds (26 W) and 0.02 seconds$< t <$ 0.04seconds (24 W). This may be due to the P&O being trapped at the local peak in both

Table 4.2: MPP Data for Prolonged Trapping at a Local Peak

Time	**Curve**	$P_{MPP}(W)$	$I_{MPP}(A)$	$V_{MPP}(V)$	**Tracked Power (W)**
$t < 0.02$	A	49.78	2.98	16.7	26
$0.02 < t < 0.04$	B	31.63	0.95	33.3	24
$0.04 < t < 0.06$	C	49.22	1.49	33.03	49
$0.06 < t < 0.08$	D	48.94	1.49	32.84	49
$0.08 < t < 1$	E	53.87	1.51	35.67	55

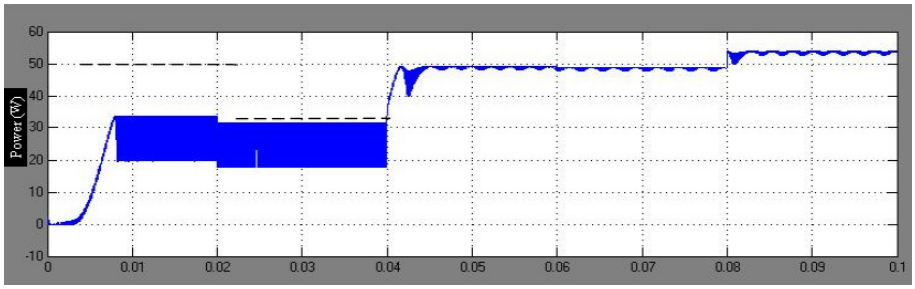

Figure 4.12: Graph of PV module power against time for prolonged trapping at a local peak

curves, hence tracking the local peak as opposed to the global peak. This is expected since the two curves have multiple peaks.

It can also be noted from Figure 4.12 that there were large oscillations in power in the first 40 ms of simulation. This may be attributed to the boost converter causing voltage ripples to appear in the converter output due to its modelling as an exact circuit.

In this run, the P&O algorithm was trapped longer at the wrong peak (the local peak) than was the case in the previous run during the first 40 ms of simulation. In this period, the solar module was experiencing partial shading. However in the subsequent 80 ms of simulation when the solar module was experiencing uniform insolation, the P&O algorithm was able to track the MPP of the solar module.

The results of this run show that the P&O can be trapped longer at the wrong peak but still continue to track the global peak of the PV array.

4.3.3 Effect of the Arrangement of Peaks

The irradiance and temperature changes for this run are shown in Figure 4.13 while the P-I curves of the PV arrays for every 0.02s are shown in Figure 4.14.

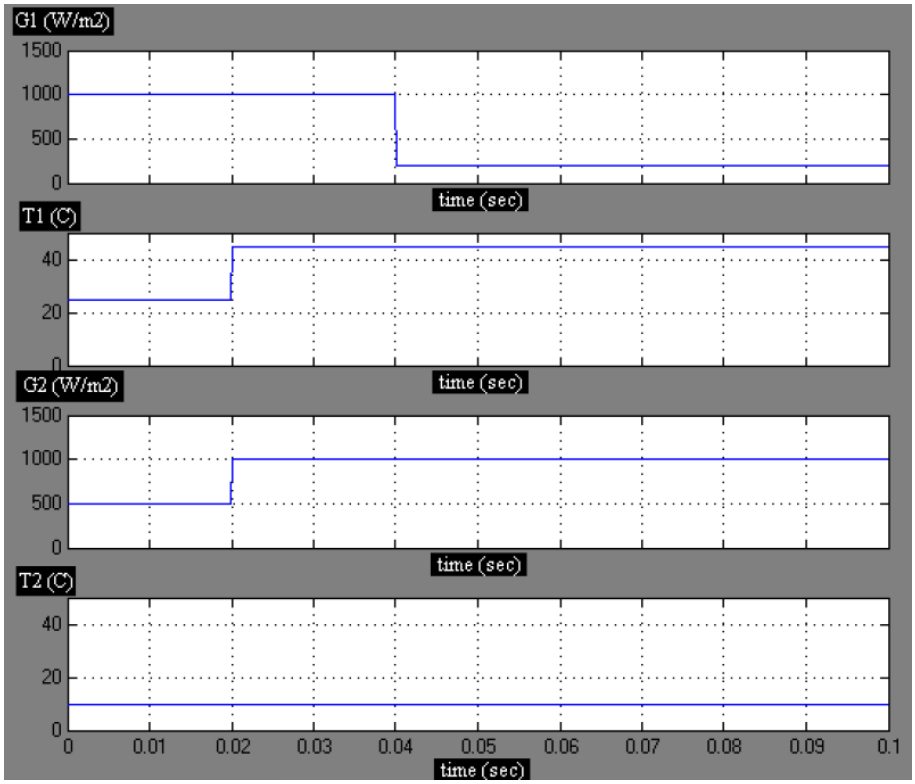

Figure 4.13: Graphical display of irradiance and temperature changes for the effect of arrangement of peaks

As can be seen in Figure 4.14, there are three curves (A, B and C), with each curve generated after 20 ms such that curve A is generated within the first 20 ms of simulation, curve B is generated in the preceding 20 ms of simulation and so on till curve C is generated. Curves A and C have multiple peaks as a result of the solar module experiencing partial shading during the duration of generation of these curves while curve B has just one peak as a result of the solar module experiencing uniform insolation during the duration of generation of curve B. Further, the first peak of curve A is the global peak while the second is the local peak. This could be explained by the fact that from Figure 4.13 in curves A and C, the iradiation incident on the array during this period of simulation causes the two modules to receive different levels of irradiation. While in curve B, the irradiation incident on the modules in the array is equal.

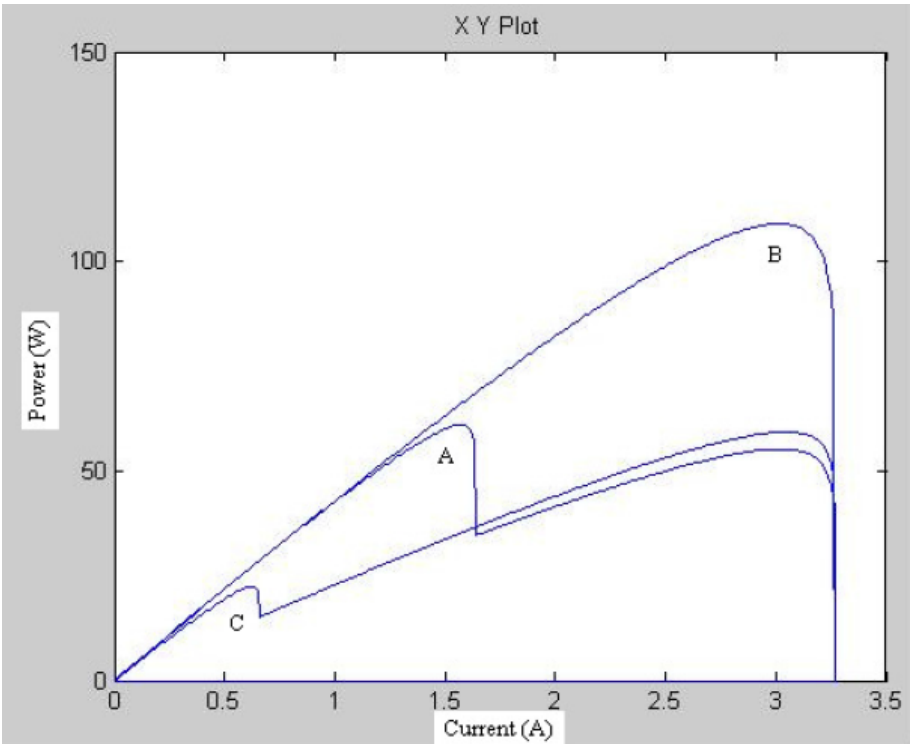

Figure 4.14: P-I curves for the effect of arrangement of peaks

Table 4.3 shows the theoretical values of the power, voltage and current at MPP and the actual value of the MPP tracked by the P&O while the waveform of the PV array power against time are shown in Figure 4.15.

Table 4.3: MPP Data for the Effect of Arrangement of Peaks

Time	**Curve**	$P_{MPP}(W)$	$I_{MPP}(A)$	$V_{MPP}(V)$	**Tracked Power (W)**
$t < 0.02$	A	61.06	1.58	38.64	58
$0.02 < t < 0.04$	B	109	3.01	36.22	100
$0.04 < t < 0.06$	C	59.32	3.04	19.51	54

From Figure 4.15, the value of tracked power is 58 W, 100 W and 54 W for curves A, B and C respectively. These values are close to the theoretical value of PMPP of 61.06 W, 109 W and 59.32 W respectively. These results show that the P&O was able to track the global MPP in all the three curves. For curve A, this may be explained by the fact that the algorithm gets stuck at the first peak. However, this peak happens to be the global MPP and as such tracks the global MPP. In curve B, there is only one peak and as such, the algorithm is expected to naturally converge around the real MPP. As the

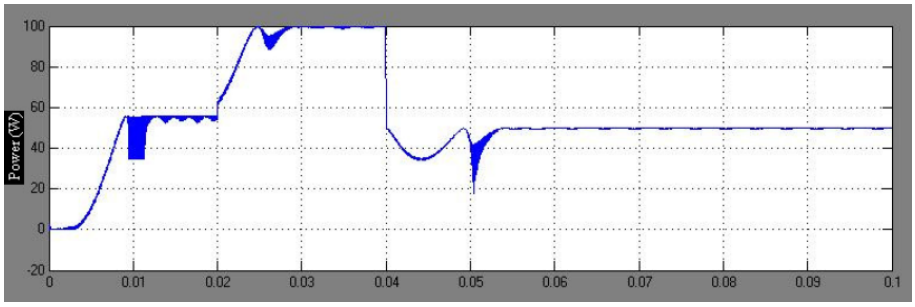

Figure 4.15: Graph of PV module power against time for the effect of arrangement of peaks

system shifts to curve C, the voltage operating point is already closer to the voltage at GMPP (similar to the reason presented in "temporary trapping at a local peak") and since the first peak is in a far region, then the system also happens to converge to the real GMPP.

The result of this run shows that sometimes, the P&O could find the global MPP by chance because of the arrangement of peaks on the curves, as is the case where the first peak encountered by the P&O is the global peak.

4.3.4 Effect of Sustained Partial Shading

The irradiance and temperature changes for this run are shown in Figure 4.16 while the P-I curves of the PV arrays for every 0.02s are shown in Figure 4.17.

As can be seen from Figure 4.17, all curves have multiple peaks as a result of the solar module being fully under partial shading for the entire duration of this simulation. Further, in each of the curves, the first peak is the local peak, and the the second peak is the global peak, with the operating points of both peaks being far from each other. This could be explained by the fact that from Figure 4.16, for the entire duration of generation of the curves, the iradiation incident on the array during this period of simulation causes the two modules to always receive different levels of irradiation.

Table 4.4 shows the theoretical values of the power, voltage and current at MPP and the actual value of the MPP tracked by the P&O.

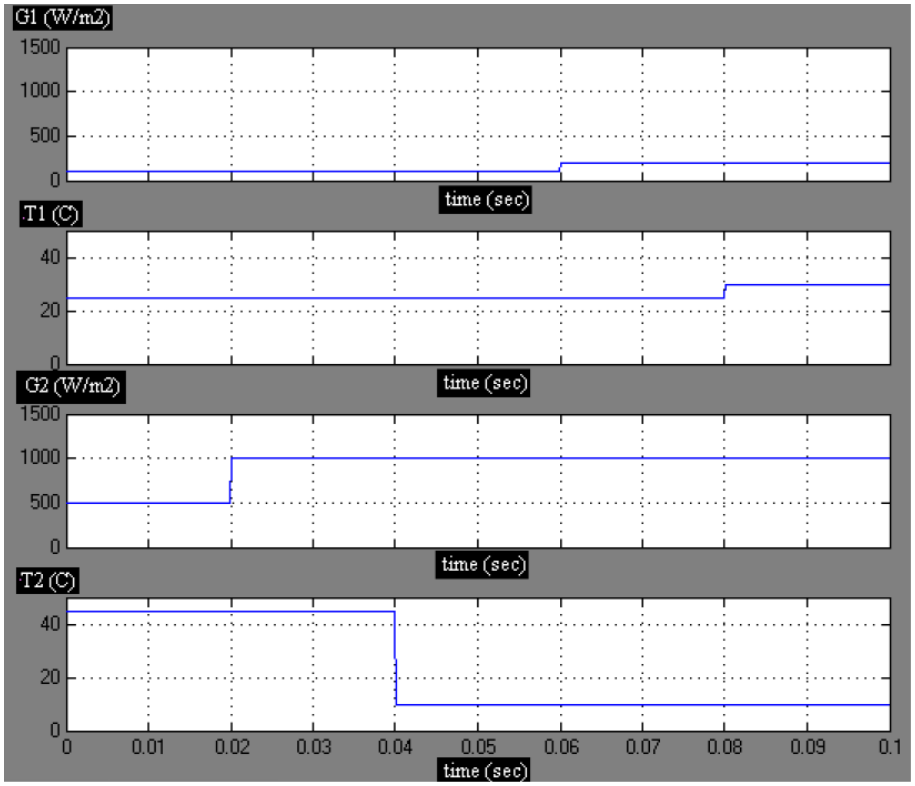

Figure 4.16: Graphical display of irradiance and temperature changes for sustained partial shading

Table 4.4: MPP Data for Sustained Partial Shading

Time	**Curve**	$P_{MPP}(W)$	$I_{MPP}(A)$	$V_{MPP}(V)$	**Tracked Power (W)**
$t < 0.02$	A	23.21	1.48	15.69	9
$0.02 < t < 0.04$	B	49.78	2.98	16.7	9
$0.04 < t < 0.06$	C	59.32	3.04	19.51	9
$0.06 < t < 0.08$	D	59.32	3.04	19.51	24
$0.08 < t < 1$	E	59.32	3.04	19.51	24

Figure 4.18 shows the waveform of the PV modules power against time.

It can be noted from Figure 4.18 that there were large oscillations in power during the entire period of simulation. This may be attributed to the boost converter causing voltage ripples to appear in the converter output as a result of its modelling in an exact circuit form in simulink.

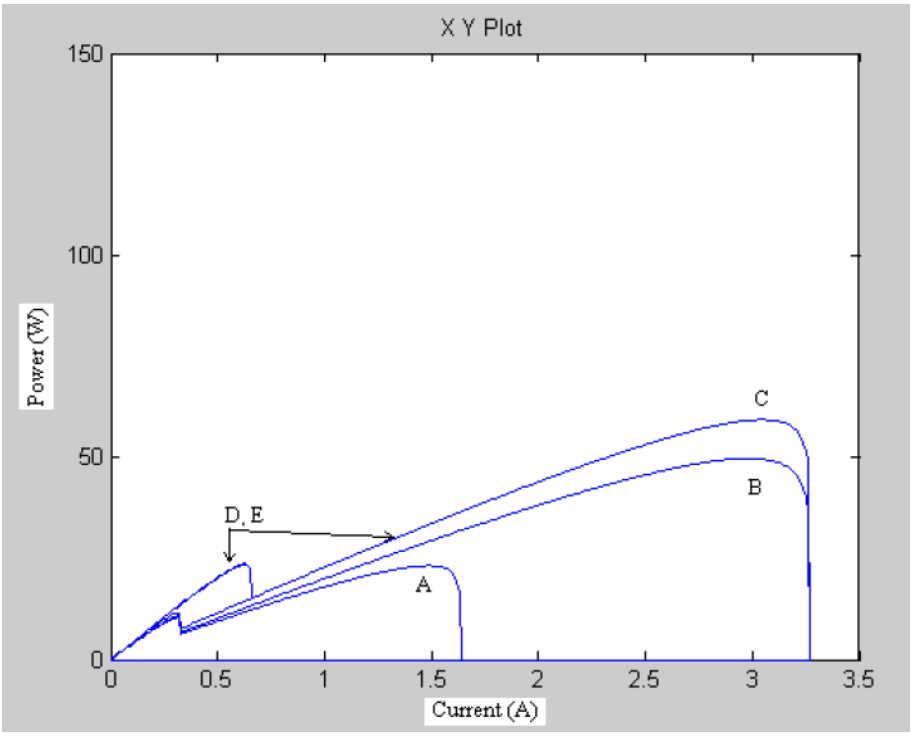

Figure 4.17: P-I curves for sustained partial shading

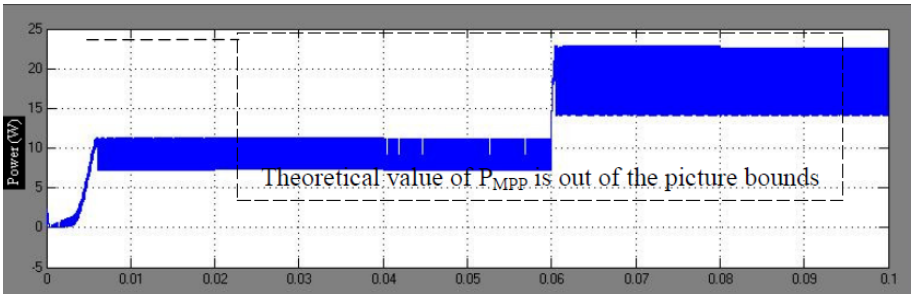

Figure 4.18: Graph of PV module power against time

In this run, the values of the tracked power of the PV array for curves A, B, C, D and E are 9 W, 9W, 9W, 24 W and 24 W respectively, which are significantly different from the value of power at the global peaks of the five curves of 23.21 W, 49.78 W, 59.32 W, 59.32 W and 59.32 W, respectively. These results show that the P&O algorithm was completely unable to track the global MPP for the entire period of simulation, with the P&O algorithm being trapped in the first peak which is not the global MPP in none of the five curves. Thus, when the P&O algorithm is faced with a solar array entirely under partial shading, where the first peak happens to be the local peak, then it completely fails to track the global MPP.

4.4 MPP Tracking of the PV System With Proposed Two-Tier Algorithm

4.4.1 Effect of Temporary Trapping at a Local Peak

The irradiance and temperature changes for this run are shown in the Figure 4.19 while the P-I curves of the PV arrays for every 0.02s are shown in Figure 4.20.

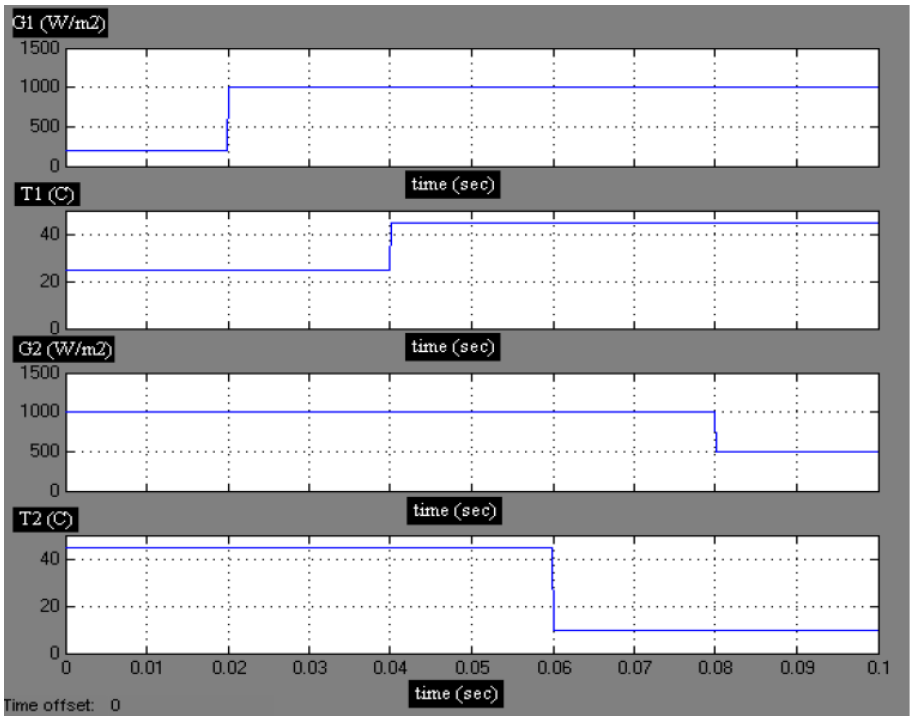

Figure 4.19: Graphical display of irradiance and temperature changes for temporary trapping at a local peak with proposed algorithm

As can be seen in Figure 4.20, there are five curves (A, B, C, D and E), with each curve generated after 20ms such that curve A is generated within the first 20ms of simulation, curve B is generated in the subsequent 20ms of simulation and so on till curve E is generated. Curves A and E having multiple peaks as a result of the solar module is experiencing partial shading during the period of generation of these curves, while curves B, C and D having just one peak as a result of the solar module is experiencing uniform insolation during the period of generation of these curves. This could be explained by

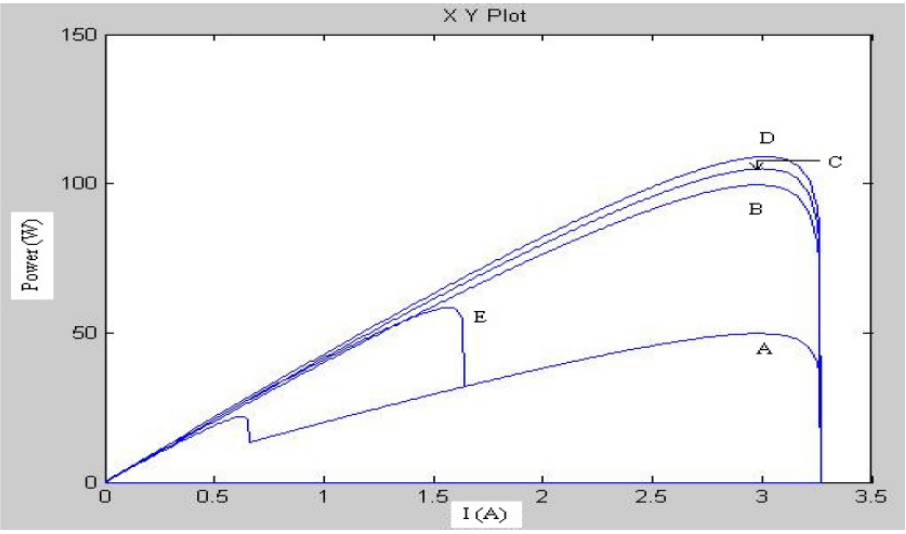

Figure 4.20: P-I curves for temporary trapping at a local peak with proposed algorithm

the fact that from Figure 4.19 in curves A and E, the iradiation incident on the array during this period of simulation causes the two modules to receive different levels of irradiation. While in curves B, C and D, the irradiation incident on the modules in the array is equal.

The MPP power that was tracked with the proposed algorithm is shown in Figure 4.21 while the Table 4.5 shows the theoretical values of the power, voltage and current at MPP and the actual value of the MPP tracked by the proposed algorithm.

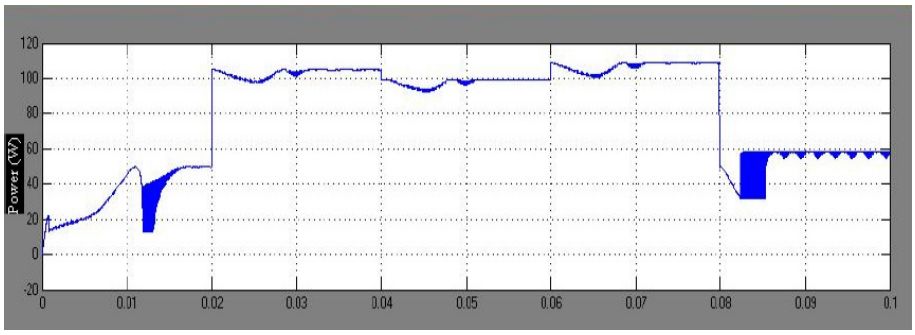

Figure 4.21: Graph of PV module power against time for temporary trapping at a local peak with proposed algorithm

In Figure 4.21, during the period of generation of curve A in which the solar module is under partial shading, the algorithm tracks the power at 20 W during the start of the simulation, but it eventually does track the theoretical power after a brief period

Table 4.5: MPP Data for Temporary Trapping at a Local Peak with Proposed Algorithm

Time	**Curve**	$P_{MPP}(W)$	$V_{MPP}(V)$	**Tracked Power (W)**	**Tracked Power (P&O)**
$t < 0.02$	A	49.78	16.7	50	18
$0.02 < t < 0.04$	B	105	34.99	105	105
$0.04 < t < 0.06$	C	99.55	33.41	100	100
$0.06 < t < 0.08$	D	109	36.22	109	109
$0.08 < t < 1$	E	58.5	37.03	58	58

with the difference in power between the theoretical MPP and tracked MPP being 0.28 W. During the period of generation of curve E, which also has multiple peaks, meaning the solar module is also experiencing partial shading, the algorithm does nearly track the power at the MPP, with the difference in power between the theoretical MPP and tracked MPP being 0.5 W. During the period of generation of curves B, C and D that have one peak, the algorithm accurately tracked the power at the MPP as expected since the curves have only one peak, the global peak. The fact that the algorithm was able to track the GMPP in curves A and E which had multiple peaks could be attributed to the fact that the first stage of the algorithm was able to approximate the loacation of the GMPP and hence enabled the by-passing of the local maxima that would have caused it to be trapped at the local peak.

Data from this run shows that the system converged at the real GMPP and was not stuck at a local maximum.

4.4.2 Prolonged Trapping at a Local Peak

The irradiance and temperature changes for this run are shown in Figure 4.22 while the P-I curves of the PV arrays for every 0.02s are shown in Figure 4.23.

As can be seen in Figure 4.23, there are five curves (A, B, C, D and E), with each curve generated after 20ms such that curve A is generated within the first 20ms of simulation, curve B is generated in the preceding 20ms of simulation and so on till curve E is generated. Curves A and B have multiple peaks as a result of the solar module is experiencing partial shading during the period of generation of these curves while curves C, D and E have just one peak as a result of the solar module is experiencing uniform

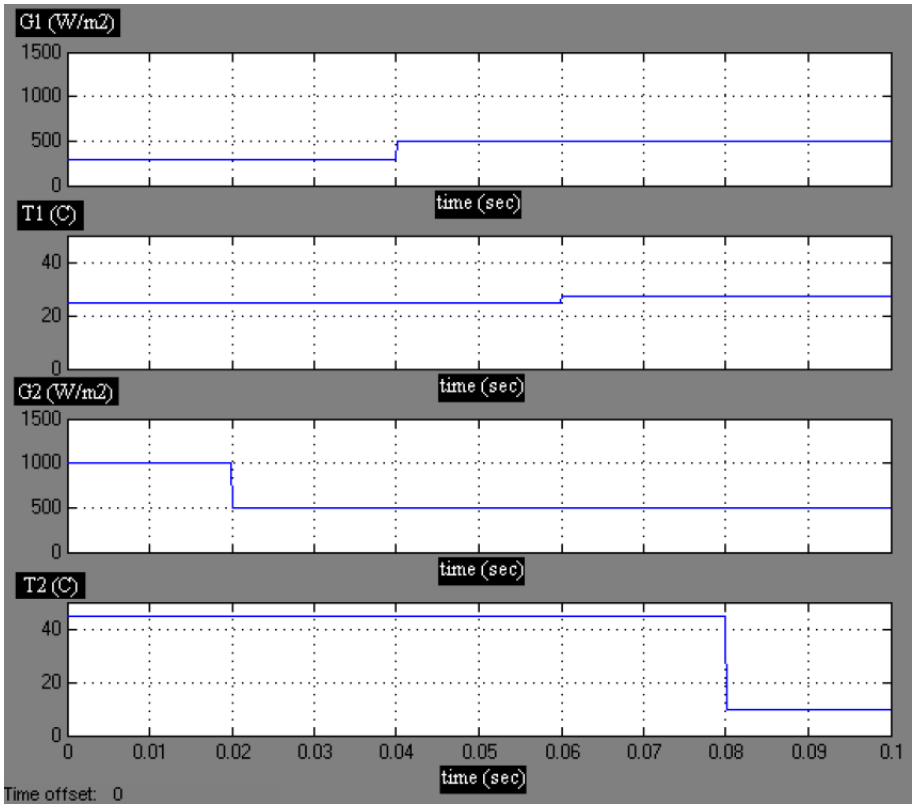

Figure 4.22: Graphical display of irradiance and temperature changes for prolonged trapping at a local peak with proposed algorithm

insolation during the period of generation of these curves. This could be explained by the fact that from Figure 4.22 in curves A and B, the iradiation incident on the array during this period of simulation causes the two modules to receive different levels of irradiation. While in curves C, D and E, the irradiation incident on the modules in the array is equal.

The MPP power that was tracked with the proposed algorithm is shown in Figure 4.24 while the theoretical values of power, voltage and current at MPP and the actual value of MPP tracked by the proposed algorithm are shown in Table 4.6.

In Figure 4.24, during the period of generation of curve A and B in which the solar module is under partial shading, the algorithm tracks the power at 49 W and 26 W respectively with the difference in power between the theoretical MPP and tracked MPP being 0.78 W and 5.63 W respectively. During the period of generation of curve C, D and E, that have one peak, the algorithm did accurately track the power at the MPP

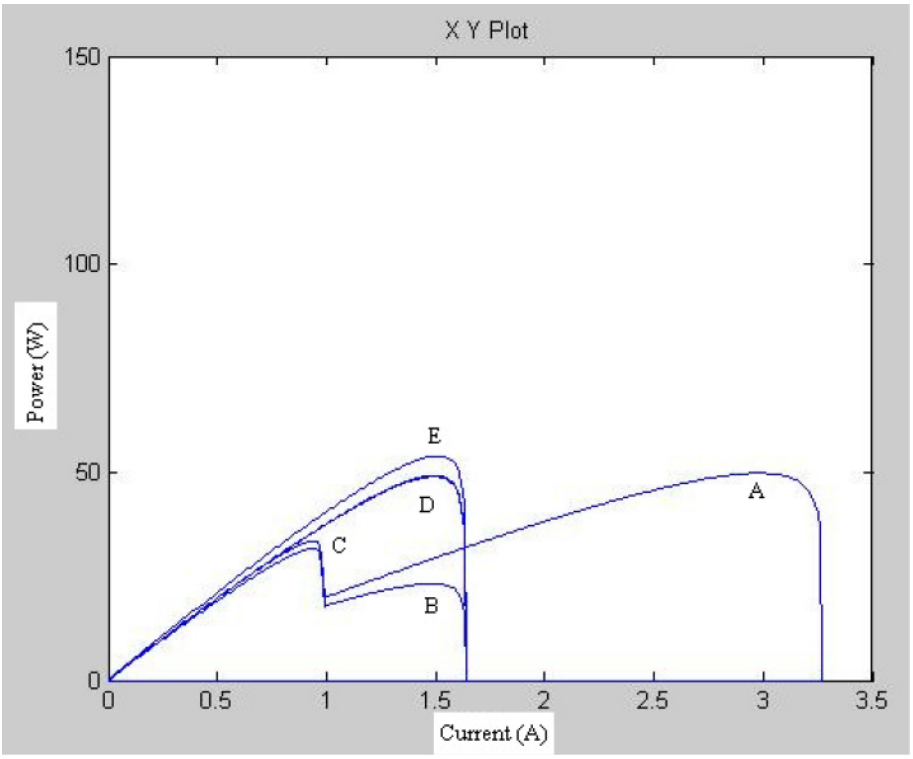

Figure 4.23: P-I curves of the PV Arrays for every 0.02s for prolonged trapping at a local peak with proposed algorithm

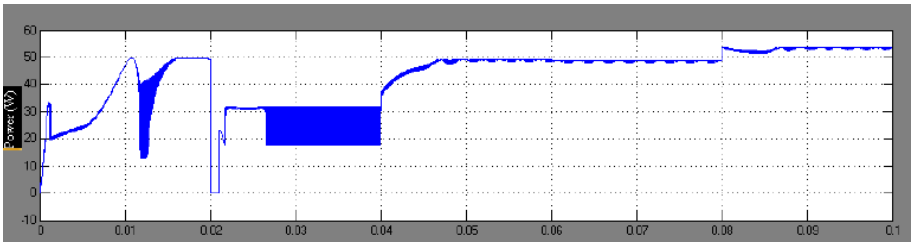

Figure 4.24: Graph of PV module power against time for prolonged trapping at a local peak with proposed algorithm

Table 4.6: MPP Data for Prolonged Trapping at a Local Peak with Proposed Algorithm

Time	**Curve**	$P_{MPP}(W)$	$V_{MPP}(A)$	**Tracked Power (W)**	**Tracked Power (P&O)**
$t < 0.02$	A	49.78	16.7	49	26
$0.02 < t < 0.04$	B	31.63	33.33	26	24
$0.04 < t < 0.06$	C	49.22	33.03	48.5	49
$0.06 < t < 0.08$	D	48.94	32.84	48	49
$0.08 < t < 1$	E	53.87	35.67	54	55

as expected since the curves have only one peak, the global peak. The difference in power between the tracked MPP and theorestical MPP being 0.72 W, 0.94 W and 0.13 W respectively.

Thus from the above data, it is clear the system converged at the real MPP and was not stuck at a local maximum in cases where both local and global maxima exist.

4.4.3 Effect of The Arrangement of Peaks

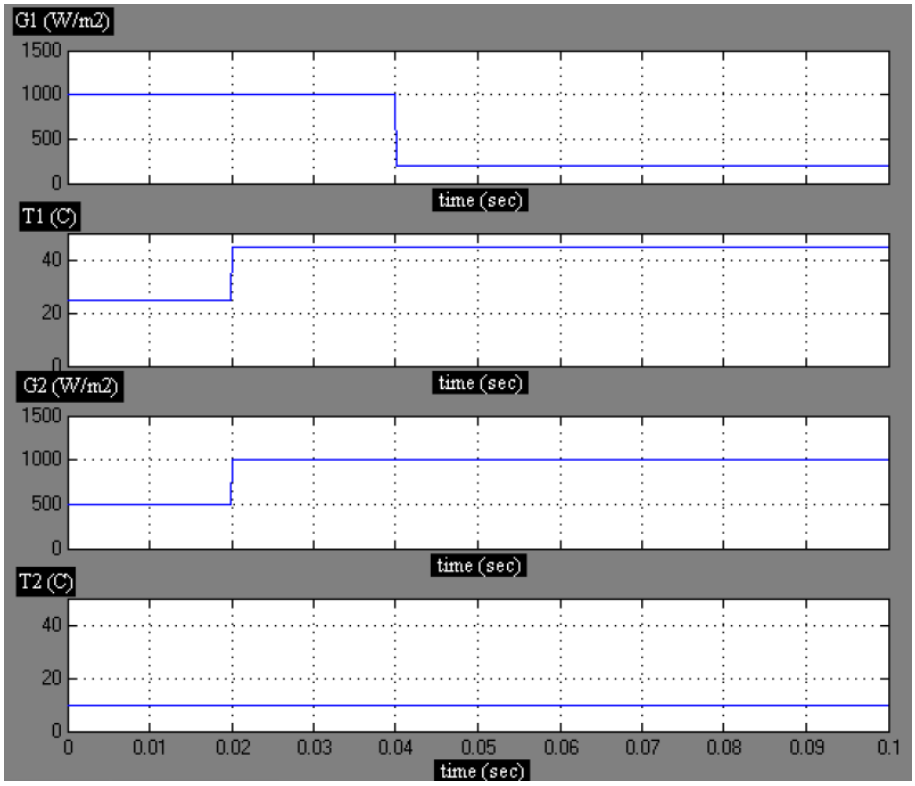

Figure 4.25: Graphical display of irradiance and temperature changes for effect of arrangement of peaks with proposed algorithm

The irradiance and temperature changes for this run are shown in Figure 4.25 while the P-I curves of the PV arrays for every 0.02s are shown in Figure 4.26. As can be seen in Figure 4.26, there are three curves (A, B and C), with each curve generated after 20ms such that curve A is generated within the first 20ms of simulation, curve B is generated in the preceding 20ms of simulation and so on till curve C is generated. Curves A and C have multiple peaks as a result of the solar module experiencing partial shading during

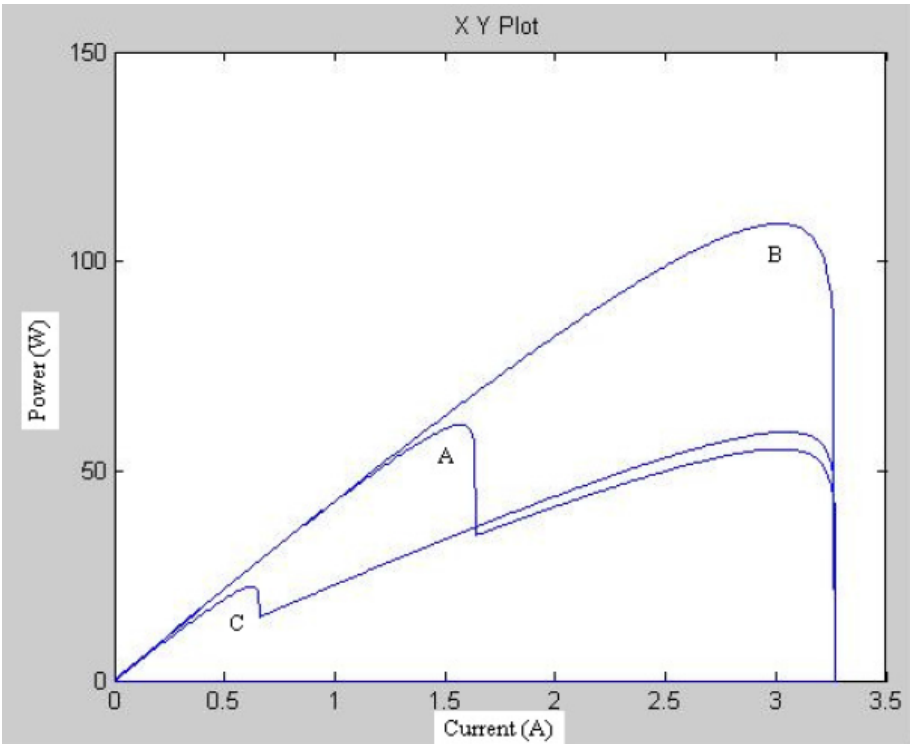

Figure 4.26: P-I curves of the PV arrays for every 0.02s for effect of arrangement of peaks with proposed algorithm

the period of generation of these curves while curve B has just one peak as a result of the solar module is experiencing uniform insolation during the period of generation of these curve. This could be explained by the fact that from Figure 4.25 in curves A and C, the iradiation incident on the array during this period of simulation causes the two modules to receive different levels of irradiation. While in curve B, the irradiation incident on the modules in the array is equal.

The MPP power that was tracked with the proposed algorithm is shown in Figure 4.27 while the theoretical values of power, voltage and current at MPP and the actual value of MPP tracked by the proposed algorithm are shown in Table 4.7.

Table 4.7: MPP Data for Effect of Arrangement of Peaks with Proposed Algorithm

Time	**Curve**	$P_{MPP}(W)$	$V_{MPP}(A)$	**Tracked Power (W)**	**Tracked Power (P&O)**
$t < 0.02$	A	61.06	38.64	60.5	58
$0.02 < t < 0.04$	B	109	36.22	110	100
$0.04 < t < 1$	C	59.32	19.51	59	54

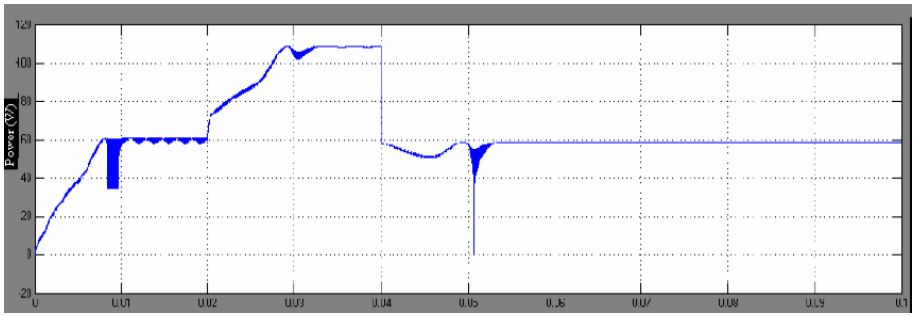

Figure 4.27: Graph of PV module power against time for effect of arrangement of peaks with proposed algorithm

In Figure 4.27, during the period of generation of curve A and C in which the solar module is under partial shading, the algorithm tracks the power at 60.5 W and 59 W respectively with the difference in power between the theoretical MPP and tracked MPP being 0.56 W and 0.32 W respectively. During the period of generation of curve B, that has one peak, the algorithm did accurately track the power at the MPP as expected since the curves have only one peak, the global peak. The difference in power between the tracked MPP and theorestical MPP being 1 W.

Thus from the above data, it is clear the system converged at the real MPP and was not stuck at a local maximum in cases where both local and global maxima exist.

4.4.4 Effect of Sustained Partial Shading

The irradiance and temperature changes for this run are shown in Figure 4.28 while the P-I curves of the PV arrays for every 0.02s are shown in Figure 4.29.

As can be seen in Figure 4.29, there are five curves (A, B, C, D and E), with each curve generated after 20ms such that curve A is generated within the first 20ms of simulation, curve B is generated in the preceding 20ms of simulation and so on till curve E is generated.All the curves A to E have multiple peaks as a result of the solar module is experiencing partial shading during the period of generation of these curves. This could be explained by the fact that from Figure 4.28, for the entire duration of generation of the curves, the iradiation incident on the array during this period of simulation causes the two modules to always receive different levels of irradiation. Thus for this run, the

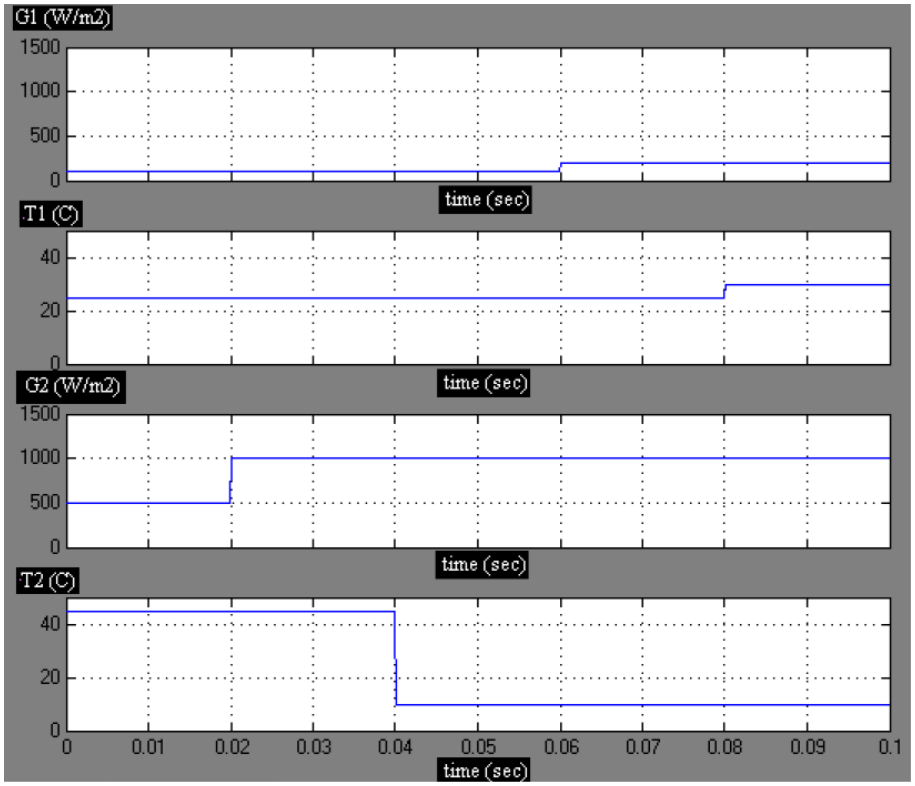

Figure 4.28: Graphical display of irradiance and temperature changes for the effect of sustained partial shading with proposed algorithm

solar module is simulated entirely under partial shading for the entire duration of the simulation.

The MPP power that was tracked with the proposed algorithm is shown in figure 4.30 while the theoretical values of power, voltage and current at MPP and the actual value of MPP tracked by the proposed algorithm are shown in Table 4.8.

Table 4.8: MPP Data for the Effect of Sustained Partial Shading with Proposed Algorithm

Time	**Curve**	$P_{MPP}(W)$	$V_{MPP}(A)$	**Tracked Power (W)**	**Tracked Power (P&O)**
$t < 0.02$	A	23.21	15.69	23	9
$0.02 < t < 0.04$	B	49.78	16.7	50	9
$0.04 < t < 10.06$	C	59.32	19.51	60	9
$0.06 < t < 0.08$	D	59.32	19.51	60	24
$0.08 < t < 1$	E	59.32	19.51	60	24

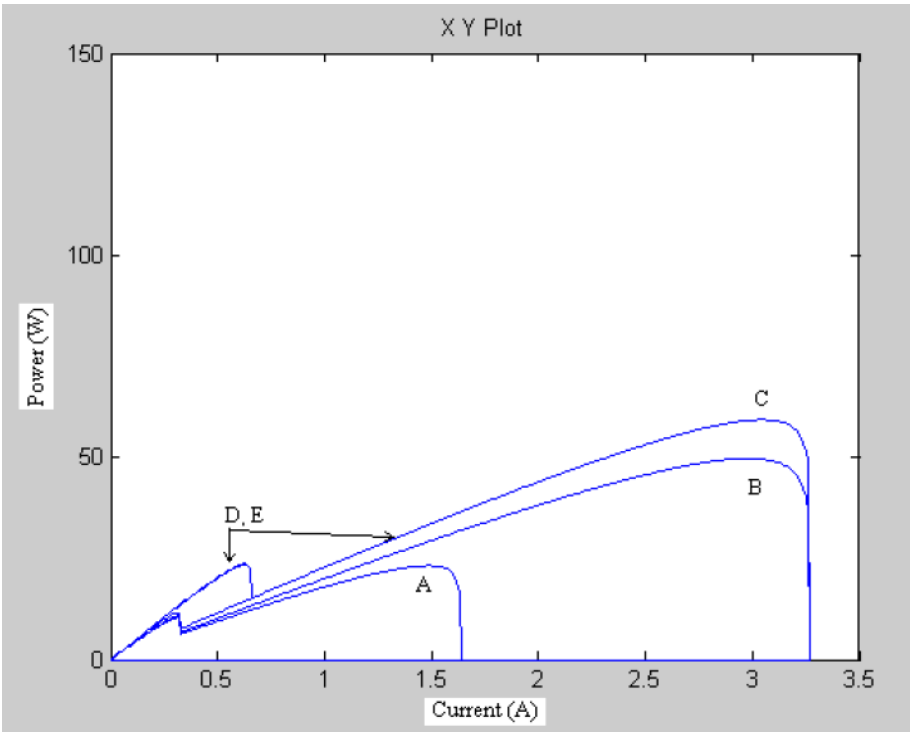

Figure 4.29: P-I curves of the PV arrays for every 0.02s for the effect of sustained partial shading with proposed algorithm

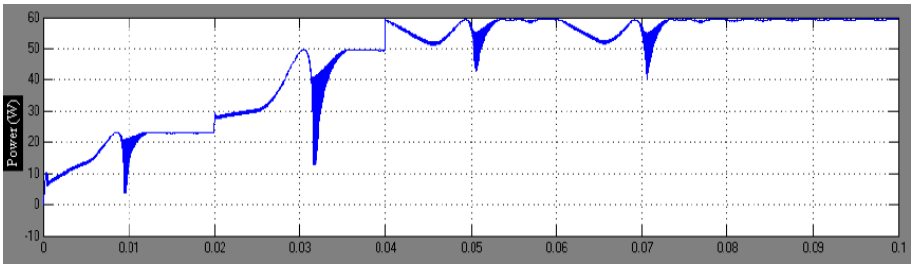

Figure 4.30: Graph of PV module power against time for the effect of sustained partial shading with proposed algorithm

In Figure 4.30, during the period of generation of curve A, B, C, D and E in which the solar module is under partial shading, the algorithm tracks the power at 23 W, 50 W, 60 W, 60 W and 60 W respectively with the difference in power between the theoretical MPP and tracked MPP being 0.21 W, 0.22 W, 0.68 W, 0.68 W and 0.68 W respectively.

Thus from the above data, it is clear the system converged at the real MPP and was not stuck at a local maximum in runs where both local and global maxima exist. This simulation is of particular importance in that, the conditions for its simulation are similar to those of the previous section under "Effect of Sustained Partial Shading" where it was

observed that the P&O algorithm did not accurately track the global MPP of the system for all the curves when the solar module was entirely under partial shading.

4.4.5 Effect of Rapidly Varying Atmospheric Conditions

The irradiance and temperature changes for this run are shown in Figure 4.31 while the P-I curves of the PV arrays for every 0.02s are shown in Figure 4.32.

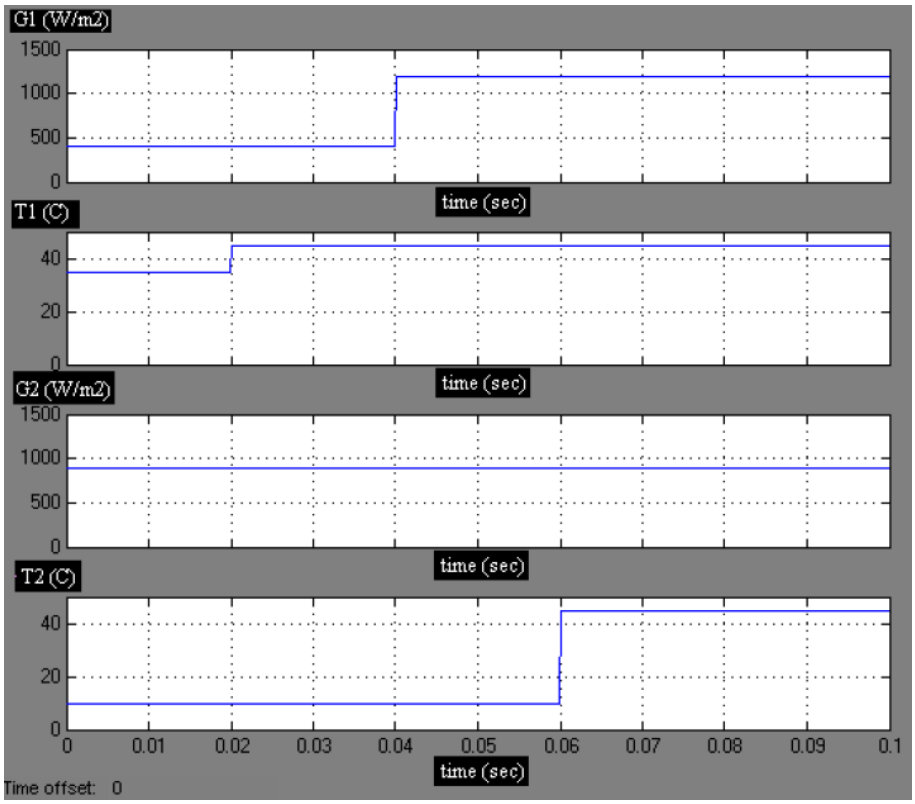

Figure 4.31: Graphical display of irradiance and temperature changes for effect of rapidly varying atmospheric conditions

As can be seen in Figure 4.32, there are five curves (A, B, C, D and E), with each curve generated after 20ms such that curve A is generated within the first 20ms of simulation, curve B is generated in the preceding 20ms of simulation and so on till curve E is generated. All the curves have multiple peaks as a result of the solar module is experiencing partial shading during the period of generation of these curves, with curve D and E being the same since the solar modules experience the same conditions of tempereature and irradiance.

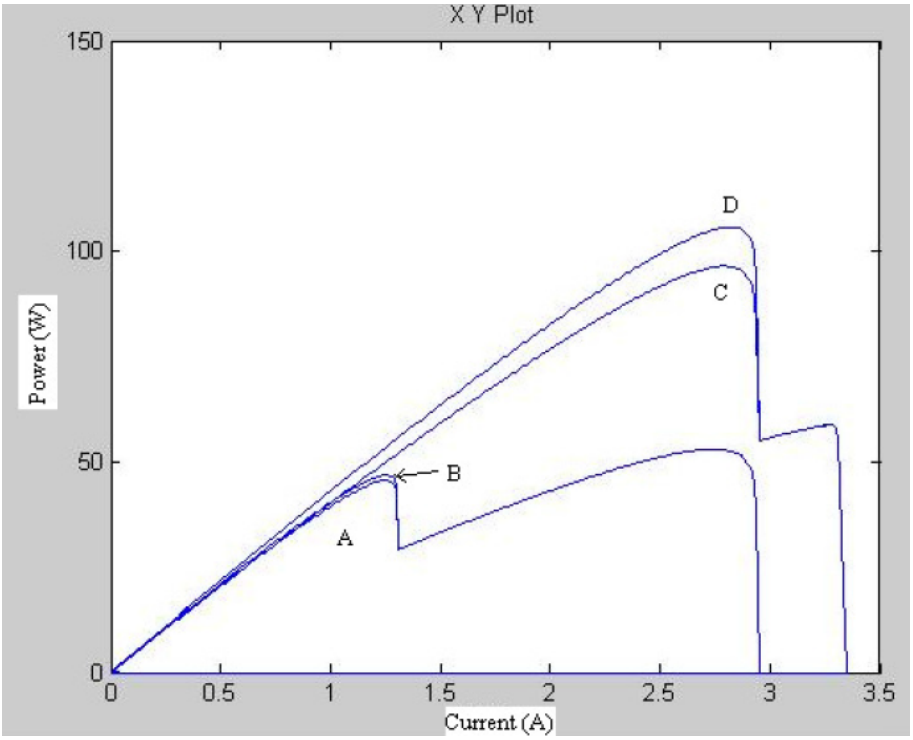

Figure 4.32: P-I curves of the PV arrays for every 0.02s for effect of rapidly varying atmospheric conditions

The MPP power that was tracked with the proposed algorithm is shown in figure 4.33 while the theoretical values of power, voltage and current at MPP and the actual value of MPP tracked by the proposed algorithm is shown in Table 4.9.

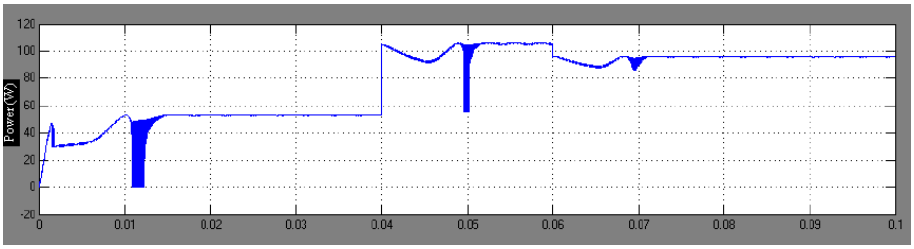

Figure 4.33: Graph of PV module power against time for effect of rapidly varying atmospheric conditions

In Figure 4.33, during the period of generation of curve A, B, C and D in which the solar module is under partial shading, the algorithm tracks the power at 55 W, 55 W, 107 W and 95 W respectively with the difference in power between the theoretical MPP and tracked MPP being 2.02 W, 2.02 W, 1.3 W and 1.48 W respectively.

Table 4.9: MPP Data for Effect of Rapidly Varying Atmospheric Conditions

Time	**Curve**	$P_{MPP}(W)$	$V_{MPP}(A)$	**Tracked Power (W)**
$t < 0.02$	A	52.98	19.33	55
$0.02 < t < 0.04$	B	52.98	19.33	55
$0.04 < t < 0.06$	C	105.7	33.84	107
$0.06 < t < 0.08$	D	96.48	34.46	95
$0.08 < t < 1$	E	96.48	34.46	95

It can be considered that under constantly varying atmospheric conditions, the PV system using the proposed algorithm converged at the real MPP and was not stuck at a local maximum in runs where both local and global maxima exist. This simulation is of particular importance in that, these conditions are what would practically be expected in our country.

4.5 Experimental Validation of the Proposed Algorithm

To ensure the model developed for this research was accurate, validation was carried out by connecting the PV module directly to a variable resistor load. The resistance was then varied from short circuit to open circuit and electrical measurements of current and voltage taken from which the measurement of power was derived. The value of electrical measurements collected experimentally were then compared to those obtained during simulation. Figures 4.34 and 4.36 show the simulated I-V and P-V characteristic curves respectively, while Figures 4.35 and 4.37 show the experimental validation of I-V and P-V characteristic curves respectively.

From the superimposed results of PV characteristics in Figures 4.38 and 4.39, the experimental results show a slightly different value of short circuit current and open circuit voltage compared to the simulated results. This may be attributed to the variation in temperature while recording the experimental measurements which in turn affected the output of the PV module. The series resistance of the solar cell may also have contributed

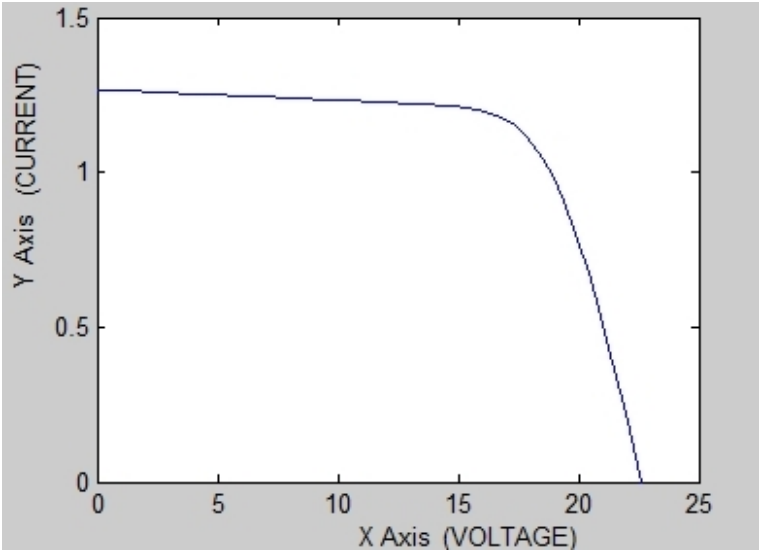

Figure 4.34: Simulated results of current-voltage characteristics

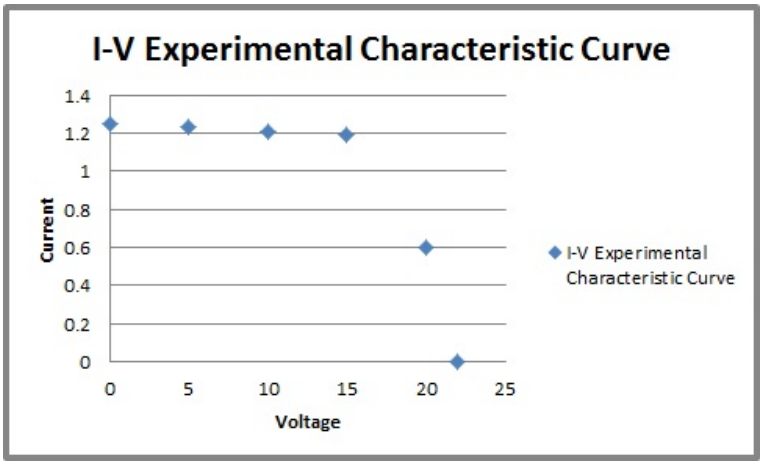

Figure 4.35: Experimental validation of current-voltage characteristics

to the mismatch in simulated and experimental characteristic curves.

The performance of the PV system (with one module partially covered by translucent gelatin paper) was first tested with the P&O MPPT algorithm and the output power recorded alongside the time duration. The proposed MPPT algorithm was then connected to the PV system and the set-up tested by recording the maximum power attained at a particular instant in time along with the time duration. Figure 4.40 shows the maximum power attained with the proposed MPPT algorithm and the nominal operating power (with P&O) in one of the test runs. The system with the proposed MPPT algorithm was found to attain an average power of 37W, corresponding to the maximum

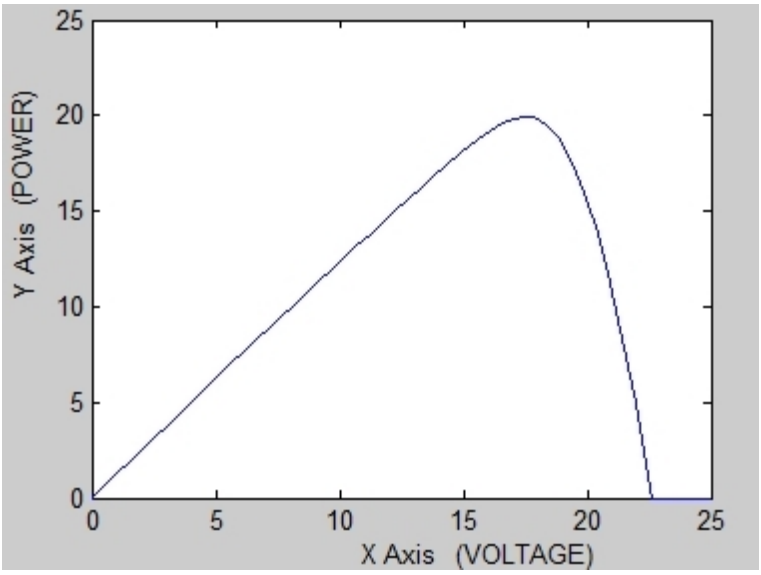

Figure 4.36: Simulated results of power-voltage characteristics

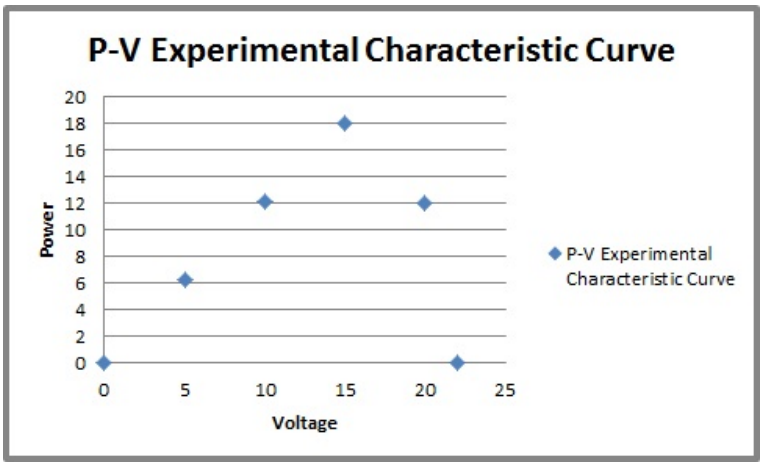

Figure 4.37: Experimental validation of power-voltage characteristics

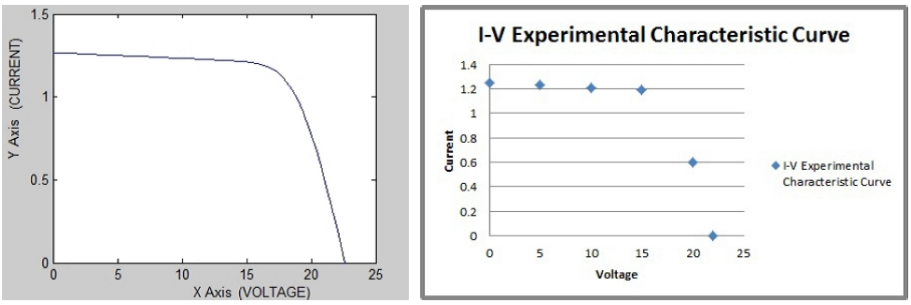

Figure 4.38: Superimposed results for simulated and experimental I-V characteristics

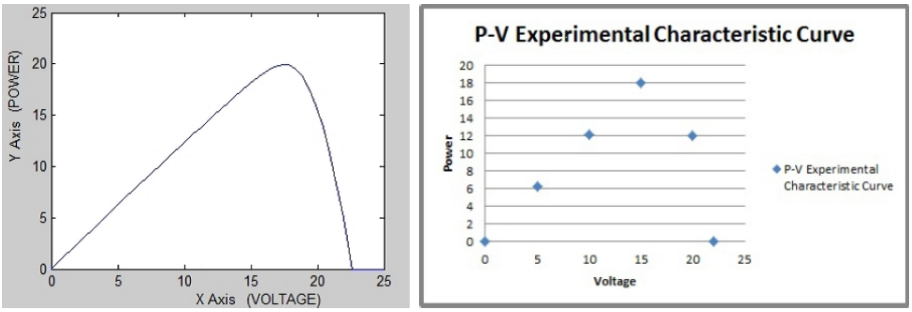

Figure 4.39: Superimposed results for simulated and experimental P-V characteristics

power attained at the global peak. It is clear the module power is maintained at an optimum value with slight variations due to noise in voltage and current measurements. Figure 4.40 also shows that the power attained for the same load in the system with P&O is only 16W, corresponding to the maximum power attained at the local peak. These results indicate an increase of about 130% in PV output power in the prescence of the proposed MPPT algorithm. This is explained by the fact that the first stage of the developed algorithm was able to approximate region of occurence of the GMPP and as such was able to guide the second stage of the controller into by-passing the local MPP and as such, was able to track the GMPP.

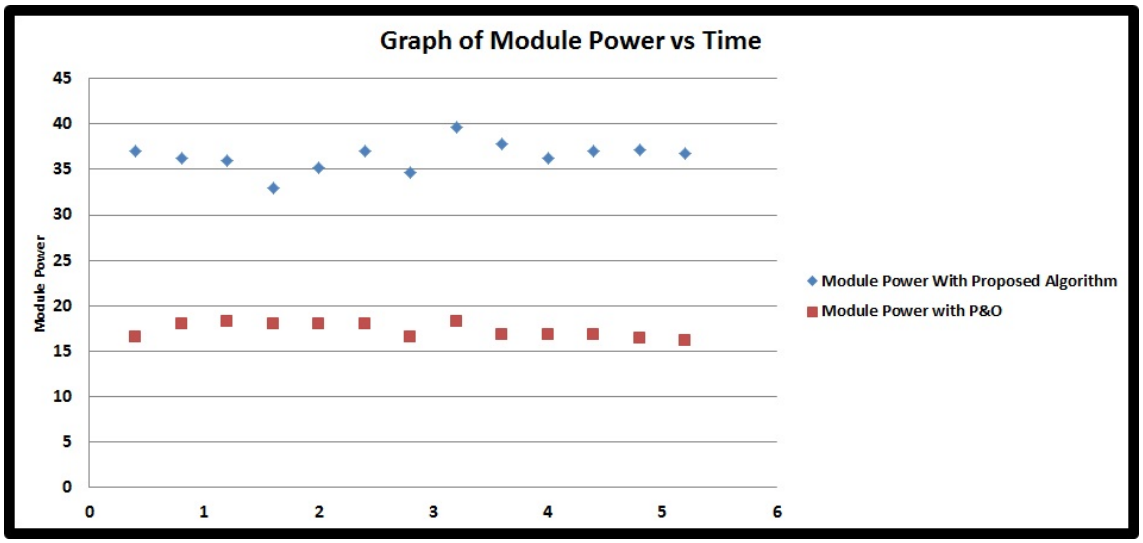

Figure 4.40: Measured results on a clear sunny day

4.6 Comparative Studies

According to Hohm and Ropp [47], the MPPT efficiency is given by (4.1). This equation shows the ratio of the integral of the actual power tracked by the MPPT technique over the integral of the theoretical MPP.

$$\eta_{MPPT} = \frac{\int_0^t P_{actual}(t)dt}{\int_0^t P_{max}(t)dt} \tag{4.1}$$

From values of output power shown in the tables in section 4.4, its can be seen that that the error between the theoretical and actual MPPs was always less than 4%. Thus, the tracking efficiency of the proposed technique can be approximated to be around 95% or even higher from other cases. Under any scale, this value of efficiency would be considered as not only acceptable, but good.

The convergence time of the proposed MPPT is split into two parts. When the two stages are run, the convergence time of the MPPT ranges between 12 and 15ms. This includes the 5 ms of the stabilization time for the first stage before the second stage is run and 7 to 10 ms for reaching the GMPP using the second stage. When the second stage is run without the first stage, the convergence time is less than 1 ms. This short amount of time is due to the fact that the P&O algorithm is run alone only when the MPP stays in a region close to the previous MPP. Thus, the average convergence time for the system cam be considered to be 13.5 ms. In [48], the authors were impressed by a convergence time of 10 ms to the MPP for a change of irradiance on a single array from 1000 to 900 W/m^2. This shows that the convergence time of the proposed technique is not only acceptable, but also high.

Comparing this technique with [41], it is noted that the convergence time in [41] is around 250 ms for a step response even though the simulation was done for 1 second which is much larger than the simulation time in this work. However, the efficiencies of both techniques are very close because they both track the global MPP accurately.

The convergence time in [49] was around 300 ms in a simulation that resembles real life which is also much higher than the one achieved in this work. However, the efficiency of was 100 % which is higher than the one achieved. This is mainly due to the fact

that their simulations did not have oscillations due to the large scale used in the power curves.

In [39], the oscillations in tacked power reached 50 W, constituting 10% of the 500 W peak power value. This reduced the efficiency of the tracked power by around 25 W while in the technique used in this work, the magnitude of the resulting oscillations was in the order of milli-watts. Further, because of the simulation time was large, the convergence time could be accurately determined. However, from graphs available in [39] the convergence time can be estimated to be around 7-10 seconds which is larger than the convergence time achieved using the technique utilized in this work.

5. CHAPTER FIVE CONCLUSIONS AND RECOMMENDATIONS

5.1 Conclusions

In this research, the effect of partial shading on the charcteristic curves of PV arrays were successfully investigated. A model for predicting the occourence of local and multiple peaks was successfully developed in Matlab/ Simulink platform. Theperformance of the conventional Perturb and Observe in tracking the global peak of a PV array was also successfully investigated. A model of the Perturb and Observe maximum power point tracking algorithm was implemented in Matlab/ Simulink platform for the purpose of determining the algorithim's performance in the prescence of multiple peaks. A modified maximum power point algorithm (two tier algorithm) for tracking the global peak in the prescence of partial shading was developed and tested in this work. In order to implement the algorithm, a system model was needed. The various subsystems were modelled and combined together in Matlab/ Simulink to produce a complete maximum power point tracking model. Experimental implementation of the proposed algorithm to determine its performance in a practical set-up and validation of the accuracy of the PV model was then carried out.

Simulation results show that under uniform insolation, the power-current and power-voltage curves have only one peak, the global peak, but under partial shading, these curves develop multiple peaks with one peak being the global peak and the rest being local peaks. Similarly, the I-V curve has only one step under uniform insolation but under partial shading conditions, the curve develops multiple steps. A significant outcome of this observation was that the power peaks under partial shading were displaced from each other by a multiple of 8% of open circuit voltage V_{OC} i.e. $(n \times 0.08 \times V_{OC})$. Further, the different levels of irradiation incident on the PV modules in the PV array determine the number of peaks observed on the PV characteristic curves.

Simulation results also show that in the prescence of multiple peaks, the P&O algorithm could find the global peak by chance, because of the arrangement of peaks on the curves as is the case where the first peak encountered by the P&O algorithm is the global peak. Further, the P&O algorithm could be trapped at the wrong peak for a while, but still continue to track the global peak. However, it was noted that when all the curves have multiple peaks, meaning the solar array is entirely under partial shading and further, the first peak is the local peak, and the second peak is the global peak, with the operating points of both peaks being far from each other, then the P&O algorithm was totally unable to track the global MPP. However, simulation results also showed that compared to the P&O algorithm, the proposed modified MPPT algorithm provides improved performance in tracking the global MPP in the prescence of multiple peaks.

Experimental results of the validation of the developed MPPT algorithm show that it is able to track the global peak in the prescence of multiple peaks. The results also indicate that a significant amount of additional energy can be extracted from a photovoltaic array under partial shading when using the proposed algorithm compared to when the traditional P&O algorithm is used resulting in improved operation of the photovoltaic system, which is expected to increase cost savings in the long haul.

On the whole, it is conluded that the overall objective of optimizing the energy extraction in a photovoltaic power system under partial shading conditions has been met. Although there still exists room for more work that should still be done, the the work in this thesis has created a foundation to allow that work to continue.

5.2 Recommendations for Future Work

As part of future work, the following points are proposed.

1. As an advancement in this field, it is proposed that a study be carried out to explore the possibility of an algorithm that directly relates the occurence and location of both the local maximum power points and global maximum power points on the PV characteristic curves to the changes in irradiance and temperature. And as such, enable the prediction of occurence of multiple peaks.

2. The algorithm proposed in this thesis should be expanded so as to design a search algorithm that would be able to locate the global maximum in the presence of several local maxima. In particular, the concept of utilizing simulated annealing in cases of large numbers of P-I points should be explored.

3. In practical applications of photovoltaic power systems, the goal may not necessarily be to deliver the maximum possible power to the load but rather only as much as is needed at any particular time. This is reffered to as power matching. The usable power that is not extracted from the panel due to the fact that it is not operating at the MPP will be dissipated as heat through the surface. Future work on this MPPT circuitry should include ways of determining how much power is needed at any particular time and and perform maximum power point tracking only to a level where power requierments are met with the usable power that is not extracted being either stored or used to carry out useful work.

REFERENCES

[1] Q. Li, P. Wolfs, "A Review of the Single Phase Photovoltaic Module Integrated Converter Topologies With Three Different DC Link Configurations", *IEEE*, May 2008, vol. 23, pp. 1320-1333.

[2] V. Devabhaktuni, M. Alam, R. C. Green, D. Nims, C. Near, " Solar Energy: Trends and Enabling Technologies," *ELSEVIER*, vol. 19, pp. 555-564, March 2013.

[3] D.J.MacKay,"Sustainable Energy Without the Hot Air, "*UIT Cambridge*, 2009. [online].Available: http://www.inference.phy.cam.ac.uk/sustainable/book/tex/cft.pdf, [Accessed 28/01/2013].

[4] M. Green, K. Emery, Y. Hishikawa W. Warta, E. Dunlop, "Solar Cell Efficiency Tables (Version 45)," *Progress in photovoltaics: Reseach and Applications*, vol. 23, pp 1-9, 2015.

[5] Survey, "Trends in photovoltaic applications. Survey report of selected IEA countries between 1992 and 2009," *International Energy Agency, Report IEA-PVPS Task 1 T1-19:2010*, 2010. [Online]. Available: http:// http://www.iea-pvps.org/fileadmin/dam/public/report/statistics/tr2009neu.pdf [Accessed 28/01/2013].

[6] Product Catalogue, "Sunny Family 2010/2011. The Future of Solar Technology," *SMA*, 2011. [Online].Available:http://www.solartechnologycentre.co.uk/STC20SMA20Prod2011.pdf [Accessed 02/02/2013].

[7] L. Piegari, R. Rizzo, "Adaptive perturb and observe algorithm for photovoltaic maximum power point tracking," *IET*, vol. 4, Issue. 4, pp. 317-328, July 2010.

[8] R. Faranda, S. Leva, "Energy comparison of MPPT techniques for PV Systems, *wseas transactions on power systems*, Vol. 3, Issue 6, June 2008.

[9] J. S. Kumari, Ch. S. Babu, "Comparison of maximum power point tracking algorithms for photovoltaic system," *IJAET*, Vol. 1, Issue 5, pp. 133-148, November 2011.

[10] T. Esram, P.L. Chapman,"Comparison of Photovoltaic Array Maximum Power Point Tracking Techniques", *IEEE Transactions on Energy Conversion*, vol. 22, no. 2, pp. 439 - 449, June 2007.

[11] B. Mishra, B. P. Kar, "Matlab Based Modeling of Photovoltaic Array Characteristics," *Bsc Project, National Institute of Technology, Rourkela*, May 2012.

[12] G. Shankar, V. Mukherjee, "MPP detection of a partially shaded PV array by continuous GA and hybrid PSO," *ASEJ*, 2012.

[13] P. A. Lynn, "Electricity from Sunlight: An Introduction to Photovoltaics," *John Wiley and Sons*, 2010, p. 238.

[14] H. Haberlin, "Photovoltaics System Design and Practice," *John Wiley& Sons*, ISBN 978-1-119-99285.

[15] M. Seyedmahmoudian, S. Mekhilef, R. Rahmani, R. Yusof, E. T. Renani,"Analytical Modeling of Photovoltaic Systems", *Energies 2013*, 6, 128-144.

[16] Y. J. Wang, P. C. Hsu, "Analytical modelling of partial shading and different orientation of photovoltaic modules", *IET 2010*, 4, 272282.

[17] A. Durgadevi, S. Arulselvi, S. P. Natarajan,"Photovoltaic Modeling and its Characteristics", *Proceedings of International Conference on Emerging Trends in Electrical and Computer Technology (ICETECT)*, March 2011; pp. 469475.

[18] S. Alsadi, B. Alsayid,"Maximum Power Point Tracking Simulation for Photovoltaic Systems Using Perturb and Observe Algorithm", *International Journal of Engineering and Innovative Technology (IJEIT)*,Volume 2, Issue 6, December 2012.

[19] S. Said, A. Massoud, M. Benammar, S. Ahmed,"A Matlab/Simulink-Based Photovoltaic Array Model Employing SimPowerSystems Toolbox", *Journal of Energy and Power Engineering*,6 (2012) 1965-1975.

[20] G. M. S. Azevedo, M. C. Cavalcanti, K. C. Oliveira, F. A. S. Neves, Z. D. Lins,"Evaluation of maximum power point tracking methods for grid connected photovoltaic systems",*in Proc. IEEE PESC*, 2008, pp. 1456-1462.

[21] T. C. Yu, Y. C. Lin, "A Study on Maximum Power Point Tracking Algorithms for Photovoltaic Systems," December 2010.

[22] D. L. King, J. A. Kratochvil, W. E. Boyson, "Temperature coefficients for PV modules and arrays: measurement methods, difficulties and results," *IEEE*, October 1997, pp. 1183-1186.

[23] T. Markvart, "Solar Electricity," *Wiley*, 2000, p. 280.

[24] S. B. Kjaer, J. K. Pedersen, F. Blaabjerg, "A Review of Single-Phase Grid-connected Inverters for Photovoltaic Modules," *IEEE*, October 2005, vol. 41, pp. 1292-1306.

[25] N. Femia, G. Petrone, G. Spagnuolo and M. Vitelli,"Optimizing sampling rate of P and O MPPT technique", *in Proc. IEEE PESC*, 2004, pp. 1945- 1949.

[26] N. Onat, "Recent Developments inMaximumPower Point Tracking Technologies for Photovoltaic Systems,"*IJP*, ISSN: 2231-1963, Nov. 2012.

[27] F. O. Karray, C. De Silva, "Soft Computing and Intelligent Systems Design,"*PEARSON, Addison Wesley.*

[28] A. Panda, M. K. Pathak, S.P.Srivastava,"Fuzzy Intelligent Controller for the Maximum Power Point Tracking of a Photovoltaic Module at Varying Atmospheric Conditions," vol. 1, no. 2, 2011.

[29] A. Elgharbi, D. Mezghani, A. Mami,"A maximum power point tracking method based on artificial neural network for a pv system," *IJAET*, Nov 2012.

[30] M. Salhi and R. El-Bachtiri,"A Maximum Power Point Tracking Photovoltaic System using a Proportional Integral Regulator," *Science Academy Transactions on Renewable Energy Systems Engineering and Technology*, Vol. 1, No. 2, June 2011.

[31] M. Azab,"A New Maximum Power Point Tracking for Photovoltaic Systems," *International Journal of Electrical and Electronics Engineering*, 2009.

[32] R. Ramabadran, B. Mathur,"Effect of Shading on Series and Parallel Connected Solar PV Modules," *CCSE*, 2009, vol. 3, No. 10.

[33] A. Garcia, M. C. Ruiz, F. Chenlo,"Experimental study of mismatch and shading effects in the I -V characteristic of a photovoltaic module," *Solar Energy Materials and Solar Cells*, 2006, vol. 90, no.3, pp 329-340

[34] C. Lashway,"Photovoltaic system testing techniques and results," *IEEE Transactions on Energy Conversion*, vol. 3, no.3, pp 503-506, 1988

[35] H. Patel, V. Agarwal,"MATLAB-Based Modeling to Study the Effects of Partial Shading on PV Array Characteristics," *IEEE Transactions on Energy Conversion*, vol. 23, no.1, pp 302-310, 2008

[36] T. Noguchi, S. Togachi, R. Nakamoto,"Short Current Pulse-based Maximum Power Point Tracking Method for Multiple Photovoltaic and Converter Module System," *IEEE*, vol. 49, no.1, pp 217-223, 2002

[37] N. Ahmed, M. Miyatake,"A novel maximum power point tracking for photovoltaic applications under partially shaded insolation conditions," *Elsevier*, vol. 78, pp 777-784, 2008

[38] T. Nguyen, K. Low, "A Global Maximum Power Point Tracking Scheme Employing DIRECT Search Algorithm for Photovoltaic Systems," *IEEE*, vol. 57, no. 10, pp 3456 - 3467, 2010

[39] T. Mishima, T. ohnishi,"A Power Compensation and Control System for Partially Shaded PV Array," *Electr Eng Jpn*, vol. 146, pp 74-82, 2004

[40] M. Miyatake, T. Inada, I. Hiratsuka, H. Zhao, H. Otsuka, M. Nakano,"Control characteristics of a Fibonacci-search-based maximum power point tracker when a photovoltaic array is partially shaded," *in Proc. IEEE IPEMC*,2004, vol. 2, pp. 816821.

[41] K. Kobayashi, I. Takano, Y. Sawada,"A study of a two stage maximum power point tracking control of a photovoltaic system under partially shaded insolation conditions," *Sol. Energy Mater. Sol. Cells*,vol. 90, no. 18/19, pp. 29752988, Nov. 2006.

[42] A. Swathy, R. Archana, "Maximum Power Point Tracking Using Modified Incremental Conductance for Solar Photovoltaic System," *IJEIT*, vol. 3, No. 2, pp 333-337, 2013

[43] E. Karatepe, T. Hiyama, M. Boztepe, M. Colak, "Voltage Based Power Compensation System for Photovoltaic Generation System Under Partially Shaded Insolation Conditions," *Elsevier*, vol. 49, pp 2307-2316, 2008

[44] K. Ishaque, Z. Salam,"A Deterministic Particle Swarm Optimization Maximum Power Point Tracker for Photovoltaic System under Partial Shading Condition," *IEEE*, 2012.

[45] KL050 Datasheet, *www.klsolar.com/images/SOLARPICS/MODULES/PDF*

[46] N. Mohan, T. Undeland, W. Robbins,"Power Electronics: Converters, Applications, and Design," 3rd ed. New Jersey: John Wiley and Sons, 2003.

[47] D. P. Hohm, M. E. Ropp,"Comparative Study of Maximum Power Point Tracking Algorithms," *Progress in Photovoltaics: Research and Applications*, vol. 11, pp 47-62.

[48] P. Midya, P. T. Krein, R. J. Turnbull, R. Reppa, J. Kimball,"Dynamic maximum power point tracker for photovoltaic applications," *27th Annual IEEE Power Electronics Specialists Conference*, vol. 2, pp 1710-1716, 1996.

[49] J. Park, J. Ahn, B. Cho, G. Yu,"Dual-Module-Based Maximum Power Point Tracking Control of Photovoltaic Systems," *IEEE Transactions on Industrial Electronics*, vol. 53, pp 4, 2006.

APPENDIX A: Microcontroller Code

```
/*
* vi_sense.c
*
* Created: 1/6/2015 15:33:34
*  Author: VIncent Lengoiboni
*/

#define F_CPU 8000000L

#include <avr/io.h>
#include <util/delay.h>
#include <stdio.h>
#include <stdlib.h>
#include <string.h>
#include <math.h>


#include "adc_read.h"
#include "usart.h"

#define switchPin  PORTB0
#define currentFault PORTB1

#define vSensePin ADC0
#define csensePin ADC1
#define crSensePin ADC2

#define tT 100

#define R1 19650.0
#define R2 2450.0
#define CR 4.7

#define sysV 5.60
```

```
#define maxAdc 1023.0

uint16_t vSense = 0;
uint16_t cSense = 0;
uint16_t crSense = 0;

double voltage = 0.0;
double cAverage = 0.0;

void printFloat(double number, uint8_t digits);
void FreqGen(uint16_t voltage, uint16_t current);
void delayUs(int tm);

int main(void)
{
        usart_init(57600);
        adc_init();

        int delayTime = 0;

        DDRB &= ~_BV(currentFault);
        DDRB |= _BV(switchPin);

        char buff[10];
        //float caverage = 0.0;


        while(1)
        {
                vSense = adc_read_16bit(vSensePin);
                _delay_ms(1);
                cSense = adc_read_16bit(csensePin)/*-519*/;
                _delay_ms(1);
                crSense = adc_read_16bit(crSensePin);
```

```
                /* printFloat(cSense, 2);
                usart_puts(", ");
                printFloat(((voltage/(R1+R2))*1000), 2);
                usart_puts(", ");
                printFloat(cAverage, 2);
                usart_puts("\r\n");*/
                sprintf(buff, "%04d,%04d\n", vSense, crSense);
                usart_puts(buff);
                _delay_ms(50);

                delayTime = 1000;
                while(delayTime--)
                {
                        FreqGen(vSense, crSense);
                }

        }
}

void printFloat(double number, uint8_t digits)
{
        char buff[4];

        if (isnan(number))  usart_puts("nan");
        if (isinf(number))  usart_puts("inf");
        if (number > 4294967040.0) usart_puts("ovf");  // constant determine
        if (number <-4294967040.0) usart_puts("ovf");  // constant determine

        // Handle negative numbers
        if (number < 0.0)
        {
                usart_Transmit('-');
                number = -number;
        }
```

```
        // Round correctly so that print(1.999, 2) prints as "2.00"
        double rounding = 0.5;
        for (uint8_t i=0; i<digits; ++i)
        rounding /= 10.0;

        number += rounding;

        // Extract the integer part of the number and print it
        unsigned long int_part = (unsigned long)number;
        double remainder = number - (double)int_part;
        sprintf(buff, "%d", (int)int_part);
        usart_puts((char *)buff);

        // Print the decimal point, but only if there are digits beyond
        if (digits > 0) {
                usart_puts(".");
        }

        // Extract digits from the remainder one at a time
        while (digits--> 0)
        {
                remainder *= 10.0;
                int toPrint = (int)(remainder);
                sprintf(buff, "%d", toPrint);
                usart_puts((char *)buff);
                remainder -= toPrint;
        }
}

void FreqGen(uint16_t cVoltage, uint16_t cCurrent)
{

        double dutyCycle = 0.0;
        int tOn = 0.0;
        int tOff = 0.0;
```

```
        int tTotal = 100;

        voltage =  ((double)((sysV/maxAdc)*cVoltage) / R2) * (R1+R2);
        cAverage = ((double)(cCurrent*(sysV/maxAdc)) / CR);// - 22.72;

        dutyCycle = (double)(1- sqrt(voltage/(2*560*cAverage)));

        tOn = tTotal * dutyCycle;
        tOff = tTotal - tOn;

        PORTB |= _BV(switchPin);
        delayUs(tOn);
        PORTB &= ~_BV(switchPin);
        delayUs(tOff);
}


void delayUs(int tm)
{
        while(tm--)
                _delay_us(1);
}
```

APPENDIX B: Switch Testing Code

```
/**
* Switch test simulation firmware
* MCU - ATTiny85-P
*
* Author : Vincent Lengoiboni
* Date: 25-12-2014
*
**/

#include <inttypes.h>
#include <avr/io.h>
#include <avr/interrupt.h>
#include <avr/sleep.h>

#ifndef F_CPU
#define F_CPU 8000000L
#endif

#include <util/delay.h>

int main()
 {
   // Write your code here
    DDRB |= _BV(PORTB0);
   while (1)
   {
      PORTB |=  _BV(PORTB0);
       _delay_ms(500);
      PORTB &= ~_BV(PORTB0);
       _delay_ms(500);
   }
   return 0;
 }
```

APPENDIX C: PV Datasheet

Electrical and Mechanical Data

Model	KL045	KL050	KL055
Maximum power (Pmax)	45 Wp	50 Wp	55 Wp
Open Circuit Voltage (Voc)	21.5 V	21.5 V	21.5 V
Maximum power point voltage (Vmpp)	17.1 V	17.1 V	17.1 V
Short circuit current (Isc)	2.94 A	3.28 A	3.60 A
Maximum power point current (Impp)	2.64 A	2.93 A	3.22 A
Tolerance of Pmax	±10%	±10%	±10%
Cell Size (mm)	66 X 156	66 X 156	66 X 156
No. of cells	36	36	36
Dimensions (mm) ± 1	670 x 665 x 38	670 x 665 x 38	670 x 665 x 38
Maximum system voltage	1000	1000	1000
Module Efficiency	10.10%	11.22%	12.34%
Weight (kgs)	5.0	5.0	5.0

Standard Test Condition: Irradiance 1,000 W/sq.m, Temperature 25deg C Air mass 1.5 spectrum)

Performance of Thermal Characteristics

Temperature co-efficient	NOCT (^{O}C)45	NOCT (^{O}C)45	NOCT (^{O}C)45
Power [Pmax]	-0.43 %/K	-0.43 %/K	-0.43 %/K
Open-circuit voltage [Voc]	-0.36 %/K	-0.36 %/K	-0.36 %/K
Short circuit current (Isc)	+0.06 %/K	+0.06 %/K	+0.06 %/K

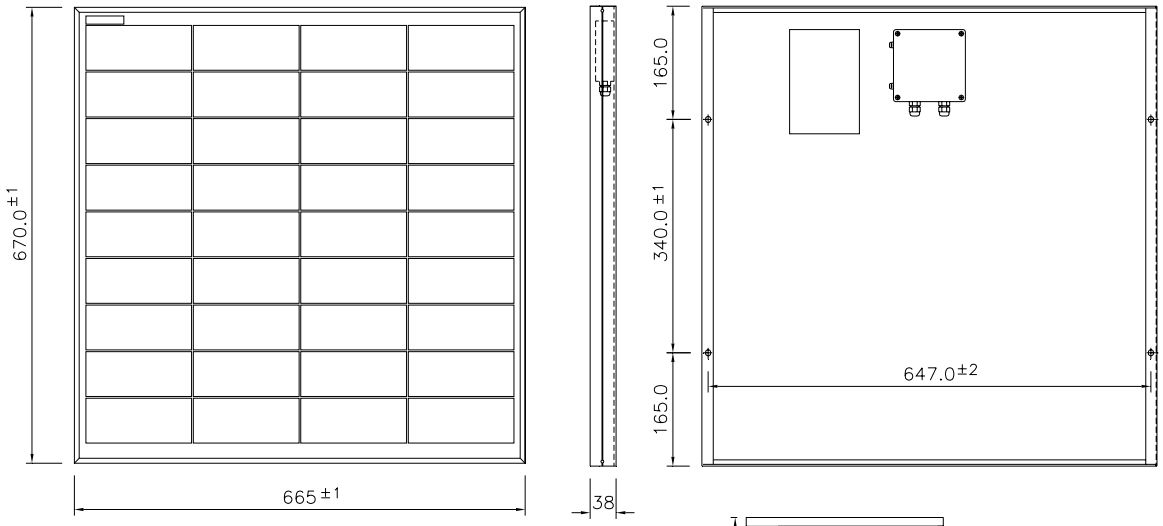

All dimensions are in mm

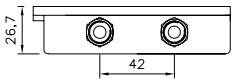

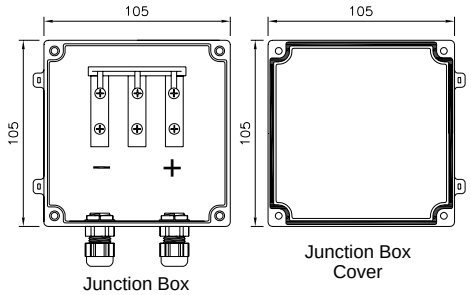

Junction Box

Junction Box Cover

Qualification and certificates

The Photovoltaic Modules certified to
IEC61215 & EN IEC 61730 Class A, Safety Class II

Our Company Certified by TUV according to ISO 9001:2008 · Reg.No. 85 100 001 06696

KL SOLAR COMPANY PVT LIMITED,
1/482B, Transport Nagar, Neelambur, Coimbatore – 641 062. INDIA.
Phone : +91 422 6563638 / Fax : +91 422 2567562, email : info@ klsolar.com / www.klsolar.com

APPENDIX D: P&O M-file

```
function d = P_and_O (Pnew, Pold, Vnew, Vold, dold, dsearch, reset)



if (reset == 1)
        d=dsearch;
elseif (reset == 0 && Pnew >= Pold && Vnew > Vold)
        d=dold-0.005;
elseif (reset == 0 && Pnew < Pold && Vnew > Vold)
        d=dold+0.005;
elseif (reset == 0 && Pnew < Pold && Vnew <= Vold)
        d=dold-0.005;
elseif (reset == 0 && Pnew >= Pold && Vnew <= Vold)
        d=dold+0.005;
elseif (Pnew == Pold))
        d=dold;
else
        d=dold;
end;
```